Numerical Limit Analysis of Reinforced Concrete Structures

Computational Modeling with Finite Elements for Lower Bound Limit Analysis of Reinforced Concrete Structures.

Larsen, Kasper Paaske

Publication date:
2011

Document Version
Publisher's PDF, also known as Version of record

Numerical Limit Analysis of Reinforced Concrete Structures

– Computational Modeling with Finite Elements for Lower Bound Limit Analysis of Reinforced Concrete Structures.

Kasper Paaske Larsen

Ph.D. Thesis

Department of Civil Engineering
Technical University of Denmark

2010

Numerical Limit Analysis of
Reinforced Concrete Structures
– Computational Modeling with Finite Elements for Lower Bound Limit Analysis of Reinforced Concrete Structures.

Printed by
Department of Civil Engineering
Technical University of Denmark
ISBN: xxxxxxxxxxxxx
ISSN: xxxx-xxxx

Preface

This thesis is submitted as a partial fulfillment of the requirements for the Danish Ph.D. degree. The study has taken place at Ramboll Denmark and the Department of Civil Engineering at the Technical University of Denmark (DTU Byg) in the period September 2007 to October 2010. The project is funded by Ramboll Denmark and the Danish Ministry of Science, Technology and Innovation. Associate Professor Peter Noe Poulsen has been the projects principal supervisor and associate professor Leif Otto Nielsen has been co-supervisor, both are affiliated to DTU Byg. From Ramboll Denmark, Bent Feddersen and Bent Steen Andreasen have supervised the project.

The first part provides an introduction to the field of research and a summary of the findings and conclusions. The second part is a collection of three papers presenting the research in greater details.

Copenhagen, October 2010

Kasper Paaske Larsen

Acknowledgements

I would like to thank my supervising team for their invaluable input and guidance throughout the project: Associate professors Peter Noe Poulsen and Leif Otto Nielsen for their feedback and assistance on developing the numerical models and Bent Feddersen and Bent Steen Andreasen for their guidance to keep the project focused on practical engineering application.

I would also like to acknowledge Dr. Johan Löfberg, research associate at Linköpings University for his assistance on generating the numerical models passed to the convex optimization algorithms. Especially his YALMIP interface have been an invaluable tool for implementation and experimentation throughout the project.

I would also like to thank my colleagues at Ramboll for their support and interest in the project which have kept my spirit high during the project. Also a special thanks to my good friend and colleague Kåre Flindt Jørgensen for proofreading the manuscript.

Last, but definitely not least, I would like to thank my family and friends for their support. Most of all, I would like to thank my wonderful and lovingly girlfriend Marie for her patience and support throughout the project.

Abstract

For more than half a century, limit state analysis based on the extremum principles have been used to assess the load bearing capacity of reinforced concrete structures. Extensive research within the field has lead to several techniques for performing such analysis manually. While these manual methods provide engineers with valuable tools for limit state analysis, their application becomes difficult with increased structural complexity. The main challenge is to solve the optimization problem posed by the extremum principles.

This thesis is a study of how numerical methods can be used to solve limit state analysis problems. The work focuses on determination of the load bearing capacity of reinforced concrete structures by employing the lower bound theorem and a finite element method using equilibrium elements is developed. The recent year's development within the field of convex optimization is applied to solve the limit state problems.

Three different element types have been developed and tested. The first is a solid tetrahedral element with a linear stress distribution. The tri-axial stress state in the element is decomposed into concrete and reinforcement stresses, to which separate yield criteria are applied. The reinforcement is assumed to carry axial stresses only and is constrained by simple upper- and lower limits while the modified Coulomb criterion is applied to the concrete stresses. The element is verified by analytical solutions and used to model and analyze a console beam with complex reinforcement layout.

The second element is a beam element capable of carrying loads in three dimensions. The element employs a zone model which provides a discrete representation of the internal stress state in the beam. By applying the yield criterion on a stress state level, the element circumvents the need for a complex section force based yield criterion. The stresses are, similar to the solid model, decomposed into concrete and axial reinforcement stresses to which separate yield criteria are applied. An approximation to the modified Coulomb criterion using second-order cone constraints is developed for improved performance. An example is given in which an inverse T-beam is analyzed and the numerical results are compared to laboratory tests.

The third and final element is a plane shell element capable of modeling membrane and plate bending behavior. The element employs a layered disk approach to create a discrete representation of the internal stresses. The stress state is separated and yield criteria are applied similar to the solid element. Because the transverse shear stresses are included in the modified Coulomb criterion, the element is capable of modeling the effects and

combined section forces such as plate bending and transverse shear. Examples are given which illustrates how the element can model plate and disk structures and the importance of taking transverse shear into account for structural problems with combined bending and transverse shear is illustrated.

Resumé

I mere end et halvt århundrede har brudstadieberegninger baseret på extremal principperne været anvendt til at vurdere bæreevnen af armerede betonkonstruktioner. Omfattende forskning indenfor området har resulteret i flere metoder til manuel brudstadie beregninger. Imens disse metoder har givet ingeniørerne et værdifuldt værktøj til at lave brudstadie beregninger, bliver de dog hurtigt utilstrækkelige når konstruktionerne bliver komplicerede.

Denne afhandling er et studie af hvordan numeriske metoder kan anvendes til at udføre brudstadieberegninger. Arbejdet fokuserer på bestemmelse af konstruktioners bæreevne ved hjælp af nedreværdi sætningen og et finite element system baseret på ligevægts elementer er udviklet. De seneste års udvikling indenfor konveks optimering udnyttes til at løse brudstadie problemerne.

Tre forskellige element typer er udviklet og testet. Det første er et solid tetraeder element med lineær spændingsfordeling. Den tre-aksede spændingstilstand i elementet er opdelt i beton- og armeringsspændinger hvorpå separate flydebetingelser er anvendt. Armeringen antages kun at optage en-aksede spændinger og simple øvre og nedre grænser er anvendt på disse mens den modificerede Coulomb betingelse anvendes på betonspændingerne. Elementet er bl.a. brugt til at modellere og analysere en konsolbjælke med et kompliceret armeringsarrangement.

Det andet element er et bjælkeelement, der kan optage laster i tre dimensioner. Elementet benytter en zone model til at beskrive den interne spændingstilstand i bjælken, og ved at opfylde flydebetingelsen på spændingsniveau undgås en kompliceret betingelse baseret på snitkræfter. Spændingerne er, ligesom for solid elementet, opdelt i beton og armeringsspændinger hvorpå forskellige flydebetingelser er anvendt. En approksimation til den modificerede Coulomb betingelse er udviklet ved brug af anden-ordens keglebetingelser hvilket giver mere effektive beregninger. Elementet er anvendt til at modellere en omvendt T-bjælke og resultaterne er sammenlignet med laboratorie forsøg.

Det tredje og sidste element er et plant skal element der kan modellere membran kræfter og plade bøjning. Elementet anvender en lagdelt skivemodel til at beskrive de interne spændinger. Spændingerne er igen opdelt og flydebetingelser som for solid elementet er anvendt. Der er givet eksempler på hvordan elementet kan bruges til at modellere både plade og skive konstruktioner og vigtigheden af at medtage tværforskydning i pladekonstruktioner udsat for kombineret bøjning og tværforskydning er vist.

Table of Contents

Part I

Introduction and summary

Chapter 1

Introduction

1.1 Reinforced Concrete Structures: Historical Overview

Concrete has been used as a structural material for millennia. Today it is often mixed with reinforcement and is the most widely used construction material in the world. Analyses have shown that concrete type materials were applied by the Egyptians as early as 3000 B.C. in the construction of the Pyramids. Concrete was also used by the Roman Empire for construction of aqueducts, arches and domes such as the one found at The Pantheon. The Roman concrete used a mortar based on quicklime and pozzolana (volcanic ash) which was mixed with aggregates such as rock pieces, ceramic tiles or brick rubble. While reinforcement in the form of steel bars were not used, the Romans knew that adding horse hairs to the mortar mixture could reduce cracks caused by shrinkage.

In 1824, the British cement manufacturer Joseph Aspin obtained a patent for Portland-cement but it was his son William Aspin who, in the early 1840's, further developed the Portland-cement used in modern concrete. Not long after, at the Parish Exposition of 1867, the French gardener Joseph Monier exhibited iron-reinforced troughs for horticulture for which he obtained a patent the same year. He expanded on his invention in the following years and obtained patents for iron-reinforced pipes and basins (1868), bridges (1873) and reinforced concrete beams (1878).

While concrete has the ability to be cast in many shapes, the process of creating moulds and casting the concrete structures on-site is often labor intensive. The use of pre-cast concrete elements has greatly reduced the construction cost of reinforced concrete structures because the elements can be cast at specialized plants. The process of pre-cast concrete was pioneered by the French engineer François Hennebique who had seen Joseph Moniers invention at the Parish Exhibition, and in 1882 he patented a system for reinforced concrete elements such as beams and columns. The first building to use the system was the Weaver Building in Swansea, Wales, see Fig. 1.1.

Not long after the introduction of reinforced concrete, it was discovered that tensile strength of reinforcement could be exploited further by subjecting the rebars to tension and thereby inducing compression to the concrete. Even though the process of post-

Figure 1.1: *Weaver Mill Building in Swansea, Wales was constructed using François Hennebique patented system.*

tensioning was patented by the American engineer P. Jackson in 1872 shortly followed by C.W. Doehring's patent for pre-stressing in 1888, it was not until French engineer Eugne Freyssinet in the beginning of the 19th century discovered that high strength steel should be utilized that the method became applicable for structural designs.

In the second half of the 20th century, during the rebuild of Europe after the Second World War, reinforced concrete was widely used in the construction of residential and industrial buildings due to the speed at which they could be erected. Because the main concern was to provide people with affordable homes and do it as quickly as possible, little attention was given to architectural expression and reinforced concrete attained a reputation of being dull and unsuitable for architecturally complex structures. Over the last decades, this has been changing though, and architects have opened up to the potential of reinforced concrete. One such structure is the 23 storey Bella Sky Hotel, designed by the Danish architectural firm 3xN and engineered by Ramboll Denmark, currently under construction in Copenhagen, Denmark, see Fig. 1.2b. With an inclination of approximately 15°, it fully utilizes the compressive capabilities of the concrete as well tensile strength added by the reinforcement. With the increased desire to build exiting and complex buildings using reinforced concrete comes a need for even more advanced design tools. While technology, and especially the numerical tools, have improved significantly over the last decades, limit state analysis of reinforced concrete structures still pose a significant challenge for structural engineers. The focus of this thesis is to develop a numerical tool which enables engineers to perform efficient limit state analysis of complex reinforced concrete structures.

1.2 Behaviour of Reinforced Concrete

Concrete is a composite material composed of cement paste and aggregate particles. When the components are mixed with water and allowed to hydrate, a stone like material is formed. Normally, the aggregate particles have a much higher stiffness than the cement paste, resulting in a complex stress field internally in the concrete material when the material is subjected to deformations. Stress concentrations forms around the aggre-

(a) *Architectural visualization by 3xN.*

(b) *From the official construction site webcam.*

Figure 1.2: *Bella Sky Hotel in Copenhagen, Denmark.*

gate particles which lead to crack formations at the interface between cement paste and aggregate. These cracks are often very small and formed at stress levels far below the compressive strength of the composite material. The cracks are not visible and are often referred to as *microcracks* or *internal cracks*. The existence of these internal cracks means that the concrete material cannot be considered isotropic on a micro-mechanical level, and isotropic failure conditions such as the modified Coulomb criterion presented in Section 1.3 are associated with the meso and macro scale material.
Fig. 1.3 shows a schematic illustration of the stress-strain behavior of concrete subjected to uni-axial loadings. Considering first the compressive part of the curve ($\sigma, \epsilon < 0$ is compression), the initial part of the curve, curve path $O - A$, is the elastic response of the material. The area under this curve part is the elastic energy absorbed in the material which is recoverable when unloaded. When loaded beyond the elastic limit, change occurs in the material leading to irreversible deformations, also called *plastic deformation*. In the beginning of the plastic domain, a hardening effect can be observed until the peak-load is reached at point B. Once the peak-load is passed, internal damage reduces the strength of the material and causes a softening effect as illustrated in the figure. At the point C, the strains reaches a point at which the concrete has substantially damages and the material is considered as crushed. The total energy absorbed in the material is defined by the area under the stress-strain curve. For ductile materials, the majority of the energy is absorbed in the post-peak range. A similar behavior can be observed when the concrete is subjected to tension. While the post-peak response is more brittle a softening effect is still observed due to sliding failure around the aggregate particles. Because the tensile strength highly depends on the crack formations in the material, it is unreliable and often disregarded in practical design cases. Reinforcement in form of steel bars, or *rebars*, is often added to concrete materials to compensate for the low tensile capacities of the concrete. Such structures are often referred to as *reinforced concrete* (RC) structures. These rebars exhibits significant ductility as illustrated on the schematic stress-strain curve in

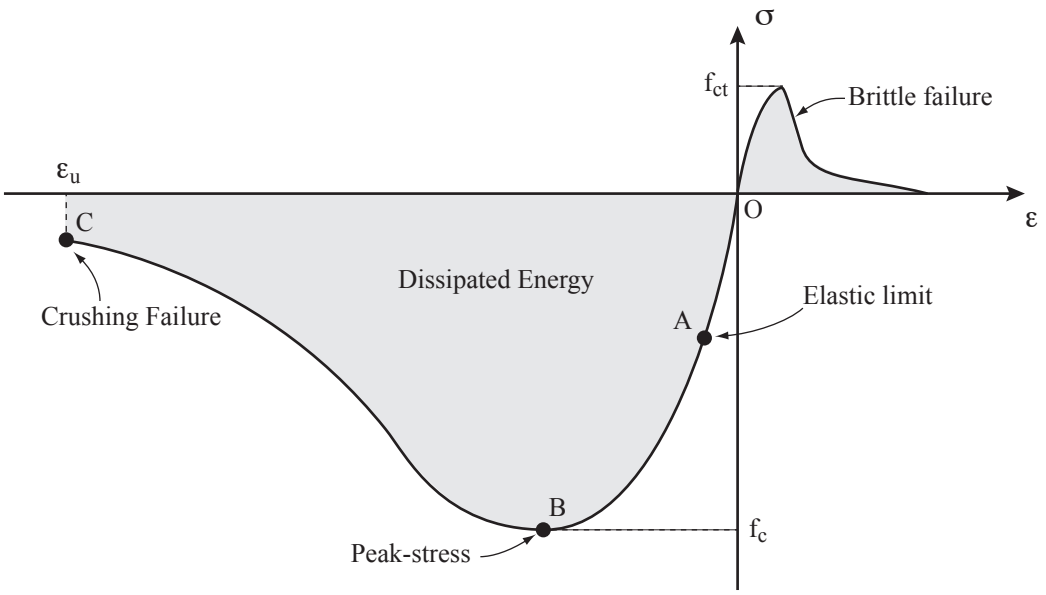

Figure 1.3: *Schematic illustration of stress-strain curve for concrete subjected to uni-axial loading.*

Fig. 1.4. The combination of concrete and steel makes RC structures able to carry both tensile and compressive stresses while maintaining a ductile behavior which is desirable for structural materials.

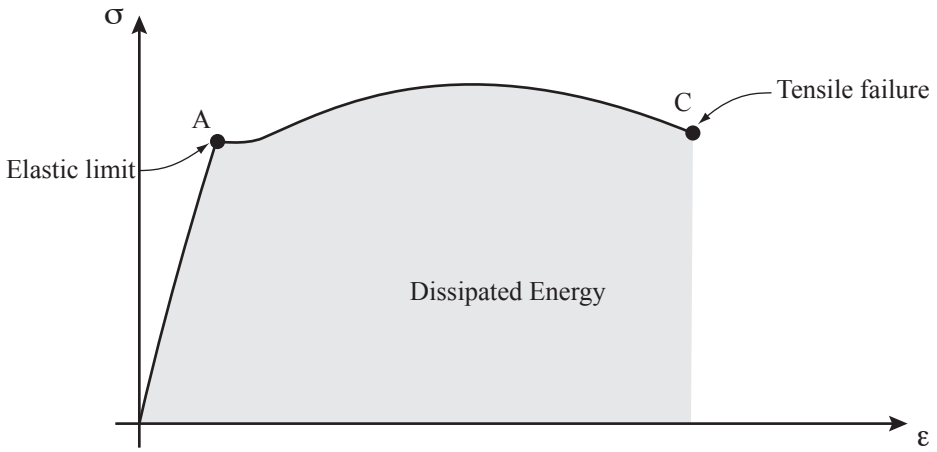

Figure 1.4: *Schematic illustration of stress-strain curve for a rebar subjected to uni-axial loading.*

1.3 Applied Material Models

Several approaches exist for analysis of RC structures. The linear elastic approach assumes a linear relation between the stress and the strain state. This method is capable of modeling the structural response in the elastic domain under the assumption that the material behaves linearly. This approach is widely adopted in commercial software packages

and is therefore often applied in practical design scenarios. If the concrete can be assumed uncracked, this method is well suited for *serviceability limit state* (SLS) analysis because it can give an estimate of structural deformations. Because this method only considers the elastic domain, *ultimate limit state* (ULS) analysis, i.e. the structural response at the point of failure is not possible.

Several approaches exist in which the non-linear behavior observed beyond the elastic limit is approximated. One approach is the use of *plasticity models*. Here, the structural response is separated into an elastic and a plastic response which governs the respective domains. The elastic stress-strain response is determined as usual by the structural stiffness, while the plastic response is determined based on the chosen *yield criterion*, or *yield surface*, and *flow rule*. The concepts of yield criteria and the flow rule are described in further detail in Section 2.2. Hardening and softening effects are modeled by expanding or contracting the yield surface. By employing this method, the structural deformations can be estimated from the initial loading all the way to failure which makes plasticity models useful for both SLS and ULS analysis. Estimation of crack widths based on these plasticity models is not straight forward though. Since the crack width is an important design parameter for RC structures, methods based on fracture mechanics have become a prime research topic in recent years. The theories of fracture mechanics have proved useful for such analysis but despite being available since 1921 (Griffith (1921)), fracture mechanics was not successfully applied to concrete until (Hillerborg et al. (1976)) presented the *fictitious crack model* (FCM). Since then, FCM have been used in finite element analysis of concrete structures. One of the most recent methods capable of modeling crack behavior is the *eXtended Finite Elements* (XFEM) (Belytschko and Black (1999)) which uses enriched finite elements to model the crack propagation through a structure. These fracture based models provides engineers with a method for estimating crack width in SLS analysis and fracture modes in ULS analysis. Despite of the significant development in the recent years, the method has just recently found its way into commercial applications such as *Abaqus FEA*. There are still several issues which must be solved before the method becomes applicable for analysis of practical problems. Some of these are:

- Multiple cracks.
- Integrated reinforcement models.
- Mixed mode material models.

It will presumably be several more years before all these problems have been solved and are available in commercial software applications.

Methods based on perfect plastic material behavior have been favored for limit state analysis of RC structures. The primary reason to do so is its relative simplicity when compared to the other methods and while good results have been obtained using these methods, they do, at the time of writing, pose considerably challenges when applied to the large-scale structures encounted in practical design problems. Perfect plastic material models makes a relatively crude approximation to the actual stress-strain behavior by assuming that the stress state is constant once yielding is initiated as illustrated in Fig. 1.5.

The behavior on a structural level is though typically close to perfectly plastic which is

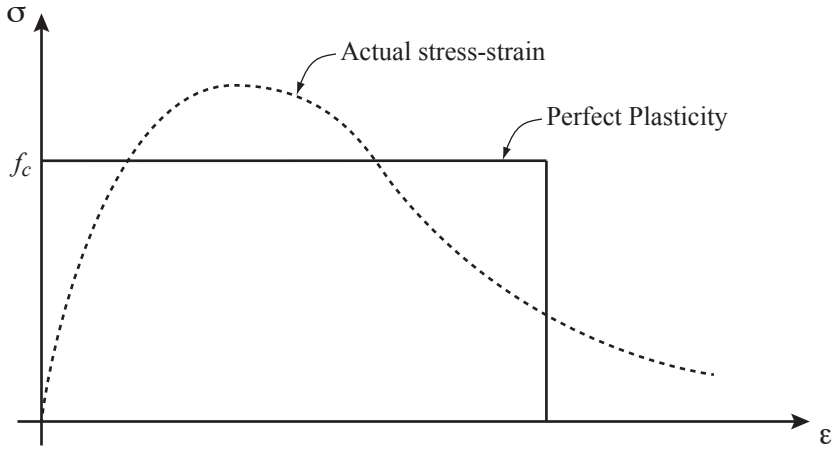

Figure 1.5: *Stress-strain curve of a perfect plastic material versus the actual stress-strain curve.*

illustrated by test data shown in Fig. 1.6. The results were presented by (Hansen (1964)) and shows the correlation between the curvature of a beam and the bending moment. From the test data, it is clear that despite being a relatively crude approximation to the material behavior, perfect plasticity is well suited for structural level ULS analysis of RC structures. Methods which employ perfect plasticity are purely aimed at ULS analysis and the obtained solutions provide no information about structural deformations or crack widths. The peak strength obtained using test specimens is often higher than the strength

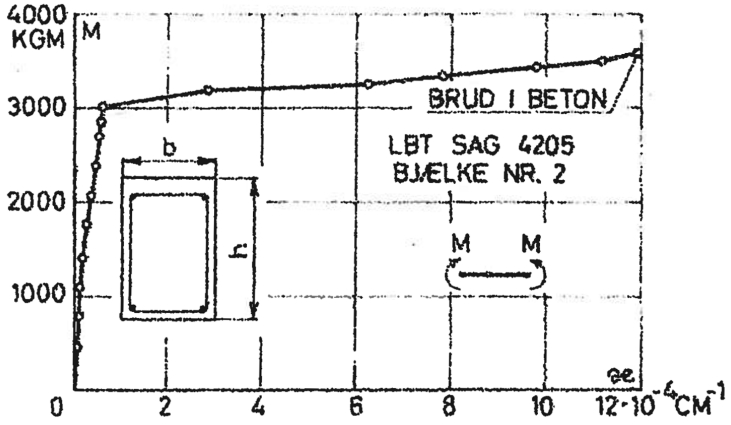

Figure 1.6: *Moment-curvature relation of an RC beam subjected to pure bending, (Hansen (1964)).*

measured directly in structures. The main reason for this is internal cracking in the concrete which reduces the strength. These cracks can, due to shrinkage, be present in the structure even before load is applied, or they can be formed at the time of loading. It is therefore necessary to insert a reduced strength, also called the *effective strength*, into the theoretical material models. The effective strength is often defined as function of the

peak strength as

$$f_{c_{ef}} = \nu f_c \tag{1.1}$$

where $\nu \leq 1$ is the effectiveness factor. When using a perfectly plastic material model the softening effects must also be accounted for, this is often done through the effectiveness factor. For practical applications, the strength values specified in this thesis should simply be replaced by the effective strength values.

From the above presentation of various material models, it is seen that the most direct and effective method available today for determining the load carrying capacity of RC structures are those based on perfect plasticity.

1.4 Scope of This Study

This thesis is concerned with numerical limit state analysis based on the lower bound theorem. The aim is to develop elements that can be implemented into a general finite element framework which enables engineers to perform limit state analysis of complete three dimensional structures. The convex optimization problems posed by the lower bound theorem is solved using generic optimization algorithms.

The major part of the work is concerned with the development of a solid reinforced concrete material model based on semidefinite programming methods. The solid material model is implemented into a finite element framework using 4-node tetrahedral elements. A 3D beam element capable of carrying loads in three dimensions is also developed and the solid material model is applied to handle the complex stress state internally in the beam. Furthermore, a material model which approximates the tri-axial stress states within the beam is developed based on second-order cone programming for improved efficiency. Finally, a shell element capable of carrying in-plane forces and bending moments is developed which employs the solid material model to consider transverse shearing in the element.

1.5 Overview of the Thesis

The thesis consists of two parts. Part I contains an introduction to limit state analysis and the problems posed when implementing these into finite element. Part I also includes a summary of the work reported in the papers appended in Part II. It should be noted that references made in the papers are not necessarily listed in the bibliography of Part I and vice versa.

Overview of Part I

This chapter opens with a historical overview of reinforced concrete as a structural material followed by a short description of its behavior under structural loadings. The chapter is concluded with an introduction to some mathematical material models applied for analysis of RC structures.

Chapter 2 introduces the extremum principles on which the numerical methods relies. These are presented along with an introduction to the concepts of yield criteria, with emphasis on the criteria employed in the present work: the modified Coulomb criterion for cohesive frictional materials and uni-axial limits for reinforcement. Finally, some manual methods for limit state analysis based on the extremum principles are presented.

Chapter 3 focuses on numerical limit state analysis. The chapter initiates with a brief presentation of the background of numerical methods for structural analysis followed by a presentation of the popular stiffness based FEM formulation. A more in-depth introduction to the equilibrium based FEM methods used in the current work is given along with a presentation of the convex optimization techniques employed.

Chapter 4, 5 and 6 summarizes the work reported in the three papers appended in Part II and includes implementation details and relevant examples.

Overview of Part II

Paper I, *"Limit State Analysis of Solid Reinforced Concrete Structures"* deals with the development of a solid reinforced material model capable of modeling solid structures subjected to tri-axial stress states. The paper presents a method in which the total stress state is decomposed into concrete and reinforcement stresses and yield conditions are enforced on these separately. The material model is verified by analytical solutions and a finite element implementation is employed for analysis of complex structures.

Paper II, *"Limit State Analysis of 3D Reinforced Concrete Frames"* presents a beam element capable of carrying loads in three dimensions. To circumvent the need for a complex yield criterion based on cross section forces the element provides a discrete representation of the internal stress state using a set of zones. The stress state is constrained by either the modified Coulomb criterion presented in Paper I or an approximated criterion based on second-order cones. The element is verified by analytical solutions and numerical results are compared to laboratory test data.

Paper III, *"Limit State Analysis of Reinforced Concrete Shells"* describes a shell element which can be used for modeling of structures subjected to in-place forces as well as plate bending. The element uses a layered disk approach in which the internal stress state is defined by shear rigid layers and the solid material model presented in Paper I is used to obtain a lower bound solution.

Chapter 2

Limit State Analysis Theorems

2.1 The Extremum Principles

Extensive research in the field of limit state analysis of reinforced concrete (RC) structures throughout the last century have resulted in numerous methods for assessing the load bearing capacity of such structures. The majority of these methods are based on the extremum principles which was first formulated by A. Gvozdev in 1936, (see english translation (Gvozdev (1960))) and independently by (Drucker et al. (1952)). The extremum principles assume a rigid plastic material model and comprise of three theorems: the *lower bound theorem*, the *upper bound theorem* and the *uniqueness theorem*.

2.1.1 Lower Bound Theorem

The lower bound theorem states that if a given stress field is statically admissible and does not violate the yield criteria at any point within the structure, then that stress field will not be able to cause collapse in the structure. For statically indeterminate structures, multiple solutions (i.e. stress fields) exists which satisfies this condition. Methods based on the lower bound theorem aims at finding *the* solution which yields the largest possible collapse load, a process which requires some sort of optimization. An attractive quality of the lower bound theorem is that the estimated collapse is safe, i.e. the load is less than or equal to the actual collapse load, hence its name.

2.1.2 Upper Bound Theorem

The upper bound theorem states that for a kinematically and possible strain field which fulfils the constitutive conditions, an upper bound on the collapse load can be found by equating the internal work, or dissipation, with the external work. Methods based on this theorem strive at finding the strain field, or *failure mechanism*, for which the determined collapse load is smallest possible. This does, similar to the lower bound theorem, pose an optimization problem in which the goal is a minimization of the ratio between internal and external rates of dissipation. The main disadvantage of the upper bound theorem is that there is a risk of overestimating the collapse load if the failure mode is not chosen carefully.

2.1.3 Uniqueness Theorem

The uniqueness theorem simply states that if a given solution is a valid lower- and upper bound solution, then that solution will be equal to the collapse load and uniquely defined.

2.2 Yield Conditions

A *yield condition* is a mathematical model which defines the stress state at which yielding in a material is initiated, i.e. $f(\sigma) = 0$ is the yield function where σ is the generalized stress state. The yield condition is also referred to as a *yield surface* because it forms a convex surface when illustrated as function of the generalized stresses.

The concept of yield criteria plays an important role in limit state analysis employing the extremum principles. Methods based on the lower bound theorem uses the yield condition to evaluate if a chosen stress state is safe. An allowable stress state is defined as one in which no stress state lies outside the convex volume enclosed by the yield surface, i.e. $f(\sigma) \leq 0$.

Methods based on the upper bound theorem uses the yield criterion to determine the dissipation of a structure when subjected to a given strain field. Here, the plastic strains are related to the stresses by *von Mises flow rule* which states that the strain state is determined as the outward directed normal to the yield surface

$$\epsilon_i = \lambda \frac{\partial f}{\sigma_i} \tag{2.1}$$

where $\lambda \geq 0$ is the plastic multiplier. A geometrical interpretation of the strain vector ϵ is an outward directed normal to the yield surface.

The majority of yield criteria employed in practical engineering today are based on hypotheses which have been evaluated by tests.

2.2.1 Yield Criterion for Frictional Materials with Cohesion

A popular yield criterion for cohesive frictional materials such as soil, concrete and masonry, is the *modified coulomb failure criterion*. This criterion assumes that failure occurs as either a *sliding failure* or a *separation failure*. The sliding criterion was proposed by (Coulomb (1776)) and assumes that failure occurs as a combined motion parallel and away from the failure surface (Coulombs work has been described by (Heyman (1997))). Failure is initiated when the shear stress $|\tau|$ exceeds the *sliding resistance*

$$|\tau| \leq c - \mu\sigma \tag{2.2}$$

where c is the *cohesion*, μ is the *frictional coefficient* and σ is the normal stress perpendicular to the sliding plane. The friction is often defined by means of the frictional angle φ: $\tan(\varphi) = \mu$. The sliding criterion is illustrated in Fig. 2.1 and it is seen that for

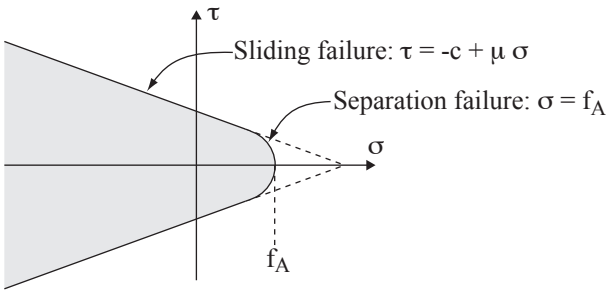

Figure 2.1: *Graphical illustration of the modified Coulomb criterion*

negative values of σ i.e. compression, increased shear strength is obtained while tensile stresses decreases the shear strength. In (Nielsen (1999)), (2.2) is rewritten as

$$k\sigma_1 - \sigma_3 \leq f_c \tag{2.3}$$

where the parameter $k = \left(\mu + \sqrt{1+\mu^2}\right)^2$ is determined from the frictional coefficient and $f_c = 2c\sqrt{k}$ is the uni-axial compression strength of the concrete. The principal stresses are sorted as $\sigma_1 \geq \sigma_2 \geq \sigma_3$. In the present work, $k = 4$ will be used which is equivalent to a frictional angle of approximately 37°.

A separation failure occurs as motion perpendicular to the failure surface and failure is initiated when the largest principal stress component, σ_1, reaches the *separation resistance*, or *separation strength*, f_A:

$$\sigma_1 \leq f_A \tag{2.4}$$

The separation strength will often be equal to the uni-axial tensile strength, f_{ct}, of the concrete. An attractive feature of the modified coulomb criterion is that the tensile capacity can be varied independently of the sliding resistance. This is useful in practical engineering applications, in which the separation strength of concrete is often assumed equal to zero.

In the principal stress space, the modified coulomb yield surface consists of six intersecting planes forming a faceted cone. Because numerical analysis including material plasticity often depends on the derivatives of the yield surface, the modified coulomb criterion has traditionally been difficult to implement. Therefore, a smoothed version of the coulomb sliding criterion is often used in such applications. The drawback of such methods is that they require smoothing parameters defined by the engineer and the choice of these parameters can greatly influence the results.

2.2.2 Yield Criterion for Reinforcent

The main purpose of reinforcement in RC structures is to compensate for the lack of tensile strength in the concrete, and reinforcement is often provided as rebars with limited bending and shear capacity. It is therefore common to consider the rebars as only being

subjected to uni-axial stresses. Applying the theory of perfect plasticity, the yield criterion for the reinforcement can be formulated as simple upper and lower limits on the axial stresses

$$-f_{Yc} \leq \sigma \leq f_{Yt} \tag{2.5}$$

where f_{Yt} and f_{Yc} are the uni-axial tensile and compression strengths.

2.3 Manual Limit State Analysis Methods

Throughout the 20th century, great effort was made by researchers to develop simple and practical analytical tools based on the extremum principles. One of the earliest methods is the *Strut-and-Tie model* (Moersch (1922)) which is based on the lower bound theorem. Here, the load is carried by compression bars (struts) and tensile bars (ties) in an interconnected network as illustrated in Fig. 2.3. The collapse load is maximized by improving the layout of the network.

The pioneering work of (Johansen (1943)), see (Johansen (1962)), introduced the yield-line method based on the upper bound theorem. Despite suffering from the potential danger of overestimating the collapse load, its intuitive work flow has made it one of the most used methods for manual limit state analysis today. The yield-line method is applicable for structures subjected to plate bending as well as disk structures subjected to plane stress states, making it a versatile tool. Fig. 2.2 shows an example of a yield line pattern for a rectangular slab simply supported along four sides and subjected to a uniform load. In this case, it is a simple problem to find the value x which gives the lowest possible collapse load.

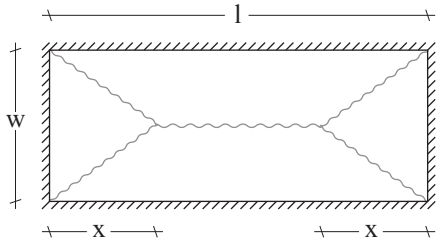

Figure 2.2: *Example of yield line pattern for a rectangular slab which is simply supported on four side.*

The *Stringer Method* (Lundgren (1949)) is based on the lower bound method and makes a coarse approximation to the stress field by discretizing the field into rectangular panels with constant shear surrounded by stringers with concentrated normal forces. This relatively crude approximation makes manual selection of the stress field easier. The stringer method is useful for structures with concentrated reinforcement which is often found in shear walls etc. Fig. 2.4 illustrates how a square wall with a hole is divided into eight shear panels with stringers placed along the edges. The *homogeneous stress field* method

approximates the stress field through a set of triangular fields in which a homogeneous stress state, comprising of normal and shear stresses, is assumed. The advantage of this method over the stringer method in its pure form is that it allows the reinforcement mesh that might be present in the structure to carry normal stresses as well as shear stresses, whereas the stringer method only uses mesh reinforcement for shear stresses. Additionally, the use of triangular fields allows for analysis of structures with more complex geometry than the stringer method which is confined to rectangular panels. The homogeneous stress fields are though not capable of utilizing concentrated reinforcement as it is by the stringer method. In (Nielsen (1999)), it is suggested to combined the above methods through superposition to exploit the benefits of both.

While the above mentioned lower bound methods are suitable for analysis of disk structures subjected to in-plane forces, (Hillerborg (1959)) suggested the strip method as a lower bound approach for structures subjected to plate bending. In this method, the plate is subdivided into orthogonal strips which carry the load as beams. Though the strip method is not as general as the yield-line method, it does provide a lower bound alternative. Regardless if the method is based on the upper bound theorem or the lower

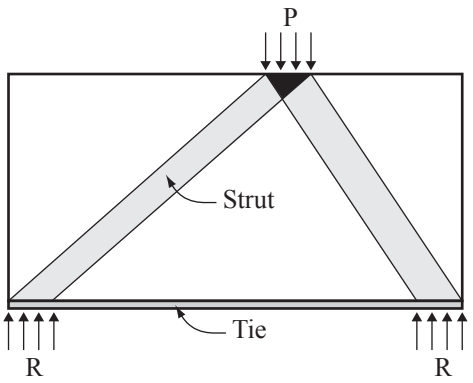

Figure 2.3: *Illustration of a Strut-and-Tie model.*

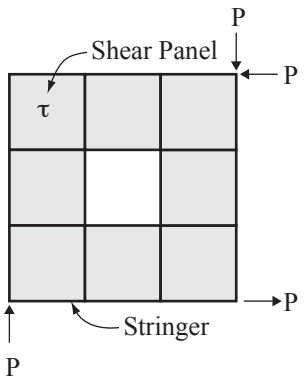

Figure 2.4: *Illustration of a Stringer model*

bound theorem, the analysis poses an optimization problem. For yield line methods, the yield line pattern which gives the minimum dissipation, and thereby the lowest upper bound solution is sought, while homogeneous stress field solutions searches for the optimal stress distribution which gives the largest possible collapse load. While these optimization problems can be addressed manually for very simple structures, the complexity increases rapidly with structural complexity. This makes numerical methods based on the extremum principles attractive for practical engineering applications. In this respect, there is one important property about these optimization problems that should be emphasized. Because the yield functions are convex, the optimization problem also becomes convex. The next section gives a brief introduction to history of numerical limit state analysis and Chapter 3.3 gives a more detailed introduction to convex optimization techniques and how they can be applied to limit state analysis.

Chapter 3

Numerical Limit State Analysis

Ever since the introduction of the modern computer in the early 1940's, extensive research have been made in the field of numerical methods for structural analysis. The exponential growth in computational power in the last decades of the 20th century made numerical tools applicable for practical engineering. While these tools have become an integral part of the structural design process, there is no commercial software readably available for limit state analysis of RC structures.

One of the most favored numerical techniques in the field of civil engineering is the *finite element method* (FEM). It's development can be traced back to (Turner et al. (1956)) and the key concepts of stiffness matrix and element assembly used today was developed in the late 1950's. While FEM originated from the need to analyze complex problems in civil and aeronautic engineering, the method has been widely adopted and is now used in fields such as product design, electromagnetism and computer animation. One of the most attractive features of FEM is its ability to handle structures with complex geometries.

FEM is used to obtain an approximate solution to problems governed by differential equations. The core concept of FEM is to discretize the structural continuum, for which an analytical solution is not readably available, into a finite number of sub-domains called *elements*. Each element thereby represents a discrete, but well defined, part of the solution. The collection of elements is referred to as the *mesh*. For structural and mechanical problems, a solution is found in form of stresses and strains or the equivalent forces and displacements. The approximate solution obtained from a discrete model can be improved by refining the mesh at the cost of computational time. The application of FEM is therefore a trade-off between accuracy and computational time.

3.1 Stiffness Based Formulation

The majority of commercial FEM software packages today employ a stiffness based approach in which the structural displacements field u is related to the stress field through the structural stiffness. Fig. 3.1 shows a simple illustration of a plane stress structure modeled using two *constant strain triangle* (CST) elements. The structural response is defined by the nodal displacement values $n^{(i)} = (u_x^i, u_y^i)$ and nodal values are shared among

adjacent elements, i.e. $n^{(2)}$ represents the displacement in the corner of both elements. Nodal displacements are coupled through the stiffness of the individual elements. Solving a linear elastic problem using the stiffness based approach is simply a matter of solving a system of linear equations on the form

$$R = KV \tag{3.1}$$

where V is a vector containing the unknown nodal values, or *degrees of freedom*, R is a vector containing the system loads and K is the quadratic system stiffness matrix which defines how nodal displacements affects one another. Because algorithms for solving problems of this type are very fast and robust on modern computers, linear FEM is the most common numerical tool used by structural engineers today.
If a non-linear material model such as the plasticity- or fracture mechanics model briefly presented in Section 1.3 is used, the problem is solved as a sequence of linear problems similar to (3.1) in which the stiffness matrix is updated between iterations to reflect the changes in material properties.

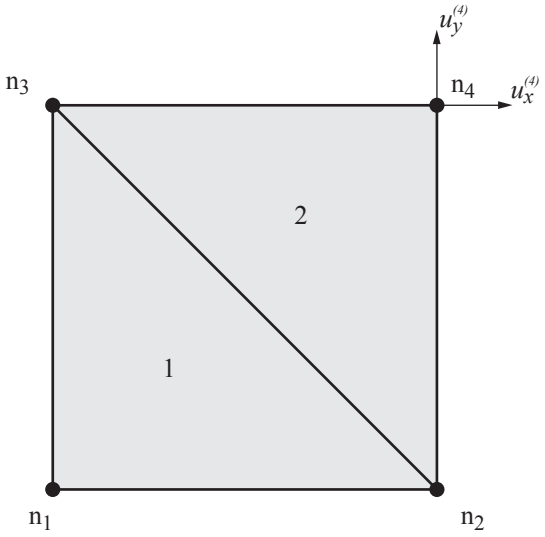

Figure 3.1: *Illustration of simple plane stress structure modelled using CST elements.*

3.2 Equilibrium Based Formulation

The stiffness based approach briefly described in the previous section is by far the most widely used method today. Alternative approaches for limit state analysis does exist though, which provides a more direct formulation of the extremum principles presented in Section 2.1. One of these approaches is the equilibrium based FEM formulation which is based on the lower bound theorem.

Rather than approximating the structural displacement field, equilibrium based FEM methods approximates the structural stress field. Fig. 3.5 illustrates a simple plane stress structure which is modeled using two linear stress triangle elements. The stress state in

element i is defined by the nodal stress values $(\sigma_1^{(i)}, \sigma_2^{(i)}, \sigma_3^{(i)})$. It should be noted here, that the nodal values are unique to each element and not shared between adjacent elements as is the case for stiffness based methods. Equilibrium between elements is ensured by statically admissible traction equilibrium as illustrated in the figure. In the case of the linear stress element, a statically admissible stress field is ensured through equilibrium at two points along each edge. For higher order elements, additional equilibrium nodes must be used along the edges. Furthermore, a set of internal element equilibrium equations must be satisfied in order to obtain a statically admissible solution. These equilibrium equations must be fulfilled at a sufficient number of points within the element, which once again depends on the chosen stress field. For the linear stress triangle, the equilibrium is ensured by fulfilling the equilibrium equations at one point as indicated in the figure. This can be written in matrix form as

$$H\ \Psi = R \tag{3.2}$$

where Ψ is a vector containing all the nodal stress values and R is the system load vector. The matrix H is called the system equilibrium matrix and contains all equilibrium equations. For statically indeterminate structures, the number of nodal stress variables

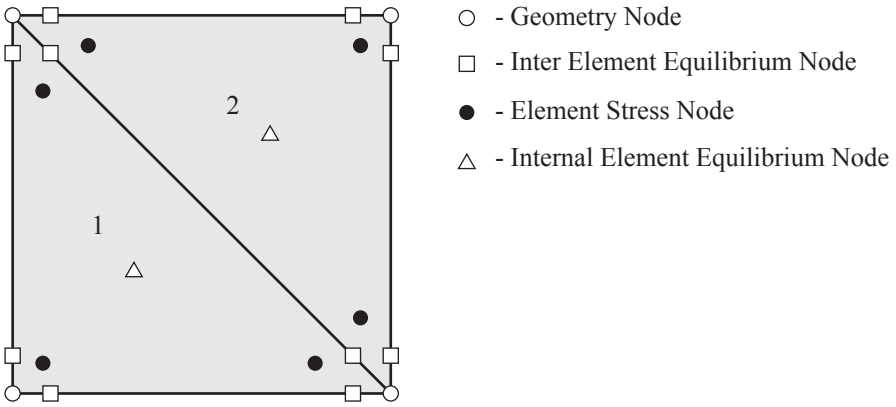

Figure 3.2: *Illustration of simple plane stress structure modeled using equilibrium based linear stress triangles.*

becomes greater than the number of equations in H, i.e. $\Psi \in \Re^n$ then $H \in \Re^{m \times n}$ where $n > m$. Because multiple solutions exists which satisfies the condition (3.2), anyone of these will provide a statically admissible stress field as required by the lower bound theorem. To obtain a lower bound solution though, the chosen stress field must also be safe, i.e. it must obey the yield criterion at all points within the field. In addition to (3.2) a set of constraints must be applied to the chosen stress state such that

$$f(\Psi) \leq 0 \tag{3.3}$$

where the inequality constraint function f is the yield criterion. The above inequality will define the boundaries on the feasible region from which a solution can be chosen. Because yield criteria are convex functions, the feasible region will be convex as well.

While (3.2) and (3.3) provides a convex set from which a valid lower bound solution can be chosen, it is often desirable to find the best possible solution with respect to a given objective. This could be the solution which yields the highest possible collapse load or to determine a minimum amount of reinforcement required to carry a given load. This thesis focusses on load optimization, but the subject of material optimization have been treated in (Prager (1962); Poulsen and Damkilde (2000))

While the equilibrium formulation described above is an interpretation of the lower bound theorem, a similar approach can be made in terms of the upper bound theorem. Here, a kinematically admissible velocity field is ensured by application of the flow rule and a given set of velocity boundary constraints. The objective for such problems is to minimize the power dissipated by plastic deformations in the structure. The upper bound approach have been described in further detail by (Bottero et al. (1980); Sloan (1989); Makrodimopoulos and Martin (2007)).

Whether an upper- or lower bound approach is used or if the objective is load- or material optimization, finite element limit state analysis poses a convex optimization problem. In the following sections a presentation of some numerical optimization techniques are given with focus on how these can be applied to solve the limit state problems presented here.

3.3 Application of Convex Optimization

As described in section 3.2, limit state analysis based on the extremum principles poses a convex optimization problem. Here, a brief overview of numerical techniques for solving convex optimization problems is given with emphasis methods readably applicable to limit state analysis of RC structures.

The mathematics of convex optimization have been studied for about a century and the first numerical methods for solving some of these problems were developed around the time of the first electronic computers in the mid 20th century. The increased efficiency of numerical algorithms over the last decades combined with the rapid increase in the computational power of computers have lead to the discovery of many new fields of application including electronic circuit design, automatic control systems and finance.

According to (Boyd and Vandenberghe (2004)), the *standard form* of an optimization problem is

$$\begin{array}{ll} \text{minimize} & f_0(x) \\ \text{subject to} & f_i(x) \leq 0, \quad i = 1, \cdots, m \\ & h_i(x) = 0, \quad i = 1, \cdots, p \end{array} \tag{3.4}$$

Here, x is a vector containing the *decision variables* and $f_0(x)$ is the *objective function* which is sought minimized, while $f_i(x)$ and $h_i(x)$ are the *inequality* and *equality constraint functions* respectively. The constraint functions defines the boundaries of the feasible region, or domain, of the optimization problem and any solution x located within this

domain is a *feasible* solution.

Convex optimization problems are a subset of the standard optimization problem given in (3.4). This subset must fulfil three additional requirements, (Boyd and Vandenberghe (2004)):

- the objective function must be convex
- the inequality constraints, $f_i(x)$, must be convex
- the equality constraints must be linear

Several types of convex optimization problems have been defined, and the following section briefly introduces those most relevant for limit state analysis problems: LP, SOCP and SDP. For a more in-depth introduction to convex optimization, the reader is referred to (Boyd and Vandenberghe (2004))[1].

3.3.1 Linear Programming

While the problem of solving a system of linear inequalities can be dated back to Fourier in the late 18th century, Linear Programming (LP) as a mathematical model was developed in 1940's. A general LP problem can be written as the minimization of a linear objective function subjected to linear equality and inequality constrains:

$$\begin{array}{ll} \text{minimize} & c^T x \\ \text{subject to} & Gx \leq h \\ & Ax = b \end{array} \tag{3.5}$$

Here, the problem data is defined by the vectors c, h, b and the matrices G and A. The domain of an LP problem is bounded by a n-dimensional polytope where n is the number of decision variables, i.e. $x \in \Re^n$. The polytope is defined through a set of hyperplanes, and the intersections between hyperplanes are called *edges*. A point where two or more edges intersect is called a *vertex*. A vertex defines a feasible solution x' which has the potential to be an optimal solution.

A very popular method for solving LP problems is the *simplex method* developed by (Dantzig (1963)). The basic principles of the simplex method is quite simple in that a starting vertex, i, is chosen and the objective function value, $f^i(x)$, determined at that vertex. Vertices are then traversed along edges with decreasing function values, i.e. $f^{i+1}(x) \leq f^i(x)$. If none of the edges associated with a vertex fulfils this requirement, a local, and thereby also a global, solution is found. While the simplex method has proved efficient for practical applications, it's solution time is greatly impacted by the problem size and the chosen start vertex. (Klee and Minty (1972)) presented an example in which the simplex algorithm proposed by Dantzig had to visit all vertices before finding the

[1] At the time of writing, Stanford University provided some excellent video lectures on convex optimization which could be found at http://www.stanford.edu/class/ee364a/

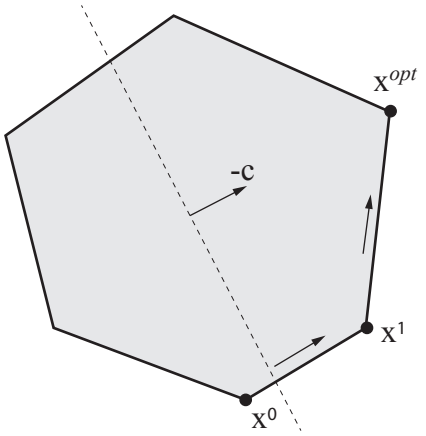

Figure 3.3: *Illustration of an LP problem solved by the simplex method.*

optimal solution, showing that the worst-case complexity of the algorithm is exponential-time i.e. $2^{O(n)}$ complexity. This makes the simplex algorithm less suitable for the large-scale problems often found in limit state analysis. In 1984, (Karmarkar (1984)) presented the *interior-point method* which is able to solve LP problems in polynomial-time i.e. $2^{O(log\ n)}$ complexity. Where the simplex method traverses the problem domain boundary in search of an optimal solution, the interior-point method traverses the interior region. The interior-point method solves the optimization problem by reducing it to a sequence of linear equality constrained problems which converges to the optimal solution. This is illustrated in Fig. 3.4. Linear programming was one of the first methods to be used for

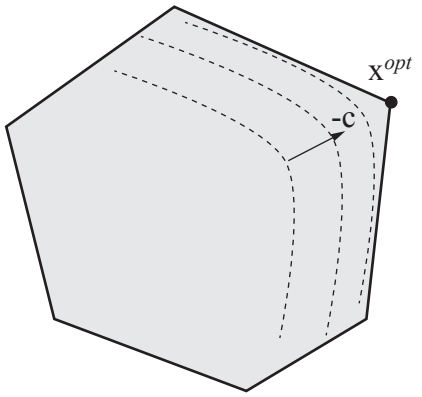

Figure 3.4: *Illustration of an LP problem solved by the interior-point method.*

numerical lower bound limit analysis, (Prager (1962); Maier (1969); Grierson and Gladwell (1971); Anderheggen and Knopfel (1972)). Because only linear inequality constraints are allowed, the non-linear yield criteria such as the conic constraints for RC disks and plates, had to be linearized to fit the format of an LP problem. A common yield criterion for RC

disks is the conic constraints presented by (Nielsen (1969)):

$$-(f_{tx} - \sigma_x)(f_{ty} - \sigma_y) + \tau^2 \leq 0 \tag{3.6}$$

$$-(f_c + \sigma_x)(f_c + \sigma_y) + \tau^2 \leq 0 \tag{3.7}$$

where σ_x, σ_y and τ are the normal- and shear stresses respectively, f_c is the uni-axial compression strength of the disk disregarding compression in the reinforcement and f_{tx} and f_{ty} are the tensile strengths in the x- and y-direction respectively. In (Poulsen and Damkilde (2000)), this criterion is linearized from the top of the cones to points on the elliptic intersection between the cones as illustrated in Fig. 3.5. While the linearization

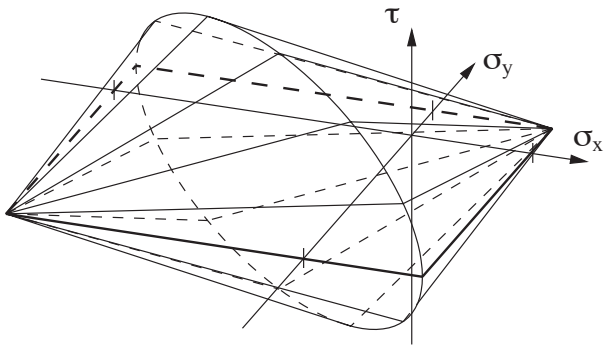

Figure 3.5: *Linearisation of the conic yield surface for RC disks. Illustration from (Poulsen and Damkilde (2000))*

provides an approximation to the yield surface, the obtained solutions will be safe due to the convexity of the yield surface. In (Olsen (1998)) a study of the error caused by linearisation is presented and here it is concluded that 16 hyperplanes provides reasonable accuracy.

3.3.2 Second-Order Cone Programming

In 1988, (Nesterov and Nemirovskii (1988)) showed that the interior-point method could be extended to handle not only LP problems, but also problems with convex constraints, see (Nesterov and Nemirovskii (1994)). It was furthermore shown, that these problems could be solved as efficiently as LP problems. This discovery gave rise to a range of new algorithms, among these the *second-order cone programming* (SOCP). In SOCP the constraint function is defined by a set of convex cones:

$$\|A_i x + b_i\|_2 \leq (c_i x + d_i)\,; \qquad i = 1, \cdots, m \tag{3.8}$$

where the matrix A_i, the vectors b_i and c_i, and the scalar d_i are problem data. $\|x\|_2$ defines the 2-norm, or Euclidean norm, which is given by $\|x\|_2 = \sqrt{\sum x_i^2}$. Two of the most common second-order constraint types are the Quadratic Cone (QC)

$$x_1 \geq \sqrt{\sum_{j=2}^{k} x_j^2} \tag{3.9}$$

and the Rotated Quadratic Cone (RQC)

$$2x_1x_2 \geq \sum_{j=3}^{k} x_j^2 \quad ; \quad x_1, x_2 \geq 0 \tag{3.10}$$

SOCP has proved very useful in the field of limit state analysis of RC structures, because the well established yield criteria for slabs (Nielsen (1963)) and disks (Nielsen (1969)) are formulated in conic form.

In recent years, SOCP has become a favored method for both upper- and lower bound limit analysis. It has been applied to the *von Mises criterion* by (Bisbos et al. (2005)) and to 2D cohesive frictional materials were modeled using the Coulomb criterion by (Makrodimopoulos and Martin (2006)). Formulation of the conic disk constraints shown in the previous section as an RQC constraint is straight forward. Considering the conic tensile constraint shown in (3.6), this can be cast as a RQC constraint by rearranging the terms as:

$$\tau^2 \leq (f_{tx} - \sigma_x)(f_{ty} - \sigma_y) \tag{3.11}$$

and introducing the auxiliary variables α_1 and α_2

$$\alpha_1 = \frac{1}{\sqrt{2}}(f_{tx} - \sigma_x) \tag{3.12}$$

$$\alpha_2 = \frac{1}{\sqrt{2}}(f_{ty} - \sigma_y) \tag{3.13}$$

Substituting back into (3.11) the following inequality is obtained

$$\tau^2 \leq 2\alpha_1\alpha_2 \quad ; \quad \alpha_1, \alpha_2 \geq 0 \tag{3.14}$$

which fits the format of an RQC constraint, (3.10). The condition $\alpha_1, \alpha_2 \geq 0$ ensures that the uni-axial tensile stresses cannot exceed the tensile strength of the disk. Similar can be done for the compression criterion which leads to a total of two RQC constraints and four additional auxiliary variables are needed to cast the conic disk constraint as an SOCP problem.

3.3.3 Semidefinite Programming

One of the latest addition to the interior-point family is *Semidefinite Programming (SDP)*. While SOCP is a generalization of LP, SDP is a generalization of both LP and SOCP. Any SOCP or LP problem can therefore be written and solved as an SDP problem. In SDP, the constraint function is defined by a set of *linear matrix inequalities* (*LMI's*), see (Vandenberghe and Boyd (1996)):

$$F(x) = F_0 + x_1F_1 + \cdots + x_nF_n \succeq 0 \tag{3.15}$$

where F_i are symmetric $k \times k$ matrices and $F(x)$ is a positive semidefinite matrix. Positive semidefinite matrices are characterized by all eigenvalues being greater than or equal to

zero, i.e. $s^T F(x)s \geq 0$ for all vectors s.
For instance, LMI constraints can be used to constrain the principle stresses in a structure since these are the eigenvalues of the stress tensor. The LMI constraint below confines the principle stresses in a volumetric body to positive values.

$$\begin{bmatrix} \sigma_x & \tau_{xy} & \tau_{xz} \\ \tau_{xy} & \sigma_y & \tau_{yz} \\ \tau_{xz} & \tau_{yz} & \sigma_z \end{bmatrix} = \sigma_x \begin{bmatrix} 1 & 0 & 0 \\ 0 & 0 & 0 \\ 0 & 0 & 0 \end{bmatrix} + \cdots + \tau_{xy} \begin{bmatrix} 0 & 1 & 0 \\ 1 & 0 & 0 \\ 0 & 0 & 0 \end{bmatrix} + \cdots \succeq 0 \tag{3.16}$$

The application of SDP in limit state analysis of RC structures became apparent when it was shown by (Bisbos and Pardalos (2007); Krabbenhøft et al. (2008)) that the Coulomb yield criteria could be formulated as LMI constraints. In Section 4.2.2 it is shown how the modified Coulomb criterion can be derived as a combination of LMI constraints and linear inequality constraints.

Chapter 4

Solid Structures

Only few attempts have been made to develop techniques for manual limit state analysis of RC structures subjected to tri-axial stress states. In (Andreasen (1989)), formulas were developed to determine the required reinforcement at a single point within a solid RC structure when the stress state was known. The formulas were reduced to a relatively simple flow diagram which could be used to determine the reinforcement design with relative ease. While these formulas enabled engineers to design reinforcement layouts in solid structures, they depend on stress states computed from linear elastic analysis methods. Therefore, it was not possible to treat the structure as a whole, and thereby exploiting the possibilities of stress redistribution. (Foster et al. (2003)) uses Mohr's circle to derive design formulas, but relies on graph look-up and the method is therefore not suitable for numerical implementations. In (Hoogenboom (2008)), an approach similar to (Andreasen (1989)) was made, though with the aim of numerical implementation rather than manual analysis. Because the method is intended as a post-processor to linear elastic calculation, it suffers from the same limitation with respect to redistribution of stresses as the earlier work.

In this chapter, a solid equilibrium element is presented. The element enables engineers to model and analyze full 3D RC structures with complex reinforcement layouts. Because the method relies on a statically admissible stress field rather than stresses obtained from linear elastic analysis, redistribution of stresses is possible.

4.1 Linear Tetrahedral Element

The volumetric stress field of the solid RC structure is approximated by 4-node tetrahedral elements with linear stress distribution as illustrated in Fig. 4.1. The geometric shape of these elements provide great flexibility when it comes to modeling of complex geometries, while the linear stress variation allows for a rigorous lower bound solution if the yield criteria are imposed at the nodes.

First, we define the stress state at a point within the solid structure by the symmetric

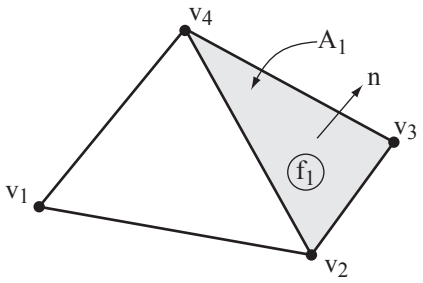

Figure 4.1: *4-node tetrahedral element with linear stress distribution.*

stress tensor σ:

$$\sigma = \begin{bmatrix} \sigma_x & \tau_{xy} & \tau_{xz} \\ \tau_{yx} & \sigma_y & \tau_{yz} \\ \tau_{zx} & \tau_{zy} & \sigma_z \end{bmatrix} \tag{4.1}$$

which can be written on vector form by its six unique components as

$$\beta = [\sigma_x, \sigma_y, \sigma_z, \tau_{xy}, \tau_{xz}, \tau_{yz}]^T \tag{4.2}$$

The stress state at a given point within the element can be determined from linear interpolation of the nodal stress values. This is easiest done in volume coordinates, ζ_i:

$$\beta(\zeta_i) = [I\zeta_1 \; I\zeta_2 \; I\zeta_3 \; I\zeta_4] \begin{bmatrix} \beta^1 \\ \beta^2 \\ \beta^3 \\ \beta^4 \end{bmatrix} \tag{4.3}$$

where β^i is the stress state at node i and I is a $[6 \times 6]$ identity matrix. The element stress field is then defined by the vector $B = [\beta^1 \; \beta^2 \; \beta^3 \; \beta^4]^T$ which contains 24 stress parameters. The complete structural stress field can be defined through the system stress vector $\Psi = [B^1, B^2, \cdots, B^m]^T$ for all elements $1, 2, \cdots, m$ in the system.

The surface tractions at a point on the element boundary surface can be determined from transformation of the stress state at that point. If we consider a point p on face f_1, i.e. $\zeta_1 = 0$, as illustrated in Fig. 4.1, the surface tractions in global coordinates can be computed from the stress state at that point and the outward face normal $n_\sigma = [n_x, n_y, n_z]$ as

$$t = P \; \beta(\zeta_i) \tag{4.4}$$

where $t = [t_x, t_y, t_z]^T$ are the tractions and P is the stress transformation matrix

$$P = \begin{bmatrix} n_x & 0 & 0 & n_y & n_z & 0 \\ 0 & n_y & 0 & n_x & 0 & n_z \\ 0 & 0 & n_z & 0 & n_x & n_y \end{bmatrix} \tag{4.5}$$

Sometimes, it is convenient to define the surface tractions as normal and shear stresses in a local face coordinate system $S = [n_\sigma, n_{\tau\xi}, n_{\tau\zeta}]$. Here, n_σ is the surface normal and $n_{\tau\xi}, n_{\tau\zeta}$ are unit vectors defining the shear directions. The local tractions can be determined from

$$s = S^T P \beta \tag{4.6}$$

where $s = [\sigma_n, \tau_\xi, \tau_\zeta]$ are the normal and shear stresses acting on the plane.

4.1.1 Element Equilbrium

To ensure internal element equilibrium, the following equilibrium equation must be fulfilled

$$\sigma_{ji,j} + \lambda f_i + f_i^0 = 0 \tag{4.7}$$

where $\sigma_{ji,j}$ is the partial derivative of the stress tensor component ji with respect to j with application of the summation convention for i and j. f_i^0 and f_i are the proportional and constant volume loads respectively. Because the stress state varies linearly over the element, the partial derivatives becomes constant and it is sufficient to fulfill these at one point within the element.

The equilibrium equation can be written on matrix form as

$$H_{eq}\Psi + \lambda R_f + R_f^0 = 0 \tag{4.8}$$

where the vectors R_f and R_f^0 contains the volume loads for all elements. The system equilibrium matrix H_{eq} is a block diagonal matrix

$$H_{eq} = \begin{bmatrix} \hat{\sigma}_{ij,j}^{(1)} & & & \\ & \hat{\sigma}_{ij,j}^{(2)} & & \\ & & \ddots & \\ & & & \hat{\sigma}_{ij,j}^{(m)} \end{bmatrix}$$

where $\hat{\sigma}_{ij,j}^{(i)}$ is a 3×24 matrix containing the partial derivatives of the stress tensor at the geometric center point of element i. The system equilibrium matrix contains $3 \cdot m$ rows and $24 \cdot m$ columns.

4.1.2 Inter-Element Equilbrium

In addition to the internal equilibrium equations defined in the previous section, inter-element equilibrium must also be ensured in order to obtain a statically admissible stress field. This is achieved by requiring traction equilibrium along shared element faces. Fig. 4.2 illustrates two adjacent elements sharing the face defined by nodes $2, 3, 5$ with surface normal n. If we consider the point p on the shared face, the inter-element equilibrium equation can be written as

$$t^{p1} + t^{p2} = \lambda t_i + t_i^0 \tag{4.9}$$

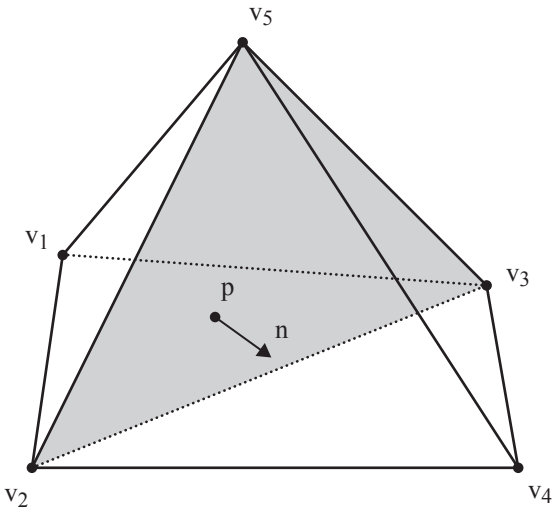

Figure 4.2: *Traction continuity along shared element boundaries.*

where t^{p1} and t^{p2} are the global surface tractions found from (4.4) at p on element 1 and 2 respectively. t_i^0 and t_i are the constant and proportional surface tractions applied to the surface. Since the stress state varies linearly over the boundary face, it is sufficient to ensure equilibrium at the three corner nodes, which leads to a total of 9 equilibrium equations per boundary face. It should be noted that the structural stress field can be discontinuous as long as inter-element traction equilibrium is ensured.

The inter-element equilibrium matrix, H_{cont}, is a $[9 \cdot f \times 24 \cdot m]$ matrix, where f is the number of boundary faces and m is the number of elements in the model:

$$H_{cont} = \begin{array}{c} \begin{matrix} B_i & \cdots & B_j \end{matrix} \\ \left[\begin{matrix} N_{ik} & \cdots & N_{jk} \end{matrix}\right] \end{array} \leftarrow k \tag{4.10}$$

Here, N_{ik} defines the contribution from element i to system face k and N_{jk} the contribution from element j to the face k. N is a $[9 \times 24]$ matrix in which each row defines a traction component on the surface. It should be noted, that a maximum of two elements can contribute to the tractions of a given face and on free boundaries, only one element contributes to the surface tractions.

If one or more traction components are supported at a point on the boundary, the associated equations are removed from the system, allowing the stresses to vary freely within the yield constraints. The resulting reactions will ensure equilibrium.

4.2 Solid Material Model

Modeling of solid RC structures often requires great attention to details because of its complex reinforcement layout. Therefore, it is important to carefully consider how the interaction between rebars and concrete should be handled. An obvious approach is to create a full 3D model in which the rebars are modeled geometrically accurate and tri-axial stresses are accounted for in both reinforcement and concrete. While highly detailed results could be obtained using this approach, the large number of elements required will impact the computational time considerably and the level of detail would increase the amount of time taken to model a structure. Additionally, attention should be paid to how stresses are transferred from the rebars to the concrete. Often, this transfer is thought of as a shear connection in which shear stresses are transferred at the interface between rebars and concrete. While some shear might be transferred due to adhesion, the primary mechanism is compression between the ribs of the rebar and the concrete. If a full solid model is employed, these ribs should be included, which would significantly increase the number of elements required.

Another approach is to consider the reinforcement as smeared over an area of the concrete. Here, full bonding between concrete and rebars is assumed and the complex interface is neglected. Additionally, the reinforcement is considered subjected to uni-axial stresses only which further simplifies the numerical model due to the simpler material constraints and fewer stress parameters.

The smeared approach has been chosen in the current work, and the remaining of this chapter will focus on implementation of this model.

4.2.1 Stress Decomposition

Here, we consider a volumetric infinitesimal at a point within the element with reinforcement in directions equivalent to the usual Cartesian coordinate system as illustrated in Fig. 4.3. The stress state is assumed constant within the infinitesimal volume and the stress state at domain boundary is given by $\lambda\sigma$ where σ is the stress tensor and λ is the load factor.
In the smeared approach, the stress state at a point within the solid structure can be described as the sum of concrete and reinforcement stresses:

$$\sigma = \sigma_c + A_s\sigma_s \tag{4.11}$$

where

$$\sigma_c = \begin{bmatrix} \sigma_{cx} & \tau_{cxy} & \tau_{cxz} \\ \tau_{cxy} & \sigma_{cy} & \tau_{cyz} \\ \tau_{cxz} & \tau_{cyz} & \sigma_{cz} \end{bmatrix} \tag{4.12}$$

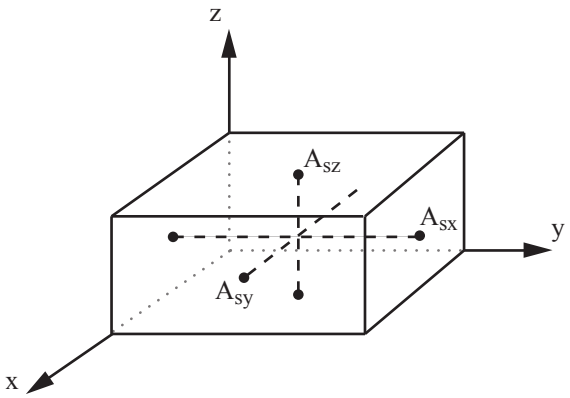

Figure 4.3: *Smeared material model for solid structures.*

is the concrete stress tensor. Because it is assumed that the reinforcement only carries uni-axial stresses, the reinforcement stress tensor only contains normal stresses:

$$\sigma_s = \begin{bmatrix} \sigma_{sx} & 0 & 0 \\ 0 & \sigma_{sy} & 0 \\ 0 & 0 & \sigma_{sz} \end{bmatrix} \tag{4.13}$$

The matrix A_s contains the reinforcement area per unit area perpendicular to the local element axes:

$$A_s = \begin{bmatrix} A_{sx} & 0 & 0 \\ 0 & A_{sy} & 0 \\ 0 & 0 & A_{sz} \end{bmatrix} \tag{4.14}$$

Since stresses are now defined separately for concrete and reinforcement, the need for a combined failure criterion is replaced by the need for a concrete criterion and a reinforcement criterion. These are fortunately readably available for both materials. Here, the modified Coulomb criterion briefly introduced in Section 2.2.1, is applied to the concrete stresses while simple upper and lower limits are applied to the reinforcement stresses:

$$-f_{Yc} \leq \sigma_s \leq f_{Yt} \tag{4.15}$$

While the upper and lower limits shown above fit directly into the framework of a convex optimization problem, the modified Coulomb criterion must be cast as LMI constraints. This formulation will be described in greater detail in the next section.

4.2.2 SDP formulation of the modified Coulomb criterion

It has recently been discovered that Semidefinite Programming (SDP) could be used to perform limit state analysis of solid structures of cohesive frictional materials. In (Bisbos

and Pardalos (2007); Krabbenhøft et al. (2008); Martin and Makrodimopoulos (2008)) it was shown how the Mohr-Coulomb criterion could be cast as a set of LMI constraints. In this section, the coulomb sliding criterion is formulated as a combination of LMI constraints and linear inequalities based on the concrete parameters f_c and k. Additionally, the separation criterion is formulated based on the concrete separation strength, f_A.

First, we consider the sliding criterion shown in (2.3) and repeated below

$$k\sigma_{c1} - \sigma_{c3} \leq f_c$$

The above condition still holds true if we rearrange the terms and introduce an auxiliary variable α_1 such that

$$-\frac{\sigma_{c3}}{k} \leq \alpha_1 \leq -\sigma_{c1} + \frac{f_c}{k}$$

This double sided inequality can now be separated into two inequalities as:

$$\sigma_{c3} + (k\alpha_1) \geq 0$$
$$-\sigma_{c1} + \left(\frac{f_c}{k} - \alpha_1\right) \geq 0$$

The left-hand side of the above inequalities simply represents the shifted eigenvalues of the stress tensor. They can therefore be transformed into matrix inequalities by replacing principal stress components σ_{c1} and σ_{c3} with the concrete stress tensor σ_c and multiplying the scalar terms (bounded by parenthesis) with the identity matrix I:

$$\sigma_c + (k\alpha_1)\, I \succeq 0 \tag{4.16}$$
$$-\sigma_c + \left(\frac{f_c}{k} - \alpha_1\right) I \succeq 0 \tag{4.17}$$

It is seen that the inequalities above matches the LMI definition given in (3.15).
The separation criterion shown in (2.4) can be cast as an LMI constraint with relatively ease by first rearranging the terms as:

$$-\sigma_{c1} + f_A \geq 0 \tag{4.18}$$

Similar to (4.16) and (4.17), the first principal stress component σ_{c1} is replaced by the concrete stress tensor and the separation strength is multiplied by the identity matrix

$$-\sigma_c + f_A I \succeq 0 \tag{4.19}$$

The modified Coulomb criterion can be formulated as three LMI constraint: (4.16), (4.17) and (4.19). The model can though be improved by expressing (4.17) and (4.19) in terms of another auxiliary variable α_2:

$$\begin{aligned} \sigma_c + (k\alpha_1)\, I &\succeq 0 \\ \sigma_c \;-\; \alpha_2\, I \;&\preceq 0 \\ \alpha_2 &\leq f_A \\ \alpha_2 &\leq \frac{f_c}{k} - \alpha_1 \end{aligned} \tag{4.20}$$

The complete criterion is then defined by two LMI's and two linear inequalities:

4.3 Example: Console Beam

This example illustrates how the solid elements presented in this chapter can be used to model and analyze an actual problem. The problem concerns the console beam shown in Fig. 4.4. The safety of the console was questioned when cracks was observed propagating from the tip of the console and manual upper and lower bound limit analysis based on plane stress theory was conducted to assess the safety of the structure. The results are presented in (Feddersen (1994)) in which the upper and lower bound collapse loads are determined to $113kN$ and $106kN$ respectively.

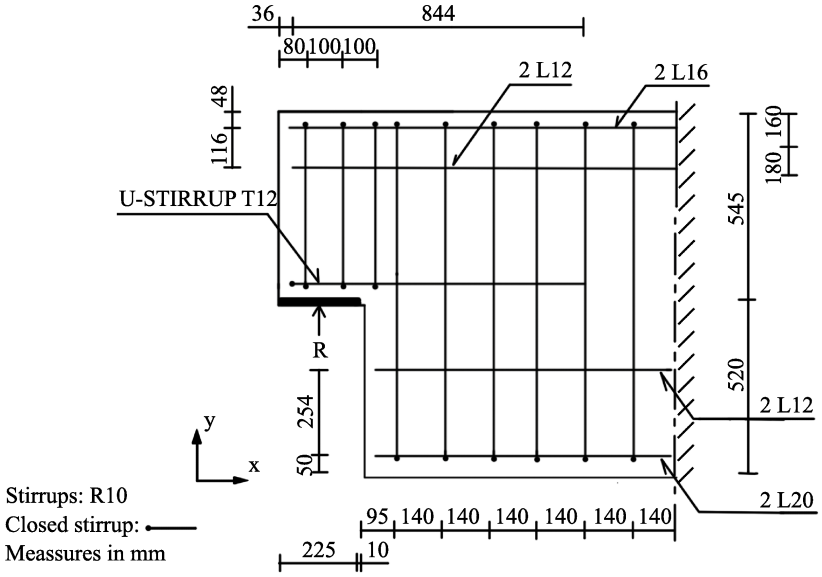

Figure 4.4: *Console beam with complex reinforcement.*

A solid model of the console beam is created and meshed using the Abaqus CAE software package. The rebars are smoothed over an area of $50mm \times 50mm$ as illustrated in Fig. 4.5. Symmetry around the center xy-plane is exploited and only one half of the console is modeled as illustrated in the figure. The model is supported in the x- and y-direction at the interface towards the remaining of the beam as illustrated in Fig. 4.4, and a support in the z-direction is added to the symmetry plane. The load is applied as a uniform pressure at the bottom of the console.

The uni-axial compression strength of the concrete is $f_c = 8.3MPa$ while the uni-axial tensile strength of the L- and T-bars is $f_{Yt} = 400MPa$. The tensile strength of the stirrups is $f_{Yt} = 171MPa$. The compression strength, f_{Yc}, of all rebars are set equal to zero as is the separation strength, f_A, of the concrete. As seen from Fig. 4.4 and Fig. 4.5, several of the longitudinal rebars are not anchored at the end of the console beam. Setting the separation strength to zero in such cases could cause problems since some tensile capacity is required to transfer the shear stresses from the rebar to the concrete. In the current problem, the stirrups provide sufficient tensile strength to anchor the rebars in the concrete. The model is analyzed using both a coarse mesh of 5501 elements and

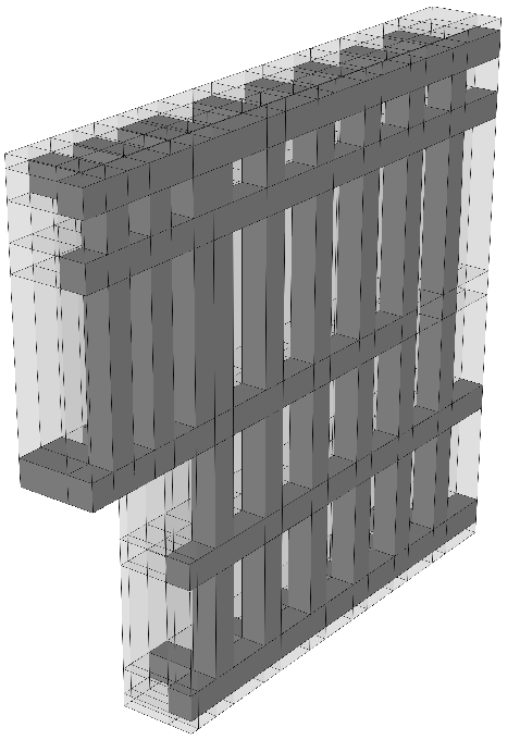

Figure 4.5: *Geometric model of console beam.*

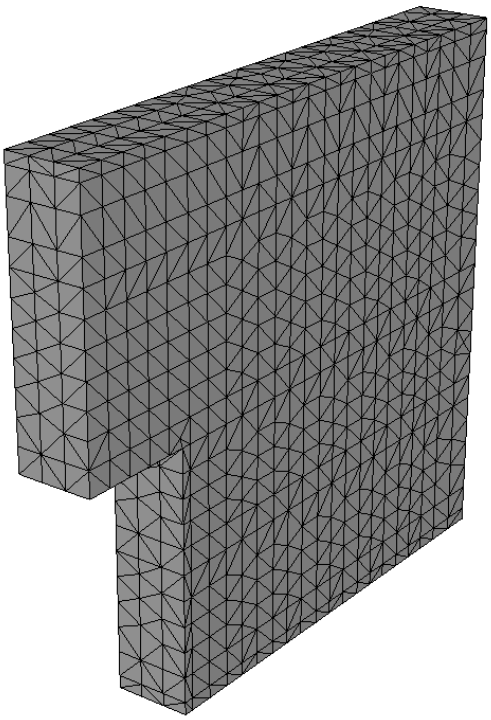

Figure 4.6: *Meshed model of the console beam using 13480 elements.*

a fine mesh of 13480 elements (shown in Fig. 4.6). Using the coarse mesh, a collapse load of $113kN$ was found which is identical to the upper bound solution determined by (Feddersen (1994)). Using the fine mesh, a collapse load of $128kN$ is found. This is not only higher than the result obtained from the coarse mesh, but also higher than the upper bound found by Feddersen. This is attainable because the upper bound solution is based on plane stress theory, while the numerical model includes the full tri-axial stress state in the concrete.

Fig. 4.7 shows a vector illustration of the third principal stress component, σ_3, where the vector length illustrates the stress intensity and the orientation of the principal direction. The image is an "x-ray" type in which stresses are visible through the volume of the model. σ_3 is interesting in this example because it can unveil areas which are prone to crack formation due to high (close to zero) values of σ_3. As seen from the figure, a band runs from just below the console towards the top of the beam in which σ_3 is close to zero and thereby prone to crack formation. It should be emphasized that it is not possible to tell whether or not a crack will exist here, just that it is a possibility.

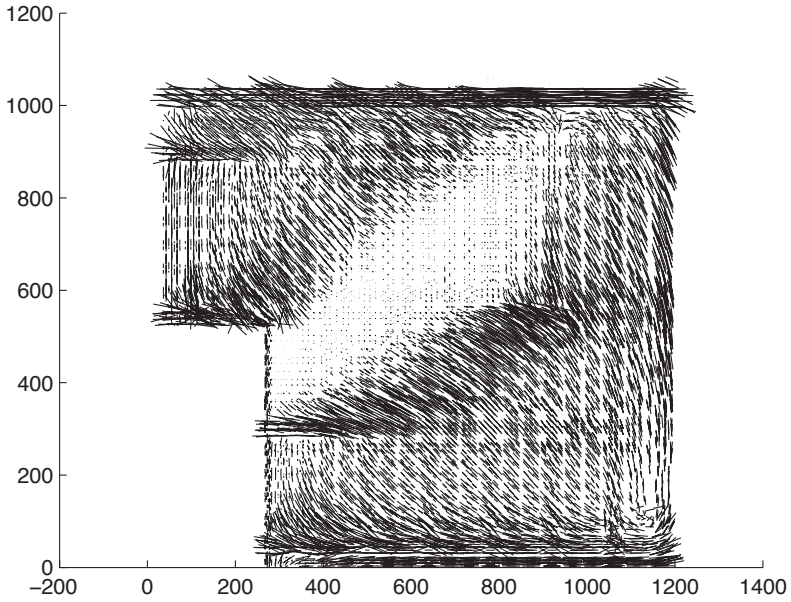

Figure 4.7: *Plot of the third principal stress component. Vectors are used for indicating the direction and magnitude of the stresses.*

Chapter 5

3D Frame Structures

Limit state analysis of RC beams subjected to a combination of cross sectional forces often relies on section force based yield criteria. The disadvantage of this approach is that construction of such yield criteria can become very difficult if the beam is subjected to loadings in 3 dimensions. A commonly used yield criterion for beams subjected to in-plane loadings is an M-N diagram, which is used to assess the safety of beams subjected to a combination of a normal force and a bending moment. If, in addition, the beam is subjected to shear, linear connections are made from the M-N curve and to the point defining the pure shear capacity. Because of the convexity of the yield surface, this provides a safe estimate of the bounding yield surface. If the beam is subjected to a more complex combination of section forces such as bi-axial bending, torsion etc., the yield criterion becomes very difficult to define manually.

In (Damkilde and Hoyer (1993)), a plane beam element was presented for which a linearized M-N curve should be provided. While this enabled engineers to analyze complex frame structures, it did not solve the problem of constructing the yield surface. In (Damkilde and Krenk (1997)) a 3D beam element is mentioned, but the actual implementation of the yield criterion is not described. For practical application of both 2D and 3D beam elements, it is vital that the yield criterion is an integral part of the element formulation, such that engineers only need to specify the cross section properties of the beam. In (Niebling et al. (2007)), this was achieved by creating a discrete representation of the internal stress state in the beam through a finite number of *zones*. The zones can be thought of as lower level elements in which the stress field is known. A stress based yield criterion can then be utilized in these lower level elements, thereby circumventing the need for a section force based yield criterion. The zone discretization must be defined by the engineer based on the cross section of the beam. The element presented in (Niebling et al. (2007)) used rectangular zones and was constrained to a 3×3 zone model as illustrated in Fig. 5.1. The reinforcement was assumed smeared over the zones and the approximated conic yield criterion for reinforced concrete disks, (Nielsen (1969)), was applied in each zone. While this model showed some excellent results, it is restricted to rectangular beam sections with a relatively simple reinforcement layout. Furthermore, the use of a plane stress yield criterion has proven inadequate for the tri-axial stress state which can exist in the cross section. This issue will be treated more in depth in Section 5.2.1.

The aim of the current work is to develop an element capable of modeling beams with

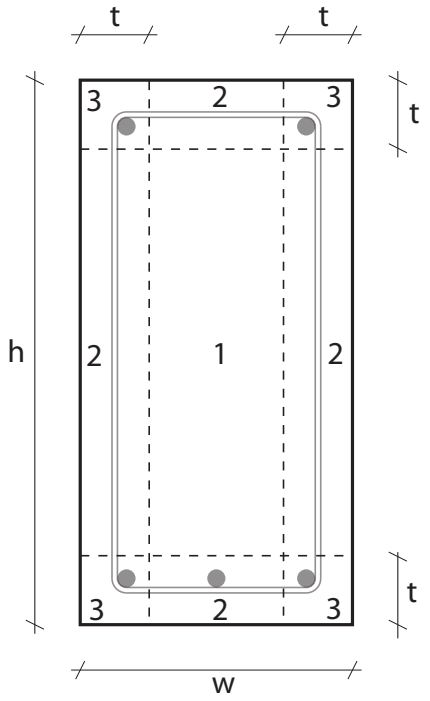

Figure 5.1: 3×3 *beam zone model presented in (Niebling et al. (2007))*

complex cross sections subjected to loadings in 3 dimensions. This requires a flexible zone model in which the zones are not predefined as well as a general yield criterion which can handle the tri-axial stress states.

5.1 Element Model

The 3D beam element is intended to be part of a full 3D structural model in which it interacts with other structural elements such as walls and floor slabs. In Chapter 6, a 3D shell element is presented which is capable of modeling both disks subjected to in-plane forces as well as elements subjected to plate bending. The shell element can carry a constant surface load perpendicular to the element plane which leads to a second order variation of the bending moments and the in-plane normal forces. For full compatibility between the shell element and the 3D beam element, the beam should be able to carry transverse loads with a second order variation. Here we consider a straight beam element with local coordinate axes as illustrated in Fig. 5.2. The element is able to carry longitudinal- and transverse loads (p_x, p_y, p_z) as well as torsional moments (t_x). The internal section forces are coupled to the external loads through the standard equilibrium equations for beams

$$p_y + V_{y,x} = 0 \tag{5.1}$$
$$p_z + V_{z,x} = 0 \tag{5.2}$$
$$t_x + M_{x,x} = 0 \tag{5.3}$$

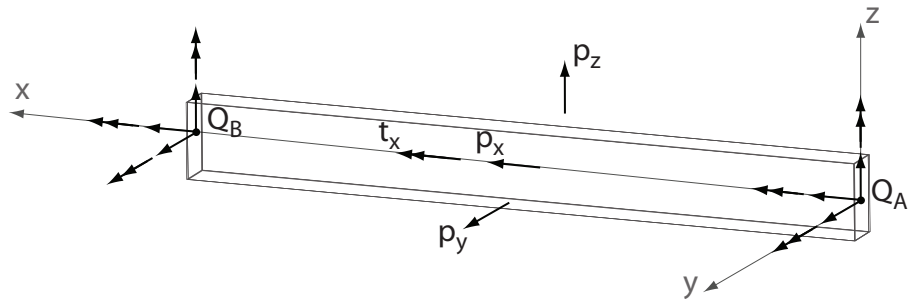

Figure 5.2: *3D Beam element model.*

where V_i is the shear force in the i'th direction and M_x is the torsional moment. The bending moments, M_y and M_z are coupled to the external load intensities through the shear forces by the following two equilibrium equations:

$$M_{z,x} + V_y = 0 \tag{5.4}$$
$$M_{y,x} - V_z = 0 \tag{5.5}$$

If we let $P_d(\zeta)$ define an arbitrary polynomium in the coordinate ζ of degree d and we chose the transverse loads and torsional moment of second degree variation along the x-axis, i.e. $p_y, p_z, t_x = P_2(x)$, then from (5.1) - (5.3) we get

$$V_x, V_y, M_x = P_3(x) \tag{5.6}$$

and from (5.4), (5.5) and (5.6) we get

$$M_y, M_z = P_4(x) \tag{5.7}$$

5.2 Zone Model

One of the main purposes of the element is to enable engineers to model and analyze beams with complex cross sections, while avoiding the need for a section force based yield criterion. This is achieved by expressing the section forces from a discrete representation of the internal stress state of the beam. The choice of discretization model greatly influences the element capabilities. The beam element presented in (Niebling et al. (2007)) used a fixed 3×3 zone model as illustrated in Fig. 5.1. A relatively rigorous material model was applied in which the zones marked by 2 was considered as reinforced disks and the conic yield criterion for such, (Nielsen (1969)), was applied. Zones marked by 3 was considered as two orthogonal disks to which the conic yield criterion was applied separately. In the center zone marked by 1, no shear reinforcement was allowed and a uni-axil constraint was employed.

While this model worked well for rectangular beams with simple cross section layouts, it provides little flexibility for the user. To extend the usability of the element, a more general zone formulation is needed. While more general shapes could be employed, we will here constrain the zones to axis aligned boxes similar to those used by (Niebling

et al. (2007)). This will constrain the element to angular cross section types such as R-, T- and I-beams but will keep the element simpler in terms of equilibrium equations and continuity constraints. The next thing to consider is how the stresses are modelled within a zone. The chosen stress state, and thereby internal stress distribution, must be able to describe the section forces needed in a 3D beam:

$$N_x = \int_A \sigma_x \, dA \tag{5.8}$$

$$V_y = \int_A \tau_{xy} \, dA \tag{5.9}$$

$$V_z = \int_A \tau_{xz} \, dA \tag{5.10}$$

$$M_x = \int_A (y \, \tau_{xz} + z \, \tau_{xy}) \, dA \tag{5.11}$$

$$M_y = \int_A z \, \sigma_x \, dA \tag{5.12}$$

$$M_z = -\int_A y \, \sigma_x \, dA \tag{5.13}$$

where A is the cross section area of the beam. From the above equations it is seen that only three stress parameters are required to define the complex set of section forces: σ_x, τ_{xy} and τ_{xz}. The stress state at a point within a zone is therefore defined by the stress tensor

$$\sigma = \begin{bmatrix} \sigma_x & \tau_{xy} & \tau_{xz} \\ \tau_{xy} & 0 & 0 \\ \tau_{xz} & 0 & 0 \end{bmatrix} \tag{5.14}$$

To keep the model simple, it is assumed that σ_x is constant over the cross section of a zone, while τ_{xy} is constant in z and linear in y and similar for τ_{xz} which is constant in y and linear in z. From 5.7 we get that σ_x must be of fourth degree along the x-direction while 5.6 gives a third degree variation of τ_{xy} and τ_{xz}. The stress distributions in a zone are summarized below

$$\sigma_x = P_4(x)P_0(y,z) \tag{5.15}$$

$$\tau_{xy} = P_3(x)P_1(y)P_0(z) \tag{5.16}$$

$$\tau_{xz} = P_3(x)P_0(y)P_1(z) \tag{5.17}$$

This choice of stresses gives the zone shown on Fig. 5.3 with 5 σ_x-nodes in the x-direction and 2 rows of shear stress nodes with 4 nodes in each row for each non-zero shear stress component - in total $5 + 2 \cdot 4 + 2 \cdot 4 = 21$ stress variables per zone.

The stress state within a zone must fulfill the following equilibrium equation

$$\sigma_{x,x} + \tau_{xy,y} + \tau_{xz,z} + f_x = 0 \tag{5.18}$$

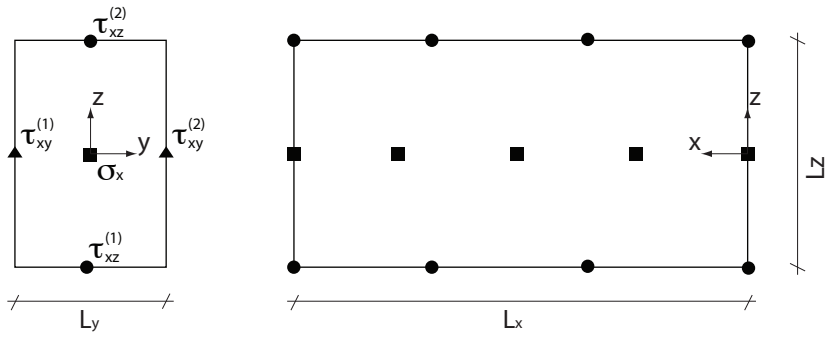

Figure 5.3: *Sketch of zone model.*

where f_x is the longitudinal volume load. It is assumed that f_x is constant over A and therefore, it can be expressed from the longitudinal load intensity as

$$f_x = \frac{p_x}{A} \tag{5.19}$$

Because the zones are axis-aligned and because the transverse normal stresses are assumed equal to zero, inter-zone continuity is ensured from simple shear stress continuity across zone borders.

5.2.1 Material Model

In the previous section it was mentioned how (Niebling et al. (2007)) considered the zones as reinforced disks oriented along the local coordinate axes, which was a feasible approach because of the rigid zone structure. When employing the more general zone described in the previous section, it is not known in advance which zones will be reinforced along which axis, and a more general material model is desired.

This is achieved by decomposing the stress state into concrete and reinforcement stresses, similar to the solid element presented in Chapter 4:

$$\sigma = \sigma_c + A_s \sigma_s \tag{5.20}$$

where

$$\sigma_c = \begin{bmatrix} \sigma_{cx} & \tau_{cxy} & \tau_{cxz} \\ \tau_{cxy} & \sigma_{cy} & 0 \\ \tau_{cxz} & 0 & \sigma_{cz} \end{bmatrix} \tag{5.21}$$

are the concrete stresses and

$$\sigma_s = \begin{bmatrix} \sigma_{sx} & 0 & 0 \\ 0 & \sigma_{sy} & 0 \\ 0 & 0 & \sigma_{sz} \end{bmatrix} \tag{5.22}$$

are the reinforcement stresses. The matrix A_s a diagonal matrix which contains the reinforcement area per unit area perpendicular to the local element axes

$$A_s = \begin{bmatrix} A_{sx} & 0 & 0 \\ 0 & A_{sy} & 0 \\ 0 & 0 & A_{sz} \end{bmatrix} \tag{5.23}$$

As is seen from the equations above, a tri-axial stress state is possible in the concrete if reinforcement is provided in both the y- and the z-direction. In (Niebling et al. (2007)), this was handled by considering the stress state as two orthogonal disks such that σ_x and τ_{xy} formed one disk and σ_x and τ_{xz} formed another. This disk analogy was used because it suited the definition of a second-order cone program very well. It should be noted though, that there is no interaction between the transverse shear stress components, and, as will be shown later, this criterion does not provide a safe stress state. In Chapter 4 it was shown how the modified Coulomb criterion in tri-axial stress states could be modeled using a combination of LMI constraints and linear inequality constraints, (4.20). This method provides a general yield criterion which can be employed in all zones, regardless of the reinforcement presented in the zone. The reinforcement stresses are, similar to the solid model, constrained by the simple upper- and lower limits shown in (4.15).

A safe stress state throughout the beam element must be ensured in order to fulfill the lower bound theorem. The yield criteria are therefore applied at a number of control points along the beam length. Because the stress distribution is of fourth degree, a rigorous lower bound solution cannot be obtained from a fixed number of control points. While it is important to use a sufficient number of control points, these must be kept reasonable since they will add to the computational time. Alternatively, the resulting stress state could be analyzed in a post-processor and additional control points could be inserted if needed.
At each control point, the yield criteria must be enforced in all zones. Because σ_x is constant over the cross section and τ_{xz} and τ_{yz} varies linearly over the cross section of a zone, it is sufficient to enforce the concrete yield criterion at the four corners of the zone. Since the reinforcement stresses are constant over the cross section of a zone, the yield criterion is simply applied at the center point.

To compare the SDP formulation employed here to the conic formulation used in (Niebling et al. (2007)), a slice of the yield surface is generated using both models. Fig. 5.4 shows the $\tau_{xy} - \tau_{xz}$ curve for both models at a point with equal reinforcement in all three direction: $\Phi = (0.1; 0.1, 0.1)$, $f_c = 1$ and $f_A = 0$. As seen from the figure, the disk approximation allows stress states which are significantly outside the actual yield surface (marked by grey in the figure). Because the conic disk criterion is an approximation, it is recommended only for reinforcement degrees less than 0.1, see (Nielsen (1999)). Since the reinforcement area in the longitudinal direction often is relatively large compared to the zone cross section, reinforcement degrees larger than 0.1 is often encountered. Fig. 5.5 shows the same comparison between the orthogonal disk model and the solid model, except that Φ_x has been increased to 1.0. From the figure it is seen that the potential unsafe area increases for larger degrees of reinforcement.

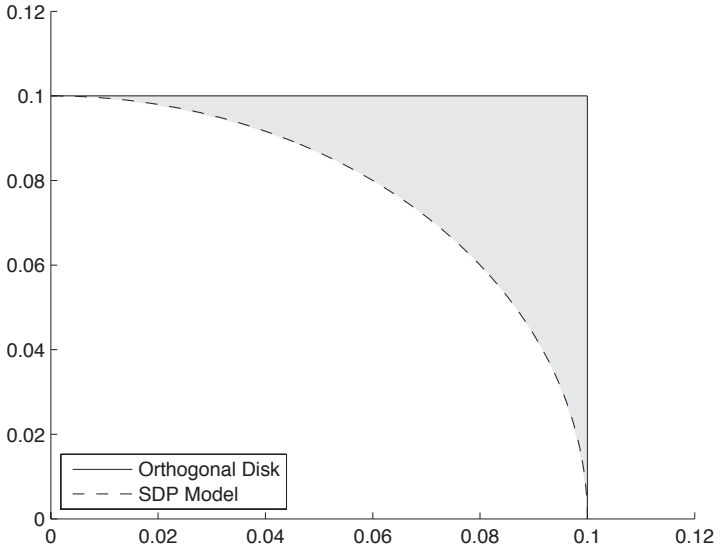

Figure 5.4: *Comparison between the orthogonal disk model used in (Niebling et al. (2007)) and the solid SDP formulation presented in Chapter 4 for low degrees of reinforcement:* $\Phi = (0.1; 0.1, 0.1)$

While the SDP formulation provides an excellent yield criterion for the general zone, the performance of numerical SDP solvers are, at the time of writing, not as good as those available for solving SOCP problems. It is therefore desirable to develop a general yield criterion based on second order cones rather than LMI's. An SOCP formulation of the general Coulomb criterion is not straightforward, but in Paper II an approximation is presented. The approximation assumes that an equal amount of reinforcement is provided in both of the transverse directions - an assumption that might seem limiting at first but actually is quite applicable. This is because tri-axial stress states often occurs in corner zones where stirrups wraps around longitudinal reinforcement. If there is not an equal amount of reinforcement in both of the transverse directions, the yield strength is governed by the direction with the smallest amount of reinforcement. If no reinforcement is provided in one of the transverse direction, the yield criterion will 'collapse' and no stresses can be carried in that zone. The approximated yield criterion should therefore only be applied to zones in which the transverse reinforcement does not differ significantly. This is a major drawback of the approximation since it prevents it from being applied generally to all zones within a beam. In Paper II, a pre-process determines to which zones the approximated yield criterion should be applied. In the remaining zones, the stress state is considered either bi-axial or uni-axial depending on whether shear reinforcement is provided or not. The approximated yield criterion for a tri-axial stress state

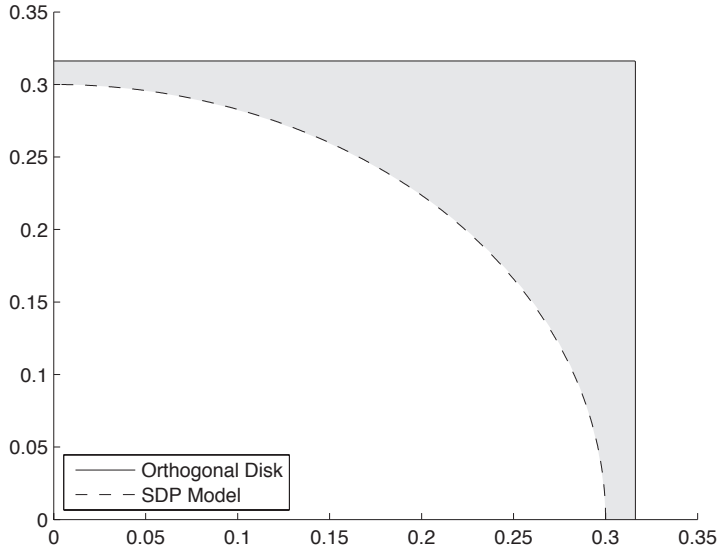

Figure 5.5: *Comparison between the orthogonal disk model used in (Niebling et al. (2007)) and the solid SDP formulation presented in Chapter 4 for high degrees of reinforcement:* $\Phi = (1.0; 0.1, 0.1)$

is summarized below and the reader is referred to Paper II for further details:

$$\sqrt{\sigma_{dz}^2 + \tau_{cxy}^2 + \tau_{cxz}^2} \leq \alpha_1 \tag{5.24}$$

$$\sqrt{\sigma_{dy}^2 + \tau_{cxy}^2 + \tau_{cxz}^2} \leq \alpha_2 \tag{5.25}$$

$$\sigma_{dz} = \frac{1}{2}\left(\sigma_{cx} - \sigma_{cz}\right) \tag{5.26}$$

$$\sigma_{dy} = \frac{1}{2}\left(\sigma_{cx} - \sigma_{cy}\right) \tag{5.27}$$

$$\alpha_1 \leq f_c - k \cdot \sigma_{cz} + \frac{\sigma_{cx} + \sigma_{cz}}{2} \tag{5.28}$$

$$\alpha_1 \leq \frac{f_c}{k} + \frac{\sigma_{cz}}{k} - \frac{\sigma_{cx} + \sigma_{cz}}{2} \tag{5.29}$$

$$\alpha_1 \leq \frac{1}{k+1}\left(f_c - \left(\frac{\sigma_{cx} + \sigma_{cz}}{2}\right)(k-1)\right) \tag{5.30}$$

$$\alpha_2 \leq f_c - k \cdot \sigma_{cy} + \frac{\sigma_{cx} + \sigma_{cy}}{2} \tag{5.31}$$

$$\alpha_2 \leq \frac{f_c}{k} + \frac{\sigma_{cy}}{k} - \frac{\sigma_{cx} + \sigma_{cy}}{2} \tag{5.32}$$

$$\alpha_2 \leq \frac{1}{k+1}\left(f_c - \left(\frac{\sigma_{cx} + \sigma_{cy}}{2}\right)(k-1)\right) \tag{5.33}$$

where α_1 and α_2 are auxiliary variables.

5.3 Example: Inverse T-Beam

In Paper II, the element is tested for various basic load cases and the numerical results are compared with analytical solutions. This example illustrates how the element can be used to model a beam with a complex cross section layout.

As part of a renovation project in Copenhagen, Ramboll was asked to assess the safety of a range of inverse T-beams in the structure. The T-beam spans $6.8m$ with a cross section as illustrated in Fig. 5.6 and the shear reinforcement varies along the length of the beam as described in the figure. The cross section is modeled using 37 zones as indicated by the dashed lines and because a single element can only have constant shear reinforcement along the length, the beam is modeled using 5 elements. The beam is subjected to a uniformly distributed line load acting along the center lines of the beam.

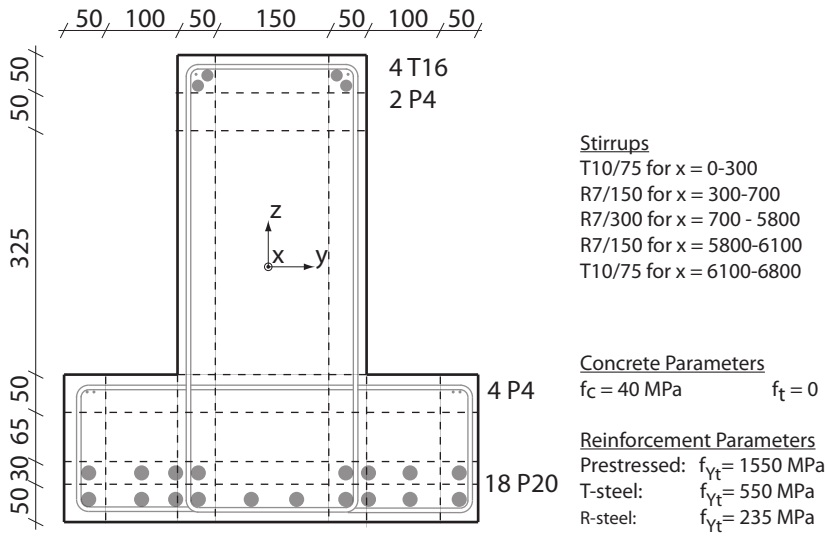

Figure 5.6: *Cross section of inverse T-beam with zone division model.*

As part of the assessment project, a series of laboratory tests was conducted in which the collapse load of the beam was determined to around $136kN/m$ (average of five tests). Fig. 5.7 shows a picture of the beam after one of the tests have been completed and, as seen from the figure, the failure mode is governed by the shear strength of the beam. From the numerical analysis, the collapse load of the beam is determined to $119kN/m$ which is around 13% less than the collapse load measured from tests. Because the numerical model is based on the lower bound theorem, this is also to be expected. While the concrete strength have been determined from tests, the strength of the rebars are those provided by the manufacturer. Such values are often lower than the actual yield strengths which could also explain the lower numerical result, since they influences the collapse load considerably.

Figure 5.7: *Failure mode of inverse T-beam. Image from Ramboll report*

Chapter 6

3D Shell Structures

Elements for limit state analysis of slabs subjected plate bending and walls subjected to in-plane forces have been developed years ago. For plate bending elements, the conic yield constraint for slabs, (Nielsen (1963)), have been employed, either in its conic form (Makrodimopoulos and Martin (2006); Krabbenhoft et al. (2007)), using SOCP optimization or in a linearized form when approximated as an LP problem, (Anderheggen and Knopfel (1972)). For disk elements, the conic yield constraints for RC disks, (Nielsen (1969)), was employed, once again in a linearized form for LP problems, (Poulsen and Damkilde (2000)) and directly as cones for SOCP problems, (Bisbos and Pardalos (2007)). In (Niebling et al. (2007)) a shell element was presented which was capable of modeling both slab and disk structures. The element utilized a layered disk model and the conic yield criterion for RC disks were then applied in each layer, thereby ensuring a safe stress distribution.

While the layered approach used by (Niebling et al. (2007)) provided good results for both plate and disk structures, it neglected the effects of the transverse shear stresses present in the cross section. The shell element presented in this chapter expands on the layered disk approach while utilizing semidefinite programming to include transverse shear stresses into the yield criterion.

6.1 Plane Shell Model

A shell structure is characterized by membrane and bending behavior. If we consider a point within the structure, the cross section forces can be defined from the internal stress

state as

$$m_x^{(j)} = \int_{-h/2}^{h/2} \sigma_x(z)\ z^{(j)}\ dz \tag{6.1}$$

$$m_y^{(j)} = \int_{-h/2}^{h/2} \sigma_y(z)\ z^{(j)}\ dz \tag{6.2}$$

$$m_{xy}^{(j)} = \int_{-h/2}^{h/2} \tau_{xy}(z)\ z^{(j)}\ dz \tag{6.3}$$

$$q_x = \int_{-h/2}^{h/2} \tau_{xz}(z)\ dz \tag{6.4}$$

$$q_y = \int_{-h/2}^{h/2} \tau_{yz}(z)\ dz \tag{6.5}$$

where j is the order of the moment and h is the height of the cross section. It should be noted that the 0th order moment is equal to the normal force i.e. $m_i^{(0)} = n_i$. Furthermore, the 1st order moment is also referred to as just moment i.e. $m_i^{(1)} = m_i$. From the above equations, it is seen that the section forces can be described from five stress components and is defined by the stress tensor

$$\sigma = \begin{bmatrix} \sigma_x & \tau_{xy} & \tau_{xz} \\ \tau_{xy} & \sigma_y & \tau_{yz} \\ \tau_{xz} & \tau_{yz} & 0 \end{bmatrix} \tag{6.6}$$

Here we assume, similar to (Niebling et al. (2007)), that the cross section is divided into three layers as illustrated in Fig. 6.1. In each layer, the normal stress components, σ_x and σ_y, and the in-plane shear stresses, τ_{xy}, are considered constant over the height of the zone which is illustrated in Fig. 6.2a. The transverse shear stresses are assumed constant

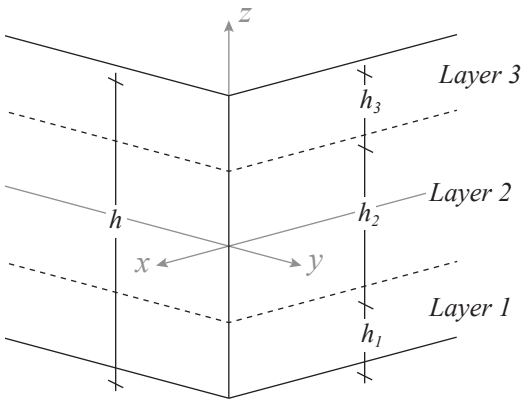

Figure 6.1: *Plane shell structure modeled using three layered disks.*

over the center zone while decreasing linearly to zero over the height of the outer zones as illustrated in Fig. 6.2b. The internal stress state must fulfill a set of equilibrium equations

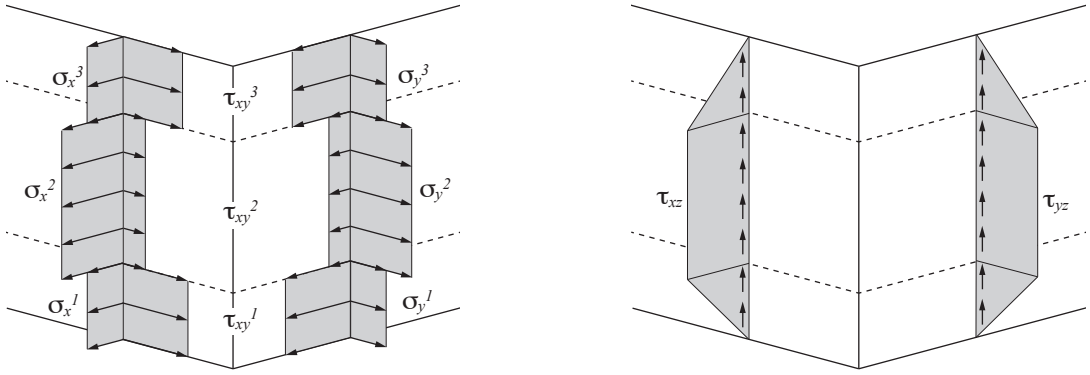

(a) *Distribution of in-plane stresses over the cross section.*

(b) *Distribution of transverse shear stresses over the cross section.*

Figure 6.2: *Stress distribution over the element cross section.*

to ensure a statically admissible stress field. In-plane equilibrium is ensured through the 'usual' set of equilibrium equations shown below

$$f_x\lambda + \sigma_{x,x} + \tau_{xy,y} + \tau_{xz,z} = -f_x^0 \tag{6.7}$$

$$f_y\lambda + \sigma_{y,y} + \tau_{xy,x} + \tau_{yz,z} = -f_y^0 \tag{6.8}$$

where f_i and f_i^0 are the proportional and constant volume loads in the i'th direction. The volume load is assumed to be constant over the height of the cross section and it can therefore be expressed from the in-plane surface loads as $p_i = hf_i$ and $p_i^0 = hf_i^0$.

Transverse equilibrium is ensured through equilibrium between the surface load and the transverse shear forces as

$$p_z\lambda + q_{x,x} + q_{y,y} = -p_z^0 \tag{6.9}$$

where p_z and p_z^0 are the proportional and constant surface loads perpendicular to the element plane respectively.

As it is seen from the stress tensor, a tri-axial stress state is possible in the cross section. This is often handled by disregarding the transverse shear stresses, thereby assuming a plane stress state. As it was shown in Chapter 4, the modified Coulomb criterion could be applied to concrete materials subjected to tri-axial stress states by means of semidefinite programming and LMI constraints. By employing the same technique here, the transverse shear stresses can be taken into account when performing the numerical analysis. The procedure is the same as for the solid element described in Chapter 4, in which the total stress state is decomposed into concrete and reinforcement stresses

$$\sigma = \sigma_c + A_s\sigma_s \tag{6.10}$$

where

$$\sigma_c = \begin{bmatrix} \sigma_{cx} & \tau_{cxy} & \tau_{cxz} \\ \tau_{cxy} & \sigma_{cy} & \tau_{cyz} \\ \tau_{cxz} & \tau_{cyz} & \sigma_{cz} \end{bmatrix} \tag{6.11}$$

is the concrete stress tensor and

$$\sigma_s = \begin{bmatrix} \sigma_{sx} & 0 & 0 \\ 0 & \sigma_{sy} & 0 \\ 0 & 0 & \sigma_{sz} \end{bmatrix} \tag{6.12}$$

is a diagonal matrix containing the normal stresses in the reinforcement. The matrix A_s contains the reinforcement area per unit area perpendicular to the local element axes

$$A_s = \begin{bmatrix} A_{sx} & 0 & 0 \\ 0 & A_{sy} & 0 \\ 0 & 0 & A_{sz} \end{bmatrix} \tag{6.13}$$

The reinforcement is assumed subjected to uni-axial stresses only as is also seen from σ_s. It should be noted that even though the total normal stresses in the transverse direction, σ_z, is assumed equal to zero, σ_{cz} and σ_{sz} does not have to be zero. This allows for transverse shear reinforcement to be applied to the shell structure.

The uni-axial stresses in the reinforcement is constrained by the simple upper- and lower limits shown in (4.15) while the concrete stresses are constrained by the combination of LMI's and linear inequality constraints shown in (4.20).

6.2 Triangular Element

The layered shell model described above is implemented into a general finite element framework using a planar triangular element as shown in Fig. 6.3. An orthogonal local coordinate system (x, y, z) is associated with the element and the geometrical shape is defined by the nodes (n^1, n^2, n^3), in an order defining the positive z-direction through the right-hand rule as illustrated in the figure. The edges are numbered in a counter clockwise direction and a local edge coordinate system (n_n, n_t) is associated with each edge. The external surface loads are chosen such that the element is capable of carrying a uniform surface load perpendicular to the element plane, i.e.

$$p_z = P_0(x, y) \tag{6.14}$$

From (6.7) - (6.9) it then follows that

$$p_x, p_y = P_1(x, y) \tag{6.15}$$

and

$$q_x, q_y = P_1(x, y) \qquad m_x^{(j)}, m_y^{(j)}, m_{xy}^{(j)} = P_2(x, y) \tag{6.16}$$

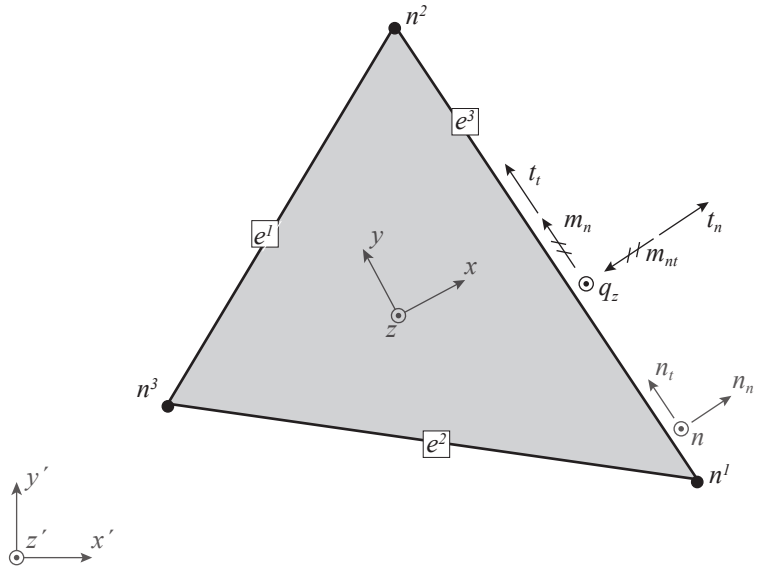

Figure 6.3: *Geometric properties of a triangular element.*

Continuity between adjacent elements is ensured through traction force continuity across shared boundaries. The traction forces along an edge can be computed by transforming the cross section forces in local element coordinates into local edge coordinates. First we write the cross section forces at a point along the element edge on vector form:

$$f = \left[n_x, n_y, n_{xy}, m_x, m_y, m_{xy}, m_x^{(2)}, m_y^{(2)}, m_{xy}^{(2)}, q_x, q_y\right]^T \tag{6.17}$$

and the transformed traction forces as

$$t = \left[t_n, t_t, m_n, m_{nt}, m_n^{(2)}, m_{nt}^{(2)}, q_n\right]^T \tag{6.18}$$

The vector f can be transformed into t by multiplication with the local edge transformation matrix T^e, i.e. $t = T^e f$. The matrix T^e is constructed from the edge normal, $n_n = (n_{nx}, n_{ny})$ as

$$T^e = \begin{bmatrix} T^m & & & \\ & T^m & & \\ & & T^m & \\ & & & T^q \end{bmatrix} \tag{6.19}$$

where

$$T^m = \begin{bmatrix} n_{nx}^2 & n_{ny}^2 & 2n_{nx}n_{ny} \\ -n_{nx}n_{ny} & n_{nx}n_{ny} & n_{nx}^2 - n_{ny}^2 \end{bmatrix} \tag{6.20}$$

and

$$T^q = \begin{bmatrix} n_{nx} & n_{ny} \end{bmatrix} \tag{6.21}$$

It should be noted here, that $m_i^{(2)}$ continuity is required. This is not necessary in order to obtain a statically admissible force distribution in the structure, but has been chosen to obtain a better stress distribution internally. Because stress continuity is not directly required across boundaries, $m_i^{(2)}$ continuity ensures that the stress distribution does not vary significantly between elements.

If adjacent elements does not lie in the same plane, the tractions have to be transformed into the same coordinate system, here the global coordinate system. This is simply done by multiplying the local transformation matrix T^e with a global transformation matrix T:

$$T = \begin{bmatrix} n_n^T & n_t^T & & & & n^T \\ & & n_n^T & n_t^T & & \\ & & & & n_n^T & n_t^T \end{bmatrix} \tag{6.22}$$

The total equilibrium equation along an edge is determined from the constant, t^0, and proportional, t, traction forces applied and a sum of all indecent elements

$$-t\lambda + \sum_{i=1}^{k} T_i P_i f = t^0 \tag{6.23}$$

6.3 Example: Triangular Plate on Column Supports

This example illustrates how the shell element can be used to model the triangular plate shown in Fig. 6.4. In Paper III, an example is shown in which the element is used to model disk behavior. The plate is supported by three columns as illustrated in the figure and subjected to a downwards point load, P, at the tip of the plate. Because point

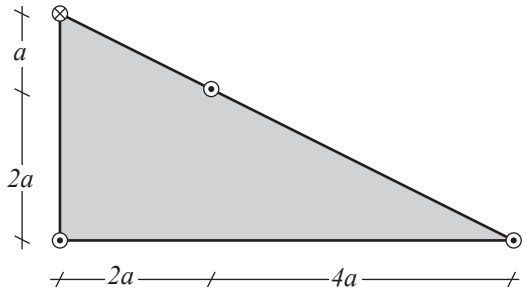

Figure 6.4: *Triangular plate supported on 3 columns and load by a pointload.*

loads and point supports are not directly applicable to the shell elements, these must be distributed over an area of the surface. Since transverse shear stresses are included in the analysis, the areas over which these are distributed have a significant impact on the load bearing capacity determined. If the area is chosen to small, larger shear stresses can occur around the loaded or supported areas.

In this example we assume that the side lengths of the plate is $6m$ and $3m$, i.e. $a = 1m$ and the supporting columns have a diameter of $0.4m$. The plate thickness is set to $300mm$ and divided into layers such that $h_1 = h_2 = h_3 = 100mm$. The concrete compression strength is set to $15MPa$ while the separation strength is assumed to be zero. Reinforcement is added to the top and bottom layers such that

$$\Phi_x^{(1)} = \Phi_x^{(3)} = 0.1 \tag{6.24}$$

$$\Phi_y^{(1)} = \Phi_y^{(3)} = 0.1 \tag{6.25}$$

which yields a plastic bending capacity of $m_p = 30kNm/m$. The plate is meshed using 351 elements as illustrated in Fig. 6.5 and the load P is applied as a constant surface load over the elements marked by grey in the figure. An upper bound solution for P_m

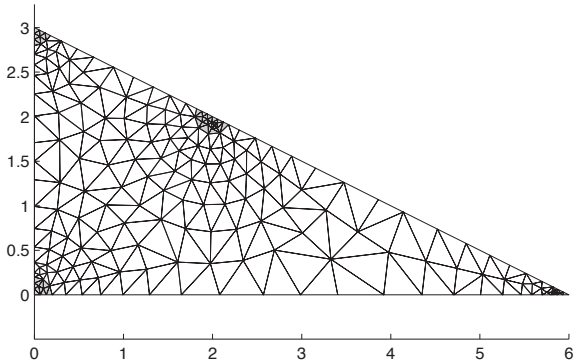

Figure 6.5: *Triangular plate meshed by 351 elements.*

(identical to a numerical lower bound solution) based on moment yield line theory and rigid in transverse shear is given by

$$P = \frac{12m_p}{2 + \sqrt{5}} \tag{6.26}$$

which gives $P = 85kN$ for $m_p = 30kNm/m$. From the numerical analysis, a load bearing capacity of $P = 36kN$ is found which is more than 60% less than the analytical upper bound solution. Fig. 6.6 shows where the yield condition in either concrete or reinforcement is (nearly) satisfied. This example illustrates the importance of including the transverse shear stresses in the yield condition when performing limit state analysis of structures subjected to plate bending.

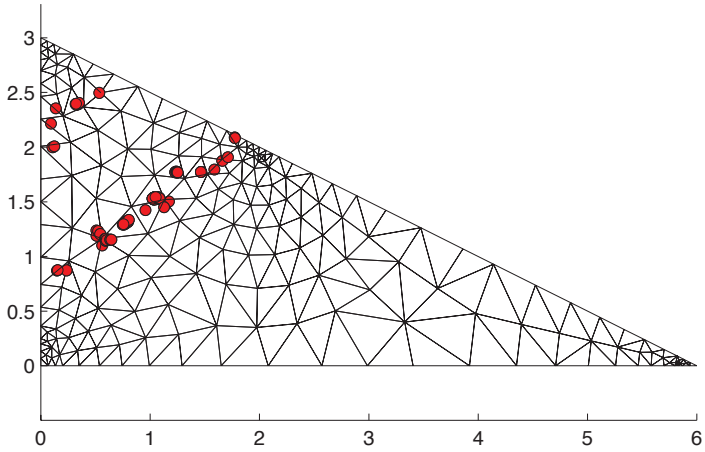

Figure 6.6: *Points at which the yield condition in either concrete or reinforcement is (nearly) satisfied.*

Chapter 7

Conclusion

A finite element framework for limit state analysis of reinforced concrete structures has been developed. Solving such limit state problems requires solving of large-scale convex optimization problems which requires specialized algorithms. The thesis contributes to further the implementation and application of numerical limit state analysis tools for practical engineering.

A solid element was developed which allows for detailed modeling and analysis of complex structures of reinforced concrete. The element implements a solid material model for reinforced concrete which includes tri-axial effects. The reinforcement is assumed to carry uni-axial stresses only and is considered smeared over the concrete. The modified Coulomb failure criterion is applied to the concrete stresses while the uni-axial reinforcement stresses are constrained by simple upper- and lower limits. The modified Coulomb criterion, which traditionally is difficult to handle numerically because of its discontinuous nature, has been implemented using a combination of linear matrix inequality and linear inequality constraints. The resulting optimization problem can be solved using Semidefinite Programming algorithms. The material model was verified by comparison with analytical solutions. The element was furthermore used to model and analyse a practical engineering problem in form of a console beam and the numerical results were in good correlation with manual calculations which have been thoroughly scrutinized.

While the solid element is capable of modeling highly detailed structures, current limitations in computational capacity restricts the application details such as the console beam example given in Paper I. A 3D beam element is developed to allow analysis of three dimensional frame structures on a larger scale. The need for a complex yield criterion based on section forces is circumvented by creating a discrete representation of the internal stress state in the beam using a zone model. The solid material model is applied to the internal stresses thereby allowing a tri-axial stress state internally in the beam. An approximate material model based on second-order cone constraints is also developed for improved performance. The model exploits the simplified stress state assumption in the beam element and allows full utilization of the tri-axial effects when an equal amount of shear reinforcement is present in both of the transverse directions. If there is not an equal amount of reinforcement in the transverse directions, the capacity is governed be

the smallest reinforcement value and therefore provides safe lower bound. The main disadvantage of the model is that it is not able to handle zones which are only reinforced in one of the transverse direction. In these zones, a conic formulation of the modified Coulomb criterion is applied. The approximated material model was validated against the solid material model and the beam element was tested when subjected to basic load cases. Furthermore the element was used to analyze an inverse T-beam and good correlation was found with laboratory tests.

The third and final element is a shell element capable of modeling membrane of plate bending behavior. The element is intended for modeling of faceted shell structures subjected to a combination of plate bending and in-plane forces. Similar to the beam element approach, the shell element employs a discrete representation of the internal stress state to avoid the need for complex section force based yield criterion. A layered disk model is used to define the internal stress state and the solid material model employed in the solid elements is used to constrain the decomposed concrete stresses while the reinforcement is, once again, subjected to uni-axial stresses only. By considering the full tri-axial stress state, the element is able to take combined cross section forces such as bending and transverse shear into consideration. It has been shown how the element can be used as a disk to create a detailed model of an unreinforced beam and good results were obtained when compared to analytical solutions. The importance of including the transverse shear stresses for some structural problems have been illustrated from analysis of a triangular plate supported on three columns and loaded by a point load. In the given example, the load bearing capacity determined using the shell element was less than half of that found when considering moments only.

7.1 Recommendations for Future Work

The beam and shell element presented in the current work employs a discrete representation of the internal stresses to which the yield criteria are applied while inter-element continuity is only required in a section force level. For the shell element, continuity in the second-order was applied to reduce stress discontinuities across element boundaries. A more in depth investigation of errors made from not requiring stress continuity is therefore to be desired.

In Paper II, an approximated formulation of the modified Coulomb criterion using second-order cone constraints was developed. The formulation exploits the assumptions made about the stress state within the beam. The formulation is able to accurately model the tri-axial effects in areas of the beam where equal reinforcement is present in the transverse directions. If though, reinforcement in the transverse directions are not equal, the obtained capacities are significantly lower than the actual capacity, and a pre-processor is therefore required to determine if the tri-axial approximation or a bi-axial formulation should be applied. The pre-processor used in the current work simply switches between the two models depending on whether transverse reinforcement is present in both directions or not. A more refined pre-processor is to be desired to avoid underestimating the capacity in cases where the transverse reinforcement differs significantly.

The elements developed here are designed to part of are complete finite element framework which facilitates modeling of full three dimensional structures. Work still remain in developing such a framework in which interfaces between element types such as beams and solids should be studied.

The current thesis focuses on estimating the load bearing capacity of existing structures. While this is useful for assessing the safety of existing structures, more design capabilities are to be desired for practical engineering purposes. Further work in extending the methods presented here to include optimal reinforcement design would increase the applicability of the framework.

List of Figures

Bibliography

Anderheggen, E. and Knopfel, H. (1972). Finite element limit analysis using linear programming. *International Journal of Solids and Structures*, 8(12):1413–1431.

Andreasen, B. S. (1989). Anchorage of ribbed reinforcing bars. *Serie R - Danmarks Tekniske Hojskole, Afdelingen for Baerende Konstruktioner*, (238).

Belytschko and Black (1999). Elastic crack growth in finite elements with minimal remeshing. *International Journal for Numerical Methods in Engineering*, 45(5):601–620.

Bisbos, C., Makrodimopoulos, A., and Pardalos, P. (2005). *Optimization Methods and Software*, 20(1):25–52.

Bisbos, C. and Pardalos, P. (2007). Second-order cone and semidefinite representations of material failure criteria. *Journal of Optimization Theory and Applications*, 134(2):275–301.

Bottero, A., Negre, R., Pastor, J., and Turgeman, S. (1980). Finite element method and limit analysis theory for soil mechanics problems. *Computer Methods in Applied Mechanics and Engineering*, 22(1):131–149.

Boyd, S. and Vandenberghe, L. (2004). *Convex Optimization*. Cambridge University Press.

Coulomb, C. (1776). Essai sur une application des regles des maximis et minimis a quelquels problemesde statique relatifs, a la architecture. *Mem. Acad. Roy. Div. Sav.*, 7:343–387.

Damkilde, L. and Hoyer, O. (1993). An efficient implementation of limit state calculations based on lower-bound solutions. *Computers and Structures*, 49(6):953–962.

Damkilde, L. and Krenk, S. (1997). Limits–a system for limit state analysis and optimal material layout. *Computers & Structures*, 64(1-4):709–718.

Dantzig, G. B. (1963). *Linear programming and extensions*. Princeton University Press, Princeton, N.J.,.

Drucker, D., Prager, W., and Greenberg, H. (1952). Extended limit design theorems for continuous media. *Quarterly of Applied Mathematics*, 9(4):381–391.

Feddersen, B. (1994). The theory of plasticity for concrete and reinforced concrete. *Bygningsstatiske Meddelelser*, 2-3-4:89–108.

Foster, S. J., Marti, P., and Mojsilovic, N. (2003). Design of reinforced concrete solids using stress analysis. *ACI Structural Journal*, 100(6):758–764.

Grierson, D. E. and Gladwell, G. M. L. (1971). Collapse load analysis using linear programming. *Journal of the Structural Division*, 97(5):1561–1573.

Griffith, A. A. (1921). The phenomena of rupture and flow in solids. *Philosophical Transactions of the Royal Society of London. Series A, Containing Papers of a Mathematical or Physical Character*, 221(582-593):163–198.

Gvozdev, A. A. (1960). The determination of the value of the collapse load for statically indeterminate systems undergoing plastic deformations. *Int. J. Mech. Sci.*, 1:322–333.

Hansen, L. P. (1964). Grundlaget for teorien for idealt plastiske konstruktioner. Ingeniøren.

Heyman, J. (1997). *Coulomb's Memoir on Statics An Essay in the History of Civil Engineering*. World Scientific Publishing Company.

Hillerborg, A. (1959). *Strimlemetoden Thestripmethod*. Svenska Riks-byggen.

Hillerborg, A., Modéer, M., and Petersson, P.-E. (1976). Analysis of crack formation and crack growth in concrete by means of fracture mechanics and finite elements. *Cement and Concrete Research*, 6(6):773 – 781.

Hoogenboom, P. (2008). Computation of reinforcement for solid concrete. *Heron*, 53(4):247–271.

Johansen, K. W. (1943). *Brudlinieteorier*. Gjellerup.

Johansen, K. W. (1962). *Yield line theory*. Cement and Concrete Association.

Karmarkar, N. (1984). A new polynomial-time algorithm for linear programming. In *STOC '84: Proceedings of the sixteenth annual ACM symposium on Theory of computing*, pages 302–311, New York, NY, USA. ACM.

Klee, V. and Minty, G. J. (1972). How good is the simplex algorithm? In Shisha, O., editor, *Inequalities*, volume III, pages 159–175. Academic Press, New York.

Krabbenhøft, K., Lyamin, A., and Sloan, S. (2008). Three-dimensional mohr-coulomb limit analysis using semidefinite programming. *Communications in Numerical Methods in Engineering*, 24(11):1107–1119.

Krabbenhoft, K., Lyamin, A., and Sloan, S. (2007). Formulation and solution of some plasticity problems as conic programs. *International Journal of Solids and Structures*, 44(5):1533–1549.

Lundgren, H. (1949). *Cylindrical Shells.* Danish Technical Press, Institution of Danish Civil Engineers.

Maier, G. (1969). Shakedown theory in perfect elastoplasticity with associated and nonassociated flow-laws: A finite element, linear programming approach. *Meccanica*, 4(3):250–260.

Makrodimopoulos, A. and Martin, C. M. (2006). Lower bound limit analysis of cohesive-frictional materials using second-order cone programming.

Makrodimopoulos, A. and Martin, C. M. (2007). Upper bound limit analysis using simplex strain elements and second-order cone programming. *International Journal for Numerical and Analytical Methods in Geomechanics*, 31(6):835–865.

Martin, C. M. and Makrodimopoulos, A. (2008). Finite-element limit analysis of mohr-coulomb materials in 3d using semidefinite programming.

Moersch, E. (1922). *Der Eisenbetonbau - Seine Theorie und Anwendung.* Verlag Konrad Wittwer, Stuttgart, 5. auflage edition.

Nesterov, Y. and Nemirovskii, A. (1988). A general approach to polynomial-time algorithms design for convex programming. *Centr. Econ. & Math. Inst., USSR Acad. Sci., Moscow, USSR,.*

Nesterov, Y. and Nemirovskii, A. (1994). *Interior-Point Polynomial Methods in Convex Programming.* Society for Industrial and Applied Mathematics.

Niebling, J., Vinther, A., and Larsen, K. P. (2007). Numerisk modellering af plastiske betonkonstruktioner.

Nielsen, M. P. (1963). Flydebetingelser for jernbetonplader (yield conditions for reinforced slabs). volume 7, pages 61–82. Nord. Betong.

Nielsen, M. P. (1969). Om jernbetonskivers styrke (on the strength of reinforced concrete discs). page 254. Polyteknisk Forlag.

Nielsen, M. P. (1999). *Limit Analysis and Concrete Plasticity.* CRC Press.

Olsen, P. C. (1998). The influence of the linearisation of the yield surface on the load-bearing capacity of reinforced concrete slabs. *Computer Methods in Applied Mechanics and Engineering*, 162(1-4):351–358.

Poulsen, P. N. and Damkilde, L. (2000). Limit state analysis of reinforced concrete plates subjected to in-plane forces.

Prager, W. (1962). Linear programming in theory of structures. *Liege Universite. Centre d'Etudes, de Recherches et d'Essais Scientifiques du Genie Civil – Memoires*, (3):33–49.

Sloan, S. (1989). Upper bound limit analysis using finite elements and linear programming. *International Journal for Numerical and Analytical Methods in Geomechanics*, 13(3):263–282.

Turner, M., Clough, R., Martin, H., and Topp, L. (1956). Stiffness and deflection analysis of complex structures. *Journal of the Aeronautical Sciences*, 23(9):805–823 + 854.

Vandenberghe, L. and Boyd, S. (1996). Semidefinite programming. *SIAM Review*, 38:49–95.

Part II

Appended Papers

Paper I

"Limit Analysis of Solid Reinforced Concrete Structures"

K.P. Larsen, P.N. Poulsen & L. O. Nielsen

Under peer-review in: *Computers and Concrete - An International Journal*

Limit analysis of solid reinforced concrete structures

K.P. Larsen[†]

Ramboll Denmark, DK-2830 Virum, Denmark,
Department of Civil Engineering, Technical University of Denmark, DK-2800 Kgs. Lyngby, Denmark
e-mail: kpl@ramboll.dk

P.N. Poulsen, & L.O. Nielsen

Department of Civil Engineering, Technical University of Denmark, DK-2800 Kgs. Lyngby, Denmark
e-mail: pnp@byg.dtu.dk and lon@byg.dtu.dk

Abstract

Recent studies have shown that Semidefinite Programming (SDP) can be used effectively for limit analysis of isotropic cohesive-frictional continuum's using the Modified Coulomb yield criterion. In the field of geotechnics, a numerical model for limit analysis of soils has been developed. In this paper, we expand on the previous work and present a solid element for lower bound limit analysis of reinforced concrete structures. The method defines the stress state at a point within the solid as a combination of concrete and reinforcement stresses and the yield criteria are applied to the stress components separately. This method allows for orthotropic reinforcement and it is therefore possible to analyze structures with complex reinforcement layouts. Tests are conducted to validate the method against well-known analytical solutions, and examples of analysis of a complex structure is carried out.
Keywords *rigid perfect plasticity; limit analysis; numerical methods; semidefinite programming*

1 Introduction

The first reinforced concrete structures came about in the last of part of the 18th century and concrete is today the most widely used construction material. In the 1970s the first numerical solutions for determination of the load-bearing capacity of reinforced concrete structures were presented by [Anderheggen and Knopfel, 1972, Fredsgaard and Kirk, 1979]. Even though solutions for different structural members were established, the application of these numerical tools was very limited. Since then, new formulations for the load-bearing capacity have been presented for a wide range of structural components: plates [Krenk et al., 1994], stringers [Damkilde et al., 1994] and disks [Poulsen and Damkilde, 2000]. These numerical solutions were all based on optimization with linear constraints which were formulated as Linear Programming (LP) problems and were solved using the simplex algorithm, [Dantzig, 1963]. Due to limitations in the simplex algorithm and in computer hardware, only problems of moderate size could be analyzed. The numerical solvers were much improved by the introduction of interior point methods [Karmarkar, 1984, Nesterov and Nemirovsky, 1988] which were applicable for both LP problems [Krabbenhoft and Damkilde, 2002, Pastor et al., 2003] and Second-Order Cone Programming problems [Makrodimopoulos and Martin, 2006, Bisbos and Pardalos, 2007], and the problem size which can be handled has increased significantly. Even though many different element types had been formulated, no real 3D modeling capabilities existed because the different elements

had been designed separately with little focus on interaction. The disk element was combined with bars and beams but still only in 2D, [Poulsen and Damkilde, 2000].
In 2007 a 3D beam element for reinforced concrete was formulated, based on a rectangular 3x3 zone model, [Niebling et al., 2007]. The zone model utilized the previously established yield surfaces for reinforced concrete disks [Nielsen, 1999] in the zones and thereby circumvented the direct formulation of the total yield surface for the beam with all of its special cases. Using the same approach, a shell element was then established on the basis of zone models, once again utilizing the disk yield surfaces. The combination of the beam element and the shell element made it possible to analyze 3D structures. The disk yield surfaces were formulated using second-order cone programming so that real size structures could be handled. In order to evaluate the assumptions made in the zone models of the 3D beam element and the shell element, a solid 3D modelling tool is required. In the area of geotechnics, solid 3D elements have been established in which the Modified Coulomb criteria is formulated as a Semidefinite Programming (SDP) problem, see [Bisbos and Pardalos, 2007, Krabbenhft et al., 2008, Martin and Makrodimopoulos, 2008]. Today only a few optimization programs are able to solve SDP problems and the present work uses SeDuMi [Sturm and Sturm, 1999, Plik, 2005] for this. SeDuMi is a software package that solves optimization problems over symmetric cones. It allows linear, quadratic, second order conic and semidefinite constrained optimization, and any combination of these. Yalmip [Lfberg, 2004] was used as the interface to the solver.
For reinforced concrete, the solid modelling in 3D of the reinforcement has to be addressed. This can be handled either by modelling each reinforcement bar with realistic dimensions or simply by smoothing the reinforcement over an area of the concrete and adding a tensile capacity in the direction of the reinforcement corresponding to the amount of reinforcement [Nielsen, 2008]. The second choice is the basis for the solid 3D modelling of reinforced concrete in the present work. This makes geometric modelling of the structure much simpler but it also introduces some assumptions concerning the transfer of stresses between the concrete and the reinforcement.
In this paper, the second example addresses this topic and shows that accurate modelling can be performed based on smoothing out the effect of the reinforcement. The first example verifies that the material model works as intended and the results are compared with some analytical solutions. In the last example a complex console beam is analyzed and the results are compared to hand calculations.

2 Finite Element Formulation of the Lower Bound Theorem

In limit analysis two different theorems are used to determine the collapse load of a structure. These are referred to as the upper- and lower bound theorems. This paper focuses on how the lower bound theorem can be implemented into a general finite element system.
The lower bound theorem of limit analysis states that a statically admissible and safe stress distribution in a structure will not be able to cause collapse in the structure. Lets assume that a given distribution of stresses $\lambda\sigma$ and loads λf, where $\lambda > 0$ is the load factor, fulfils the statement above. Then all distributions $\lambda\sigma$, λf up to a certain load factor value λ_p^- will be a lower bound solution. Because different stress distributions may give different lower bounds λ_p^- for the collapse load factor λ_p the lower bounds are maximized i.e. $max(\lambda_p^-)$. If all stress distributions are investigated, this maximum must be equal to λ_p. This leads to an optimization problem which is often difficult, if not impossible, to solve manually. The above also holds true if only a part of the external loading is proportional and the rest is constant. The constant load must of course be of a magnitude such that it alone will not cause collapse in the structure.
In this paper we present a finite element framework for limit analysis of solid reinforced concrete structures. The three dimensional stress field is approximated using four node tetrahedral elements with linear stress variation. Because of the convex properties of the yield criterion, a strict lower bound solution can be obtained by enforcing the yield criterion at the four corner nodes. For higher order elements, the yield

criterion should be enforced at several points within the elements and adaptive methods should be used to ensure that the yield criterion is not violated. Strict lower bound solutions can also be obtained by using elements with constant stress distributions, but the need for discontinuities at the boundaries can cause problems. This makes elements with a linear stress distribution attractive for lower bound implementations. The following sections give a brief overview of the implementation and appendix A describes the numerical matrix implementation of the framework. For more details, see [Lyamin et al., 2001].

2.1 Statically admissible stress distribution

As prescribed by the lower bound theorem, the chosen stress distribution must be statically admissible. For this requirement to be fulfilled when implemented in a finite element system, the internal stress state within each element as well as the inter-element stresses must be in equilibrium and the static boundary conditions must be satisfied.

2.1.1 Internal element equilibrium

Let the three dimensional stress state at a point within the volume be defined by the stress tensor

$$\sigma_{ij} = \begin{bmatrix} \sigma_x & \tau_{xy} & \tau_{xz} \\ \tau_{yx} & \sigma_y & \tau_{yz} \\ \tau_{zx} & \tau_{zy} & \sigma_z \end{bmatrix} \tag{2.1}$$

where σ_i are the normal stresses and τ_{ij} for $i \neq j$ are the shear stresses. From stress equilibrium considerations at a point it is found that σ_{ij} is symmetric i.e. $\sigma_{ij} = \sigma_{ji}$. The equilibrium equation can, with application of index and summation convention for i and j, be written as

$$\sigma_{ji,j} + \lambda f_i + f_i^0 = 0 \tag{2.2}$$

where f_i^0 and f_i are the constant and proportional body force per unit volume respectively and λ is the load factor. The tensor notation $\sigma_{ji,j}$ refers to the partial derivative of component ji with respect to direction j. For the four node tetrahedral element with a linear stress field, the partial derivatives become constant and the body force field is then approximated by piecewise constant body forces. Because equilibrium must be insured along all directions, three equilibrium equations per element are required.

2.1.2 Inter-element equilibrium

Inter-element equilibrium is ensured by requiring traction continuity at the interface between adjacent elements. Fig. 1 shows two tetrahedral elements which share a common boundary defined by the vertices v_2,v_3 and v_5. If p is a point on the interface and the stress state in each element at that point is defined by σ_{ij}^{p1} and σ_{ij}^{p2} respectively, the inter-element equilibrium can be written as

$$(\sigma_{ij}^{p1} + \sigma_{ij}^{p2}) n_j = \lambda t_i + t_i^0 \tag{2.3}$$

where n is the unit normal vector of the plane defined by v_2,v_3 and v_5. t_i^0 and t_i are the constant and proportional surface tractions at the point p and λ is the load factor. As seen here, the stress state does not have to be continuous from one element to the next as long as the sum of tractions at the shared boundary are equal to the external load. Nodes are therefore made unique to each element instead of being unique to a spatial coordinate set as in a standard finite element model. The discontinuities in the complete stress field provide greater freedom in the choice of a statically admissible stress field. Since the stress state varies linearly over the face of an element, it is sufficient to ensure continuity at three distinct points of the face. The three corner nodes defining the face is a natural choice hereof and since equilibrium must be fulfilled in all three directions, a total of nine equations per system side are added to the set of equilibrium equations.

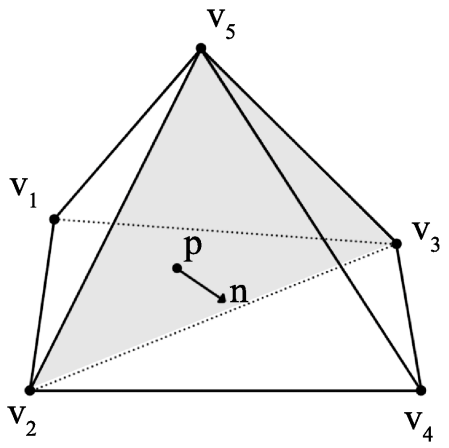

Figure 1: Inter-element equilibrium is ensured by traction continuity at the interfaces between elements.

2.1.3 Static boundary conditions

The static boundary constraints are, similar to the inter-element equilibrium in Eq. (2.3), defined by surface tractions and can be applied in either global- or local coordinates. Surface traction equilibrium in global coordinates gives

$$\sigma_{ij} n_j = \lambda t_i + t_i^0 \tag{2.4}$$

where t_i and t_i^0 are the proportional and constant surface tractions, n_j is the outward unit surface normal and λ is the load factor. In local coordinates, the stresses must be transformed using the transformation matrix $S = [n'_\sigma, n'_{\tau_\xi}, n'_{\tau_\zeta}]$ where n_σ is the surface normal and $n_{\tau_\xi}, n_{\tau_\zeta}$ are vectors defining the two shear directions. If one or more traction components are supported at a point on the boundary, the associated equations are removed from the system of equations, allowing the stresses to vary freely within the yield constraints. The resulting reactions will ensure equilibrium.

2.1.4 Safe stress distribution

A volumetric infinitesimal domain of concrete is reinforced in directions equivalent to the usual Cartesian coordinate system as shown on Fig. 2. The stresses at the boundary of the infinitesimal domain are given by $\lambda(\sigma_x, \sigma_y, \sigma_z, \tau_{xy}, \tau_{xz}, \tau_{yz})$ where λ is the load factor. The shear stresses in the rebars are disregarded and the normal stresses, σ_{si} for $i \in \{x, y, z\}$, are smoothed over the cross section area perpendicular to each of the three directions. This is standard practice in reinforced concrete analysis and a detailed study can be found in [Nielsen, 1999].

$$\begin{aligned} &\sigma_x = \sigma_{sx} A_{sx} + \sigma_{cx} \qquad \sigma_y = \sigma_{sy} A_{sy} + \sigma_{cy} \qquad \sigma_z = \sigma_{sz} A_{sz} + \sigma_{cz} \\ &\tau_{xy} = \tau_{cxy} \qquad \tau_{xz} = \tau_{cxz} \qquad \tau_{yz} = \tau_{cyz} \end{aligned} \tag{2.5}$$

where A_{sx}, A_{sy} and A_{sz} are the reinforcement areas per unit area perpendicular to the three axis and (σ_{cx}, σ_{cy}, σ_{cz}, τ_{cxy}, τ_{cxz}, τ_{cyz}) are the concrete stresses. If the reinforcement is not aligned with the Cartesian coordinate system, the equivalent orthotropic reinforcement values are used, [Nielsen, 2008].
To obtain a strict lower bound solution, the yield criteria for both concrete and reinforcement must be adhered to at all points within the solid. Since the shear stresses in the reinforcement are disregarded, the

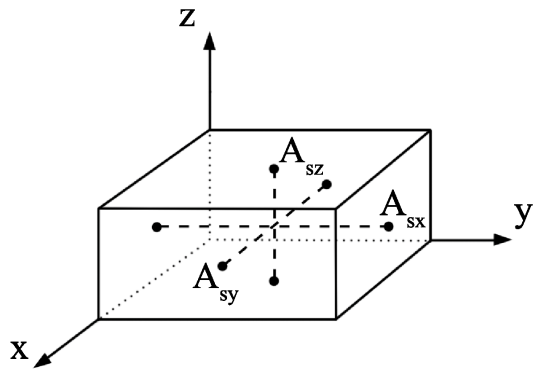

Figure 2: Solid concrete with orthogonal reinforcement.

yield criterion for the rebar's can be formulated as simple upper- and lower bounds on the normal stress components as

$$f_{Yc,i} \leq \sigma_{si} \leq f_{Yt,i} \qquad i \in \{x,y,z\} \tag{2.6}$$

where $f_{Yc,i}$ and $f_{Yt,i}$ are the compression and tensile strengths respectively.

2.2 Modified Coulomb material using Semidefinite Programming

The Modified Coulomb criterion is described in [Nielsen, 1999] and is the most commonly used yield criterion for limit analysis of concrete structures. It consists of the Coulomb sliding failure criterion combined with a separation criterion. If tensile stresses are positive, the sliding failure can, in the three dimensional case, be written as

$$k\sigma_{c1} - \sigma_{c3} \leq f_c \tag{2.7}$$

where σ_{c1} and σ_{c3} are the largest and smallest principal stress respectively. f_c is the uniaxial compression strength of the concrete and k is a parameter determined from the frictional angle ,ϕ, as

$$k = \frac{1 + sin(\phi)}{1 - sin(\phi)} \tag{2.8}$$

k is here set to 4 which results in a value of ϕ of approximately $\phi = 37°$.
The separation criterion can be formulated as

$$\sigma_{c1} \leq f_A \tag{2.9}$$

where f_A is the separation strength, which for a typical concrete is equal to the uniaxial tensile strength, f_{ct}, of the concrete.

2.2.1 Semidefinite Programming (SDP)

Semidefinite Programming (SDP) is a relatively new branch of convex optimization problems. Even though SDP problems was known in the 1960's it was not until 1988 that it was demonstrated that interior-point methods for Linear Programming (LP) could be generalized to all convex optimization problems

[Nesterov and Nemirovsky, 1988], and it became possible to solve SDP problems efficiently. SDP is now applied in such diverse fields as finance, control engineering and graph theory. The application of SDP in limit analysis of Coulomb materials has been described by several authors, e.g. [Krabbenhft et al., 2008], [Martin and Makrodimopoulos, 2008] and[Bisbos and Pardalos, 2007].
Semidefinite Programming considers the problem of minimizing a linear function of the variables $x \in \Re^m$ subjected to a set of matrix inequalities and equality constraints as

$$\begin{array}{ll} \text{minimize} & c^T x \\ \text{subject to} & F(x) \succeq 0 \\ & Ax = b \end{array} \tag{2.10}$$

where the constraint function

$$F(x) = F_0 + \sum_{i=1}^{m} x_i F_i \tag{2.11}$$

is an affine combination of symmetric matrices. The problem data are the vectors $c \in \Re^m$ and $b \in \Re^k$, the matrix $A \in \Re^{k \times m}$ and the $m+1$ symmetric matrices $F_0, \ldots, F_m \in \Re^{m \times m}$. The inequality $F(x) \succeq 0$ is called a *Linear Matrix Inequality* or *LMI* and states that the constraint function is positive semidefinite, i.e. $x^t F(x) x \geq 0$ for all $x \in \Re^m$. Since positive semidefinite cones are convex, [Vandenberghe and Boyd, 1996], the SDP is a convex optimization problem.
Of course if the matrix $F \succeq 0$ and I is a unit matrix in $\Re^{m \times m}$ then

$$-F + \lambda_F I \succeq 0 \tag{2.12}$$

for all $\lambda_F \geq \lambda_{max}$ where λ_{max} is the largest eigenvalue of F.

2.2.2 SDP formulation of the Modified Coulomb criterion

As described in section 2.1.4 the stress state at a point consists of a combination of concrete and reinforcement stresses, Eq. (2.5). The reinforcement constraints can simply be formulated as linear inequalities based on Eq. (2.6) but the Modified Coulomb criterion must be cast as semidefinite constraints.
The Coulomb sliding criterion in Eq. (2.7) can be written as a combination of two positive semidefinite cones, see [Krabbenhft et al., 2008, Martin and Makrodimopoulos, 2008, Bisbos and Pardalos, 2007]. Eq. (2.13) and 2.14 shows this formulation using the concrete material parameters f_c and k as posed by [Nielsen, 2008].

$$\sigma_{ij}^c + k\alpha_1 I \succeq 0 \tag{2.13}$$

$$-\sigma_{ij}^c + \left(\frac{f_c}{k} - \alpha_1\right) I \succeq 0 \tag{2.14}$$

where α_1 is an auxiliary variable and σ_{ij}^c is a stress tensor containing the concrete stresses.
In order to prove that Eq. (2.13) and Eq. (2.14) are equal to Eq. (2.7) we use the fact that a positive semidefinite matrix can only have non-negative eigenvalues, [Vandenberghe and Boyd, 1996]. Eq. (2.13) and Eq. (2.14) is therefore equal to

$$\sigma_{c3} + k\alpha_1 \geq 0$$

$$-\sigma_{c1} + \left(\frac{f_c}{k} - \alpha_1\right) \geq 0$$

Isolation of α_1 in the inequalities above yields

$$-\frac{\sigma_3}{k} \leq \alpha_1 \leq -\sigma_1 + \frac{f_c}{k} \Rightarrow$$
$$-\frac{\sigma_3}{k} \leq -\sigma_1 + \frac{f_c}{k}$$

which can be rewritten as

$$k\sigma_{c1} - \sigma_{c3} \leq f_c$$

which is the Coulomb criterion from Eq. (2.7).
The separation criterion given in Eq. (2.9) can be formulated directly as an LMI constraint that takes the form

$$-\sigma_{ij}^c + \boldsymbol{I}\, f_A \succeq 0 \tag{2.15}$$

Further improvements can be made to the model by expressing Eq. (2.14) and Eq. (2.15) in terms of another auxiliary variable α_2 as

$$\begin{aligned} \sigma_{ij}^c - \alpha_2 \mathbf{I} &\preceq 0 \\ \alpha_2 &\leq f_A \\ \alpha_2 &\leq \frac{f_c}{k} - \alpha_1 \end{aligned} \tag{2.16}$$

thereby reducing the yield criterion from three LMI constraints to two LMI's and two linear inequality constraints, Eq. (2.13) and Eq. (2.16).

2.3 Solving lower bound problems using the YALMIP interface

Implementing the linear constraints posed by the equilibrium constraints and the yield criteria for the reinforcement is straightforward as they are part of the general formulation of the SDP problem, Eq. (2.10). Most SDP solvers only allow for a single LMI constraint on a set of variables, so the Modified Coulomb criterion described in section 2.2.2 is more difficult to implement. Instead of reformulating the problem to fit the format of a specific solver, it is chosen to use the YALMIP interface, [Lfberg, 2004]. YALMIP provides a parametric modelling language that giving a high-level model for defining different types of optimization problems. One of the main advantages of using YALMIP is that it takes care of all the low-level modelling and is designed to obtain as efficient and numerically sound model as possible. Another advantage is that it supports a wide range of solvers, making it possible to switch from one solver to another by simply changing the optimizer settings. YALMIP was implemented as a MatLab^{TM} toolbox.

3 Numerical Examples

This section shows how the numerical lower bound model presented here can be used to solve some basic examples. There are currently only a few solvers capable of solving SDP problems. Here we use the open source solver SeDuMi, [Sturm and Sturm, 1999, Plik, 2005] which is implemented as a MatLab^{TM} toolbox [1]. All default settings are used except for the way SeDuMi handles free variables. By default, SeDuMi places free variables in a quadratic cone which caused stability problems. These problems were resolved by forcing SeDuMi to split the free variables instead of placing them in cones.

[1] The 64 bit version of SeDuMi bundled with CVX is used [Grant and Boyd, 2008a, Grant and Boyd, 2008b].

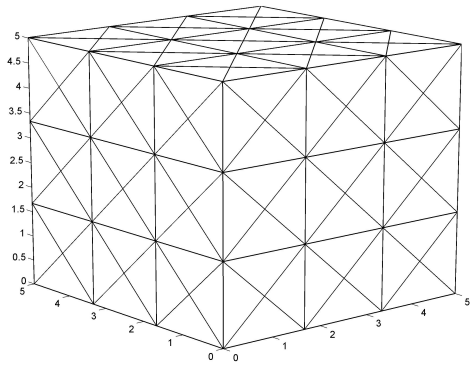

Figure 3: Square block of reinforced concrete discretized using a structured mesh.

3.1 Numerical determination of yield condition for a reinforced solid

In the first example, the numerical model will be used to determine the yield conditions for a solid block of reinforced concrete with various types of reinforcement. For these tests, a cubic block with a side length of 5 is modelled using a structured mesh of $3 \cdot 3 \cdot 3 \cdot 24 = 648$ elements as shown in Fig. 3. The yield surface is a function of the six independent stress parameters in the stress tensor σ_{ij}. To simplify visualization, only a section in the $\sigma_x \tau_{xy}$-plane is determined here. This is done by applying cosine- and sine weighted values of σ_x and τ_{xy} to the block

$$\tau_{xy}^0 = \lambda \ sin(v) \qquad \sigma_x^0 = \lambda \ cos(v) \tag{3.1}$$

where $0 \leq v \leq \pi$.
For all tests the material parameter k is set equal to 4 and unless otherwise is noted, the separation strength f_A is set to zero. The reinforcement degree is defined as

$$\Phi_i = \frac{A_{si} f_{Yi}}{f_c} \tag{3.2}$$

3.1.1 Isotropic Disc

In [Nielsen, 1999] the yield condition for a reinforced concrete disc was determined based on the lower bound theorem. In this example we will show how the yield surface for a disk can be replicated using the numerical model. The complete surface is complex, but Fig. 2.2.11 in [Nielsen, 1999] shows the curve of intersection between the yield surface and the $\sigma_x \tau_{xy}$-plane, and the expression for this curve is summarized below

$$\tau_{xy}(\sigma_x) = \begin{cases} \sqrt{\Phi f_c (\Phi f_c - \sigma_x)} & \text{if } -(1-2\Phi) f_c \leq \sigma_x \leq \Phi f_c \\ \sqrt{\Phi (1-\Phi)} f_c & \text{if } -f_c \leq \sigma_x \leq -(1-2\Phi) f_c \\ \sqrt{\frac{1}{4} f_c^2 - \left[\sigma_x + \left(\frac{1}{2} + \Phi\right) f_c\right]^2} & \text{if } -(1+\Phi) f_c \leq \sigma_x \leq -f_c \end{cases}$$

The isotropic disc is easily modelled by simply removing the reinforcement in the direction perpendicular to the loaded plane, in this case the z-direction

$$\Phi_x = \Phi_y = 0.1$$
$$\Phi_z = 0.0$$

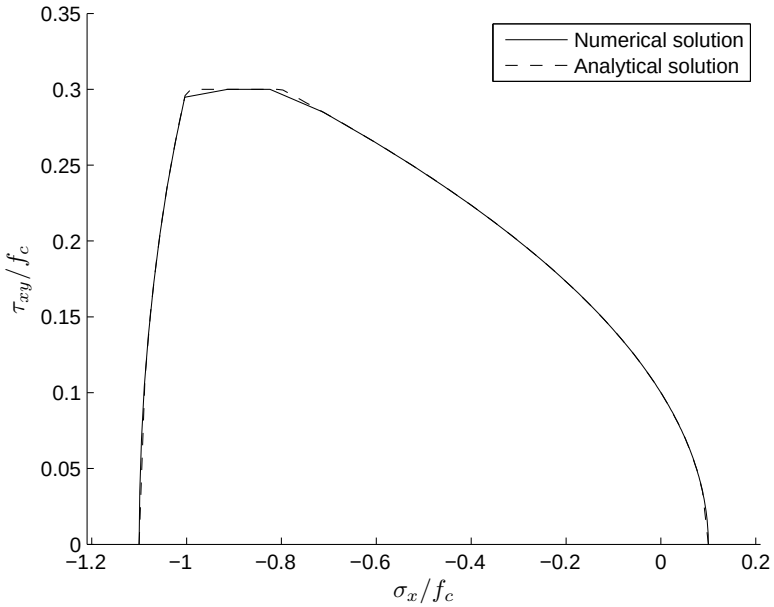

Figure 4: Comparison between the numerical and the analytical yield surface for a reinforced concrete disk. The numerical curve is determined using 100 linearly spaced values of v in the interval from 0 *to* π.

Fig. 4 shows the $\tau_{xy}\sigma_x$-section of the yield surface for both the analytical and the numerical model. As seen from the figure, very good agreement between the analytical and the numerical model was achieved. The slight differences observed on the figure are caused by the subdivision with which the numerical curve is generated.

3.1.2 Isotropic Solid

The previous example showed how the numerical model could be used to recreate a known yield condition for an isotropic disc. This example investigates the yield conditions for an isotropic solid of reinforced concrete, i.e.

$$\Phi = \Phi_x = \Phi_y = \Phi_z = 0.1$$

Fig. 5 shows the $\tau_{xy}\sigma_x$-section of the yield surface as determined by the numerical analysis and compared with the disc solution, some tri-axial effects are seen. The effects on the uniaxial compression strength should be noted: it is here computed to 1.5. This is identical to the theoretical value which can be found by assuming full utilization of the transverse reinforcement

$$\sigma_{sy} = \sigma_{sz} = A_s f_Y \tag{3.3}$$

The concrete stress components in the y- and z-direction can be determined from Eq. (2.5) when $\sigma_y^0 = \sigma_z^0 = 0$ as

$$\sigma_{cy} = \sigma_{cz} = -A_s f_Y \tag{3.4}$$

With no shear stresses acting on the cube, the normal stresses are equal to the principal stresses (there are no off-diagonal elements in the concrete stress tensor). Since the uniaxial compression strength is greater than

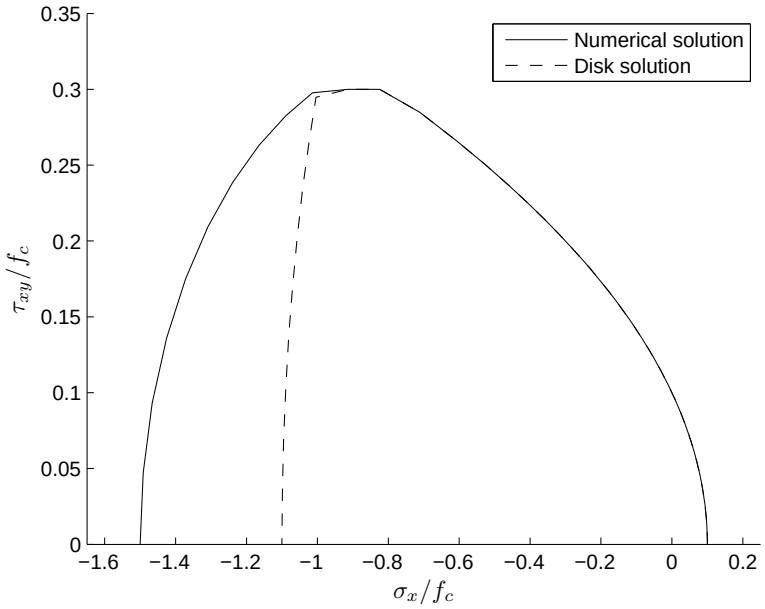

Figure 5: The yield surface of a reinforced concrete solid determined using the numerical model. The numerical curve is determined using 100 linearly spaced values of v in the interval 0 *to* π.

the transverse compression generated by the reinforcement, the principal stresses in the concrete material become

$$\sigma_{c1} = \sigma_{c2} = -A_s f_Y \qquad \sigma_{c3} = \sigma_x^0 - (-f_Y)A_s \tag{3.5}$$

The uniaxial compression strength can be determined from the sliding criterion given in Eq. (2.7).

$$\sigma_x^0 \geq -f_c(1+\Phi(k+1)) = -1.5 \cdot f_c \tag{3.6}$$

3.2 Anchorage Problem

Even though the method presented here assumes perfect bonding between the rebars and the concrete, attention must be paid to how rebars are anchored when creating detailed structural models. In this example we will investigate how the separation strength of the concrete and the area over which the rebars are smoothed effects the anchorage capacity of a rebar. An in-depth study of the subject can be found in [Nielsen, 1999] and [Andreasen, 1989], were both local and global failure modes are analyzed theoretically. Here we will only consider the global failure modes in the concrete surrounding the rebar.
A rebar with diameter d and length l is cast into a cuboid concrete specimen with side lengths $2c+w$ as shown on Fig. 6. The specimen is constrained from movements along the longitudinal direction and the rebar is subjected to a tensile force p as illustrated on the figure. In this example, the concrete compression strength is set equal to $f_c = 8.3$ *MPa* and the tensile strength of the reinforcement is $f_Y = 400$ *MPa*. The length of the test specimen is $l = 800$ *mm*, the diameter of the rebar is $d = 16$ *mm* and the cover thickness is kept constant at $c = 100$ *mm*. The rebar is smoothed over a square area with side length w as shown on the figure.
To illustrate the effect of the separation strength, f_A, on the anchorage of a rebar in pure concrete, the tensile

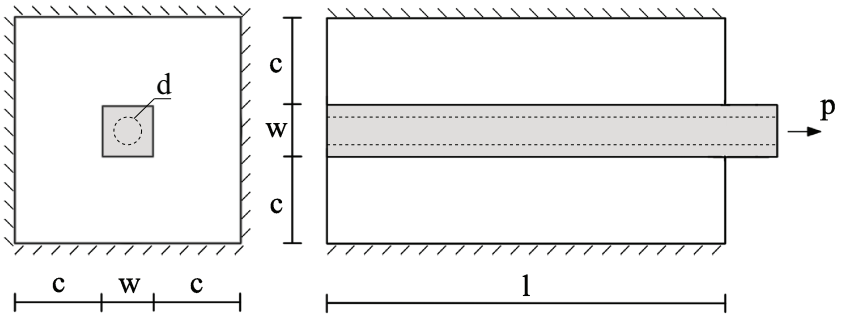

Figure 6: Cuboid test speciment for a smoothed rebar placed in unreinforced concrete.

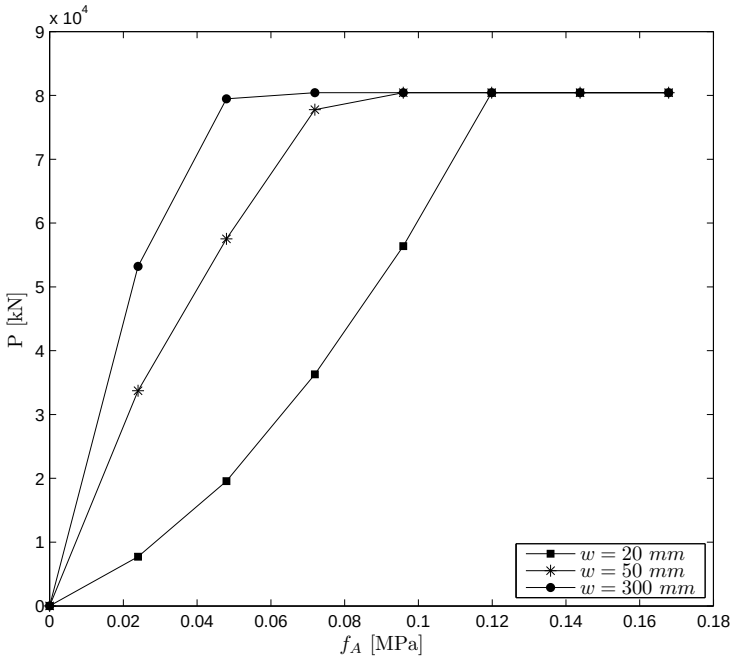

Figure 7: Anchorage capacity of the rebar as function of f_A for $w = 50$ mm and $w = 300$ mm

capacity of the rebar is determined for increasing values of f_A. Fig. 7 shows this relation when the rebar is smoothed over a 50 $mm \times 50$ mm and a 300 $mm \times 300$ mm area. From the figure it is seen that some separation strength must be present in the concrete for it to carry the shear stresses along the rebar while the strength needed to fully anchor the rebar is relatively low ($f_A \leq 0.1$ MPa). The area over which the rebar is smoothed also effects how much separation strength is required. This is caused by the larger area over which the stresses are transferred from the rebar to the concrete, resulting in smaller shear stress values. As illustrated here, it is important to keep in mind how rebars are anchored when creating highly detailed solid models. In practical applications, some form of reinforcement providing confinement is often present in the structure thereby eliminating the need for tensile stresses in the concrete. In some cases though a separation strength is required to obtain a reasonable anchorage of the rebars. If it is undesirable to apply a separation strength to all of the concrete, a small zone surrounding the end of the rebar could be modelled in which the shear stresses could be transferred from the rebar and into the concrete.

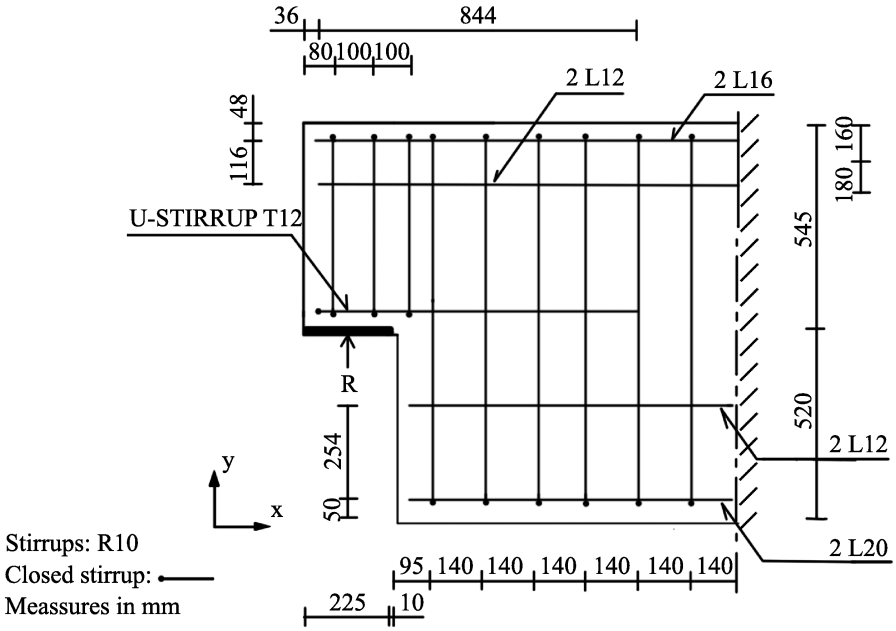

Figure 8: Console beam with complex reinforcement.

3.3 Console Beam

In the final example we will use the solid elements to determine the collapse load, R, of the console beam shown on Fig. 8. This problem has been analyzed by manual calculations using both upper- and lower bound methods in [Feddersen, 1994] and the results obtained will be compared to the numerical results determined in this example.

The concrete material is similar to that used in the previous example with a compression strength of $f_c = 8.3$MPa, and the tensile strengths of the L- and T-bars are also identical to those used previously, i.e. $f_Y = 400$MPa. The tensile strength of the stirrups is 171MPa. The compression strength of the reinforcement is set to zero so it only contributes to carry the tensile stresses in the structure. The model is created and meshed using the Abaqus CAE software package. Because the console is symmetric around the centre xy-plane only one half is modelled.

All reinforcement bars are smoothed over a $50mm \times 50mm$ area perpendicular to their direction. Fig. 9 shows the geometric model with the concrete material made transparent to show the internal rebars. The model is analyzed using both a 5501 element mesh and a 13480 element mesh (shown on Fig. 10). The load is applied as a uniform pressure on the underside of the console and the console beam is supported in the x- and y-direction at the cross section as shown on Fig. 8. All tests were performed on a Mac Pro Workstation (2 x 2.8 GHz Quad Core Xeon, 6 GB RAM) using Windows XP Pro x64 running under Bootcamp. The collapse load of the coarser model was found to be $113kN$ while the finer model was found to have a slightly higher collapse load of $128kN$. These results correspond very well to those found in [Feddersen, 1994] where lower- and upper bound vaules of $106kN$ and $113kN$ respectivly were found. It should be noted, that the numerical lower bound method results in a collapse load that is greater than the upper bound method used in [Feddersen, 1994]. This increased capacity is caused by the triaxial effects that occurs in the structure. To illustrate the stress state in the console, the smallest principal stress component is shown in Fig. 11. The figure shows that there is a band running from just below the console towards the top of the beam in which the stress component is close to zero. This indicates that a crack could form in this region which corresponds well with the optimal fracture line found in [Feddersen, 1994] and the crack

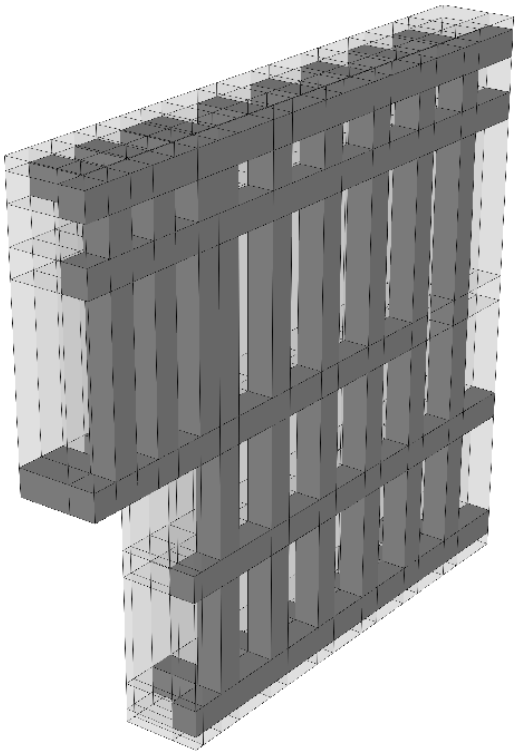

Figure 9: Geometric model of console beam.

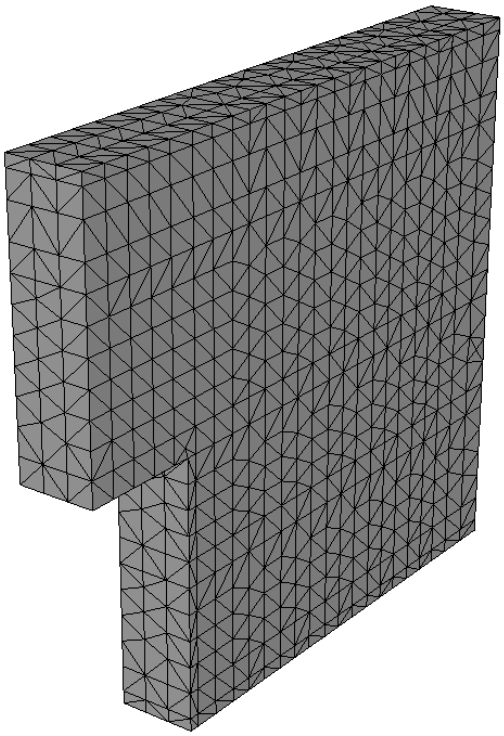

Figure 10: Meshed model of the console beam

pattern observed in the actual structure.

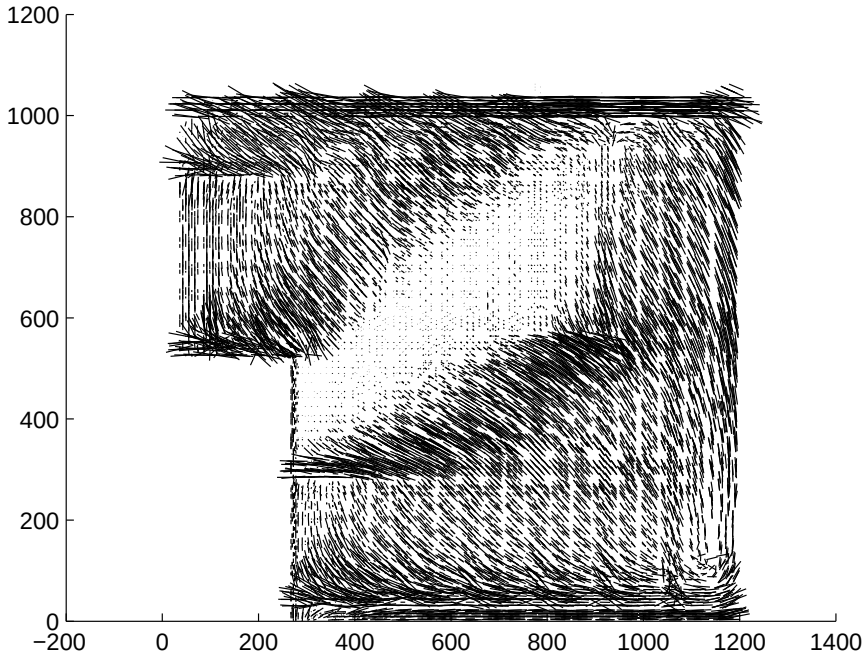

Figure 11: Plot of the third principal stress component. Vectors are used for indicating the direction and magnitude of the stresses.

4 Conclusions

We have shown a method for performing limit state analysis of solid reinforced concrete structures using a general finite element framework based on lower bound elements. To simplify the modelling of complex structures, a material model in which there is both reinforcement and concrete was considered as a homogeneous material. The stress state in this material was defined by a combination of concrete- and reinforcement stresses and yield criteria were imposed on these stress components separately.
The method uses Semidefinite Programming algorithms for solving the optimization problem posed by the lower bound method. The solver used here (SeDuMi) has proven very efficient and robust for these types of problems and models with more than 10.000 elements has been analyzed successfully on a standard workstation grade computer. The use of YALMIP as the interface made it easy to formulate the optimization problem and it's translation into the underlying solver has been very efficient.
The numerical model was verified by comparison with well-known analytical solutions and good correlation was found between the results. The approximation of considering the reinforcement and concrete as a unified material was also tested and the results were very encouraging, and comparison between numerical and manual results are very good.

A Matrix Implementation

This appendix briefly describes the matrix implementation of the solid elements presented here. Since implementation of the non-linear material constraints highly depends on the chosen solver, only the equilibrium equations and continuity conditions will be described here. In the present work, YALMIP [Lfberg, 2004]

was used as interface to the optimization software which greatly simplifies the process of applying constraints to the stress variables. Below is a short description of how the equilibrium equations and inter-element continuity condition are assembled.
Initially we define a vector containing the total stress parameters for all elements $1,2,\cdots,m$ in the system

$$\Psi = \left[\sigma^1, \sigma^2, \cdots, \sigma^m\right]^T \tag{A.1}$$

where m is the number of elements and σ^i is a vectors containing the 24 stress parameters for each element

$$\sigma^i = [\sigma_x^{1-4}, \sigma_y^{1-4}, \sigma_z^{1-4}, \tau_{xy}^{1-4}, \tau_{xz}^{1-4}, \tau_{yz}^{1-4}]^T \tag{A.2}$$

The internal stress state in each element must be in equilibrium. Because the element has a linear stress distribution, the equilibrium conditions described in section 2.1.1 needs only to be fulfilled at one point within each element. The system equilibrium matrix H_{eq} can be assembled as a diagonal matrix containing the equilibrium conditions associated with each element:

$$H_{eq} = \begin{bmatrix} \hat{\sigma}_{ij,j}^1 & & & \\ & \hat{\sigma}_{ij,j}^2 & & \\ & & \ddots & \\ & & & \hat{\sigma}_{ij,j}^m \end{bmatrix}$$

where $\hat{\sigma}_{ij,j}^i$ is a 3×24 matrix containing the partial derivatives of the stress tensor at the geometric center point of the element, see Eq. (2.2). The equilibrium conditions can be written as

$$H_{eq}\Psi + \lambda R_f + R_f^0 = 0 \tag{A.3}$$

where R_f and R_f^0 are the proportional and constant body forces and λ is the load factor. In addition to the internal equilibrium equations defined above, the stress state on each of the system faces must also be in equilibrium, see section 2.1.2 and 2.1.3. All element contributions to the system faces are assembled in the H_{cont} as illustrated below

$$\begin{matrix} & e_i & \cdots & e_j & \\ H_{cont} = & \begin{bmatrix} & & & \\ N_{ik} & \cdots & N_{jk} & \\ & & & \end{bmatrix} & & & \leftarrow f_k \end{matrix} \tag{A.4}$$

Here, N_{ik} defines the contribution from element e_i to system face f_k and N_{jk} the contribution from element e_j to the face f_k. Since the stress state varies linearly over a face, continuity must be ensured at all three face nodes, making N a 9×24 matrix. The system face equilibrium conditions can now be defined as

$$H_{cont}\Psi = \lambda R_t + R_t^0 \tag{A.5}$$

where R_t and R_t^0 are the proportional and constant surface tractions respectively.
The material stress parameters are, similarly to the total stress vector defined in Eq. (A.1), assembled into separate vectors

$$\Psi_c = \left[\sigma_c^1, \sigma_c^2, \cdots, \sigma_c^m\right]^T \tag{A.6}$$

$$\Psi_s = \left[\sigma_s^1, \sigma_s^2, \cdots, \sigma_s^m\right]^T \tag{A.7}$$

where σ_c^i and σ_s^i are the concrete and reinforcement stresses for element i. The total stresses are equal to the sum of concrete stresses and equivalent reinforcement stresses $A_s\sigma_s$:

$$\Psi = \Psi_c + A_s\Psi_s \tag{A.8}$$

The equations Eq. (A.3), Eq. (A.5) and Eq. (A.8) are assembled into a system of equations as

$$\begin{bmatrix} H_{eq} & & & R_f \\ H_{cont} & & & -R_t \\ I & -I & -A_s & \end{bmatrix} \begin{bmatrix} \Psi \\ \Psi_c \\ \Psi_s \\ \lambda \end{bmatrix} = \begin{bmatrix} -R_f^0 \\ R_t^0 \\ 0 \end{bmatrix} \tag{A.9}$$

which can be implemented directly into the numerical solver.

References

[Anderheggen and Knopfel, 1972] Anderheggen, E. and Knopfel, H. (1972). Finite element limit analysis using linear programming. *International Journal of Solids and Structures*, 8(12):1413–1431.

[Andreasen, 1989] Andreasen, B. S. (1989). Anchorage of ribbed reinforcing bars. *Serie R - Danmarks Tekniske Hojskole, Afdelingen for Baerende Konstruktioner*, (238).

[Bisbos and Pardalos, 2007] Bisbos, C. and Pardalos, P. (2007). Second-order cone and semidefinite representations of material failure criteria. *Journal of Optimization Theory and Applications*, 134(2):275–301.

[Damkilde et al., 1994] Damkilde, L., Olsen, J. F., and Poulsen, P. N. (1994). A program for limit state analysis of plane, reinforced concrete plates by the stringer method. *Bygningsstatiske Meddelelser*, 65(1):1–26.

[Dantzig, 1963] Dantzig, G. B. (1963). *Linear programming and extensions*. Princeton University Press, Princeton, N.J.,.

[Feddersen, 1994] Feddersen, B. (1994). The theory of plasticity for concrete and reinforced concrete. *Bygningsstatiske Meddelelser*, 2-3-4:89–108.

[Fredsgaard and Kirk, 1979] Fredsgaard, S. and Kirk, J. (1979). Ruptus - et program til brudstadieberegninger. *ADB-Udvalget*.

[Grant and Boyd, 2008a] Grant, M. and Boyd, S. (2008a). Cvx: Matlab software for disciplined convex programming.

[Grant and Boyd, 2008b] Grant, M. and Boyd, S. (2008b). Graph implementations for nonsmooth convex programs. *Recent Advances in Learning and Control*, pages 95–110.

[Karmarkar, 1984] Karmarkar, N. (1984). A new polynomial-time algorithm for linear programming. *Combinatorica*, 4(4):373–395.

[Krabbenhft et al., 2008] Krabbenhft, K., Lyamin, A., and Sloan, S. (2008). Three-dimensional mohr-coulomb limit analysis using semidefinite programming. *Communications in Numerical Methods in Engineering*, 24(11):1107–1119.

[Krabbenhoft and Damkilde, 2002] Krabbenhoft, K. and Damkilde, L. (2002). Lower bound limit analysis of slabs with nonlinear yield criteria. *Computers and Structures*, 80(27-30):2043–2057.

[Krenk et al., 1994] Krenk, S., Damkilde, L., and Hoyer, O. (1994). Limit analysis and optimal design of plated with equilibrium elements. *Journal of Engineering Mechanics*, 120(6):1237–1254.

[Lfberg, 2004] Lfberg, J. (2004). Yalmip : A toolbox for modeling and optimization in matlab. In *Proceedings of the CACSD Conference*, Taipei, Taiwan.

[Lyamin et al., 2001] Lyamin, A. V., Sloan, S. W., and of Newcastle (N.S.W.)., U. (2001). *Lower bound limit analysis using nonlinear programming / A.V. Lyamin and S.W. Sloan*. Dept. of Civil, Surveying and Environmental Engineering, University of Newcastle, Callaghan, N.S.W. :.

[Makrodimopoulos and Martin, 2006] Makrodimopoulos, A. and Martin, C. M. (2006). Lower bound limit analysis of cohesive-frictional materials using second-order cone programming. *International Journal for Numerical Methods in Engineering*, 66(4):604–634.

[Martin and Makrodimopoulos, 2008] Martin, C. M. and Makrodimopoulos, A. (2008). Finite-element limit analysis of mohr-coulomb materials in 3d using semidefinite programming. *Journal of Engineering Mechanics*, 134(4):339–347.

[Nesterov and Nemirovsky, 1988] Nesterov, Y. and Nemirovsky, A. (1988). A general approach to polynomial-time algorithms design for convex programming. *Centr. Econ. & Math. Inst., USSR Acad. Sci., Moscow, USSR,*.

[Niebling et al., 2007] Niebling, J., Vinther, A., and Larsen, K. P. (2007). Numerisk modellering af plastiske betonkonstruktioner (in danish). Master's thesis, Department of civil engineering, Byg-DTU.

[Nielsen, 2008] Nielsen, L. O. (2008). Concrete plasticity notes. Technical report, Department of Civil Engineering, Byg-DTU.

[Nielsen, 1999] Nielsen, M. P. (1999). *Limit Analysis and Concrete Plasticity*. CRC Press.

[Pastor et al., 2003] Pastor, J., Francescato, P., and Thai, T.-H. (2003). Interior point optimization and limit analysis: An application. *Communications in Numerical Methods in Engineering*, 19(10):779–785.

[Plik, 2005] Plik, I. (2005). Addendum to the sedumi user guide. version 1.1.

[Poulsen and Damkilde, 2000] Poulsen, P. N. and Damkilde, L. (2000). Limit state analysis of reinforced concrete plates subjected to in-plane forces. *International Journal of Solids and Structures*, 37(42):6011–6029.

[Sturm and Sturm, 1999] Sturm, J. F. and Sturm, J. F. (1999). Using sedumi 1.02, a matlab toolbox for optimization over symmetric cones. *Optimization Methods and Software*, 11(1):625–653.

[Vandenberghe and Boyd, 1996] Vandenberghe, L. and Boyd, S. (1996). Semidefinite programming. *SIAM Review*, 38:49–95.

Paper II

"Limit Analysis of 3D Reinforced Concrete Frames"

K.P. Larsen, P.N. Poulsen & L. O. Nielsen

Submitted to: *Journal of Mechanical Engineering*

Limit Analysis of 3D Reinforced Concrete Frames

Kasper P. Larsen * Peter N. Poulsen †and Leif O. Nielsen ‡

October 15, 2010

Abstract

In this paper we present a new finite element framework for lower bound limit analysis of reinforced concrete beams subjected to loadings in three dimensions. The method circumvents the need for a direct formulation of a complex section force based yield criteria by creating a discrete representation of the internal stress state in the beam. The yield criteria are formulated and applied on a stress state level. The stress state is decomposed into concrete and reinforcement stresses and separate yield criteria are applied to each component. Simple limits are used on the reinforcement stresses and a modified Coulomb criterion is applied to the concrete stresses. The modified Coulomb criterion is implemented using Semidefinite Programming and an approximation using Second-Order Cone Programming is developed for improved performance. The element is verified by comparing the numerical results with analytical solutions.

Keywords *rigid perfect plasticity; limit analysis; numerical methods; semidefinite programming; second-order cone programming*

1 Introduction

The Finite Element Method (FEM) is the most common method for numerical analysis of structures, and it has been used for limit state analysis for several decades, [Anderheggen and Knopfel, 1972, Fredsgaard and Kirk, 1979]. Different lower bound element types such as beams [Damkilde and Hoyer, 1993], plates [Krenk et al., 1994], stringers [Damkilde et al., 1994] and disks [Poulsen and Damkilde, 2000, Makrodimopoulos and Martin, 2006] have been developed over the years. These elements all employed a yield criterion based on sectional forces. The disadvantage of this approach is, that construction of the complete yield surface can become very difficult, especially if the element is subjected to loadings in three dimensions. In 2007, [Niebling et al., 2007] presented a 3D beam element which employed a discrete zone model to define the internal stress state in a beam. The yield criterion was then applied at the stress state level, thereby circumventing the need for a direct formulation of the section level yield criteria. The element presented by [Niebling et al., 2007] utilized a 3×3 zone model which allowed for modeling of rectangular beams with a simple reinforcement layout. Here, we will expand on the previous work by extending the method to handle more general cross sections. We will also address some of the simplifications made by [Niebling et al., 2007] in which the full tri-axial stress state in the beam was not accounted for. Where [Niebling et al., 2007] utilized the simplified yield criterion for reinforced concrete disks, [Nielsen, 1999], we will decompose the total stresses into

*Industrial Ph.D. Candidate, Ramboll Denmark, Hannemanns Allé 56, DK-2300 København S, Denmark, Department of Civil Engineering, Technical University of Denmark, DK-2800 Kgs. Lyngby, Denmark. E-mail: kpl@ramboll.dk.

†Associate Professor, Department of Civil Engineering, Technical University of Denmark, DK-2800 Kgs. Lyngby, Denmark. E-mail: pnp@byg.dtu.dk.

‡Associate Professor, Department of Civil Engineering, Technical University of Denmark, DK-2800 Kgs. Lyngby, Denmark. E-mail: kpl@byg.dtu.dk.

concrete- and reinforcement stresses and apply the yield criteria separately on these. This approach was used by [Larsen et al., 2009], in which an element for analysis of solid reinforced concrete structures was presented. The modified Coulomb failure criterion is applied to the concrete while simple limits are applied to the reinforcement.
Limit state analysis of reinforced concrete structures always result in a convex optimization problem. Recent advances in optimization algorithms and computational power have made it possible to solve medium to large-scale problems with complex yield criteria within reasonable time. The major challenge here is to establish a numerical formulation of the yield criteria, which is compatible with the optimization algorithms available. Linear Programming (LP) was a favorable technique in the 1970's where the simplex method [Dantzig, 1963] was used. Non-linear yield criteria had to be linearized to fit the structure of an LP problem, which often caused significant overhead. The Interior-Point method [Karmarkar, 1984] came about in the early 1980's and was capable of solving larger LP problem more efficiently than the simplex method. In 1988, [Nesterov and Nemirovsky, 1988] showed that the Interior-Point method could be generalized to handle non-linear constraints which lead to Second-Order Cone Programming (SOCP) and Semidefinite Programming (SDP). Here we will implement the modified Coulomb criterion using SDP as described in [Larsen et al., 2009]. We will also develop an approximate method based on SOCP, which can be used in special cases and solves faster and more efficiently.

2 Lower Bound Limit Analysis

The 3D beam element presented in this paper is an equilibrium element. Its application is based on the lower bound theorem, which states that *a safe and statically admissible stress distribution will not be able to cause collapse in a structure*. This encompasses all solutions that fulfils the equilibrium equations, static boundary conditions and does not violate the yield criterion at any point within the structure. Because the yield criterion is convex, the lower bound problems can be posed as convex optimization problems. Several numerical methods for solving convex optimization problems exist and, depending on the properties of the problem, different methods should be employed. The method required for solving lower bound problems is determined by the chosen yield criterion. Section 4 describes how the yield criterion employed in the beam model can be formulated as Semidefinite Programming (SDP) and Second-Order Cone Programming (SOCP) problems. These types of optimization problems will be further introduced in the next section.

2.1 Convex Optimization Problems

Due to the nature of lower bound limit analysis, numerical methods for solving convex optimization problems plays an important role in such analysis types. Especially Second-Order Cone Programming (SOCP) and Semidefinite Programming (SDP) are of great importance for analysis of reinforced concrete structures. Both SOCP and SDP problems can be solved using the Interior-Point method [Karmarkar, 1984, Nesterov and Nemirovsky, 1988], and a number of free and commercial solvers are capable of handling these types of problems. The increase in hardware- and algorithm performance over the past years has made it possible for engineers to solve medium to large-scale problems. In [Vandenberghe and Boyd, 1996] a convex optimization problem is defined as a linear function $f_0(x)$ of the variables $x \in \Re^n$ which is sought minimized when subjected to linear equality constraint functions $h_i(x)$ and non-linear inequality constraint functions $f_i(x)$, $i = \{1,2,\cdots m\}$. We will here use a formulation, which is more related to the nature of the

lower bound limit analysis problems

$$\begin{aligned} &\text{minimize} && -\lambda \\ &\text{subject to} && -R\,\lambda + H\,\Psi = R_0 \\ & && \Sigma \in C_t \end{aligned} \tag{2.1}$$

where λ is the scalar load factor sought maximized (by minimizing the negative load factor we will find the maximum load capacity) and the vector Ψ contains the n stress parameters used to define the stress state within the structure. The matrix H holds the equilibrium equations while the vectors R and R_0 are the proportional and constant load vectors respectively. Σ is the stress state at a number of control points within the structure and it is constrained by a set of convex cones, C_t. The stress state σ in a point is found from interpolation of the stress parameters as

$$\sigma = N\,\Psi \tag{2.2}$$

where N contains the interpolation functions. The following sections briefly describes the two cone types, the second-order cone and the positive semidefinite cone, which are used for modeling the convex yield criterion.

2.1.1 Semidefinite Programming

In Semidefinite Programming, constraints are applied as *linear matrix inequalities* (*LMI's*), [Grant and Boyd, 2008a, Grant and Boyd, 2008b].

$$C_t = \{X \succeq 0\} \tag{2.3}$$

where $X \succeq 0$ means that the square matrix X is positive semidefinite, i.e. $\sigma^T X \sigma \geq 0$ for any σ. LMI's allow for constraints to be applied to the eigenvalues of symmetric matrices, which is useful for modeling yield criterion based on principal stresses. Section 4.1 shows how the modified Coulomb criterion can be cast as a combination of LMI's and linear inequalities.

Second-Order Cone Programming

The constraint function for SOCP is, as the name suggests, a set of second-order cones defined by

$$C_t = \{\|A_i\sigma + b_i\|_2 - (c_i\sigma + d_i)\,; \qquad i = 1,\cdots,m\} \tag{2.4}$$

where the matrix A_i, the vectors b_i and c_i, and the scalar d_i are problem data. The most common second-order constraint types are the Quadratic Cone (QC)

$$C_t = \left\{ \sigma_1 \geq \sqrt{\sum_{j=2}^{k} \sigma_j^2} \;\; ; \;\; k \leq n \right\} \tag{2.5}$$

and the Rotated Quadratic Cone (RQC)

$$C_t = \left\{ 2\sigma_1\sigma_2 \geq \sum_{j=3}^{k} \sigma_j^2 \;\; ; \;\; k \leq n \right\} \tag{2.6}$$

Section 4.2 shows how the modified Coulomb criteria can be approximated by a combination of QC and RQC constraints.

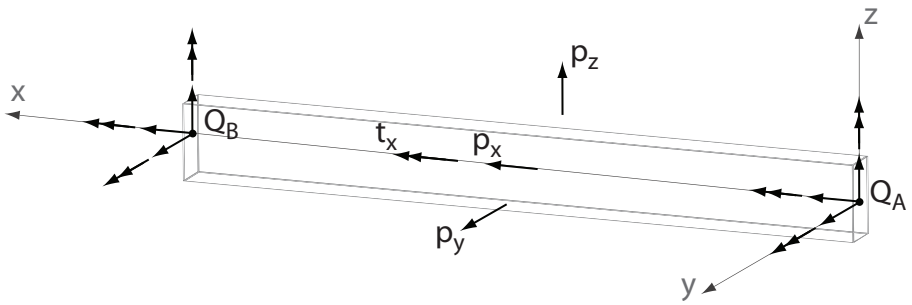

Figure 1: 3D Beam element model.

3 Element Model

Here we consider a straight beam element with local coordinate axes as shown on Figure 1. The element length is measured along the local x-axis and the width and height is measured along the y- and z-axis respectively. Here, the x direction will also be referred to as the longitudinal direction and the y- and z-direction will be referred to as the transverse directions. The element is capable of carrying loads in the longitudinal and transverse directions (p_x,p_y,p_z) as well as torsional moments (t_x) as shown on Figure 1. The element is intended to be compatible with a shell element, such that full 3D beam-shell structures can be modeled.
Static boundary conditions are applied to the beam element as nodal forces. These are applied at the beam ends, see Figure 1, and defined as

$$Q_A = \{-N_x^A, -V_y^A, -V_z^A, -M_x^A, -M_y^A, -M_z^A\} \tag{3.1}$$

$$Q_B = \{\ N_x^B,\ \ V_y^B,\ V_z^B,\ M_x^B,\ M_y^B,\ M_z^B\} \tag{3.2}$$

where N_x is the normal force, M_i is the moment around the i'th axis and V_i is the shear force in the i'th direction.
The external load intensities are coupled to the internal section forces through the following equilibrium equations:

$$p_y + V_{y,x} = 0 \tag{3.3}$$

$$p_z + V_{z,x} = 0 \tag{3.4}$$

$$t_x + M_{x,x} = 0 \tag{3.5}$$

The normal force equilibrium conditions are ensured through the internal zone equilibrium equations defined by Eq. (3.9). The bending moments are coupled to the external loads through the shear forces by two additional equilibrium equations

$$M_{z,x} + V_y = 0 \tag{3.6}$$

$$M_{y,x} - V_z = 0 \tag{3.7}$$

Zone Model

To obtain a lower bound solution, the element must be in a *safe* state i.e. the yield criterion must be obeyed at all points within the element. The yield criteria for beams are usually based on cross section forces such as M,N,V-surfaces. These yield criteria can be extremely difficult to set up, especially when the element is subjected to forces in three dimensions and support for arbitrary reinforcement layouts complicates the

process even further. To circumvent the need for a yield criterion based on section forces, we apply the material constraints on a stress state level. In [Niebling et al., 2007], a zone model was used to discretize the internal stress state in the beam element and the yield criteria was applied to the stresses within each zone. The model presented in [Niebling et al., 2007] was restricted to rectangular beams modeled by 3×3 rectangular zones. Here, we will adopt this zone model approach and extend it to work with arbitrary number of zones, hereby enabling engineers to model and analyze more complex cross sections.
The zones must be aligned with the local coordinate axes and the reinforcement is smoothed over the zone area. We will here assume that the transverse normal stresses, σ_x and σ_y, are equal to zero. Additionally, only the transverse shear stresses, τ_{xy} and τ_{xz}, are considered in the cross section. The stress state at a point within the beam is then defined by

$$\sigma = \begin{bmatrix} \sigma_x & \tau_{xy} & \tau_{xz} \\ \tau_{xy} & 0 & 0 \\ \tau_{xz} & 0 & 0 \end{bmatrix} \tag{3.8}$$

Besides the section force equilibrium equations described in the previous section, the stress state within a zone must also fulfil the following equilibrium equation

$$\sigma_{x,x} + \tau_{xy,y} + \tau_{xz,z} + f_x = 0 \tag{3.9}$$

where f_x is the volume load in the longitudinal beam direction. f_x can be expressed by the longitudinal load intensity p_x as

$$f_x = \frac{p_x}{A} \tag{3.10}$$

where A is the cross section area of the beam.
With $P_d(\zeta)$ representing an arbitrary polynomium in the coordinate ζ of degree d, the non-zero stresses in the zone are chosen

$$\sigma_x = P_4(x), \qquad \tau_{zx} = P_3(x)P_1(z), \qquad \tau_{xy} = P_3(x)P_1(y) \tag{3.11}$$

This choice of stresses gives the zone shown on Fig. 2 with 5 σ_x-nodes in the x-direction and 2 rows of shear stress nodes with 4 nodes in each row for each non-zero shear stress component - in total $5+2\cdot4+2\cdot4=21$ stress variables.
The loads are described by

$$p_x = P_3(x), \qquad p_y,\ p_z,\ t_x = P_2(x) \tag{3.12}$$

All terms in Eq. (3.9) are then of the same degree $P_3(x)$, i.e. avoiding locking. Eq. (3.3) - Eq. (3.7) give with Eq. (3.11)-Eq. (3.12)

$$V_y,\ V_z,\ M_x = P_3(x), \qquad M_y,\ M_z = P_4(x) \tag{3.13}$$

The load variation given in Eq. (3.12) provides a convenient interface for interaction with shell elements. If the shell element is capable of carrying constant surface loads perpendicular to the element plane, $p_z = P_0(x)P_0(y)$, the in-plane forces as well as the bending and torsional moments will be of second degree,

$$n_x,\ n_y,\ n_{xy},\ m_x,\ m_y,\ m_{xy} = P_2(x)P_2(y) \tag{3.14}$$

In a beam-shell structure, loads can be transferred between beam and shell elements along shared edges.
To obtain a statically admissible stress field within the element, traction continuity between zones must be

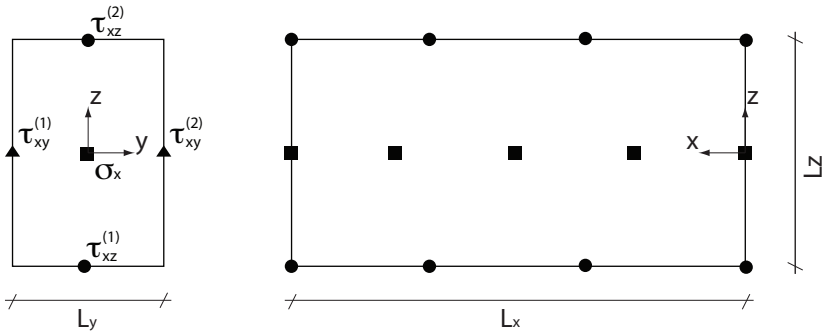

Figure 2: Sketch of zone model.

ensured. Because the zones are axis-aligned and transverse normal stresses are disregarded, this is simply done by ensuring shear stress continuity along shared zone faces.
Because the zones discretize the internal stress state, the section forces required by the equilibrium equations and the static boundary conditions can be computed from a set of summations

$$N_x = \sum_{i=1}^{n} \sigma_x \, A_i \tag{3.15}$$

$$V_y = \sum_{i=1}^{n} \frac{1}{2} \left(\tau_{xy}^{(2)} + \tau_{xy}^{(1)} \right) A_i \tag{3.16}$$

$$V_z = \sum_{i=1}^{n} \frac{1}{2} \left(\tau_{xz}^{(2)} + \tau_{xz}^{(1)} \right) A_i \tag{3.17}$$

$$M_x = \sum_{i=1}^{n} \frac{1}{2} \left(\left(\tau_{xz}^{(2)} + \tau_{xz}^{(1)} \right) y_i + \left(\tau_{xy}^{(2)} + \tau_{xy}^{(2)} \right) z_i \right) A_i \tag{3.18}$$

$$M_y = \sum_{i=1}^{n} z_i \, \sigma_x \, A_i \tag{3.19}$$

$$M_z = -\sum_{i=1}^{n} y_i \, \sigma_x \; A_i \tag{3.20}$$

where n is the number of zones, A_i is the cross section area of zone i and y_i and z_i are the geometric center point coordinates of the zone cross section.

4 Yield Criterion

The equilibrium equations defined in the previous section ensures that the obtained solution is statically admissible. Because a lower bound solution requires the structure to be in a safe state, a set of material constraints must be applied as well. The stress state is decomposed into a set of concrete- and reinforcement stresses as

$$\sigma = \sigma_c + A_s \sigma_s \tag{4.1}$$

where

$$\sigma_c = \begin{bmatrix} \sigma_{cx} & \tau_{cxy} & \tau_{cxz} \\ \tau_{cxy} & \sigma_{cy} & 0 \\ \tau_{cxz} & 0 & \sigma_{cz} \end{bmatrix} \tag{4.2}$$

are the concrete stresses and

$$\sigma_s = \begin{bmatrix} \sigma_{sx} & 0 & 0 \\ 0 & \sigma_{sy} & 0 \\ 0 & 0 & \sigma_{sz} \end{bmatrix} \tag{4.3}$$

are the reinforcement stresses. It should be noted that the transverse normal stresses in the concrete and reinforcement does not have to be zero, as long as the total transverse stresses are. This allows for modeling of the transverse reinforcement in the beam. The effect of shear in the rebars is studied in [Nielsen, 1999] and it is found that these are insignificant when the purpose of the rebars is to carry longitudinal tension and compression. The shear stress contribution from the reinforcement is therefore disregarded here. A_s is then a diagonal matrix containing reinforcement area per unit area perpendicular to the local element axes

$$A_s = \begin{bmatrix} A_{sx} & 0 & 0 \\ 0 & A_{sy} & 0 \\ 0 & 0 & A_{sz} \end{bmatrix} \tag{4.4}$$

If the reinforcement is not aligned with the local Cartesian coordinate system, the equivalent orthotropic reinforcement values are used, [Nielsen, 2008]. Since only normal stresses are considered in the reinforcement, simple upper- and lower bounds are applied to these

$$-f_{Yc} \leq \sigma_s \leq f_{Yt} \tag{4.5}$$

where f_{Yc} and f_{Yt} are the compression and tensile strength of the rebars respectively.
The modified Coulomb failure criterion, which consists of a sliding- and a separation criteria as shown in Eq. (4.6) and Eq. (4.7), will be applied to the concrete.

$$k\sigma_1 - \sigma_3 \leq f_c \tag{4.6}$$

$$\sigma_1 \leq f_A \tag{4.7}$$

Here, f_A is the separation strength and f_c is the uni-axial compression strength of the concrete. The separation strength, f_A, will often be equal to the uni-axial tensile strength, f_t of the concrete. The material parameter k is determined from the frictional angle, ϕ. Here, $k = 4$ is used which is equivalent to a frictional angle of approximately 37°. The principal stresses are sorted as $\sigma_1 \geq \sigma_2 \geq \sigma_3$. In [Larsen et al., 2009] it was shown how the modified Coulomb criterion could be defined as a set of *linear inequality matrices* and solved using Semidefinite Programming techniques.

The yield criteria on the reinforcement and the concrete will be applied in a number of control points along the length of the beam element. At a given control point, the yield criteria for the reinforcement stresses are applied once in each zone. This is sufficient because the normal stresses in the transverse reinforcement are constant within a zone. Because the shear stress varies linearly over the cross section of a zone, the concrete constraints must be applied in each of the four zone corners. Due to the high element degree, a rigorous lower bound solution cannot be obtained from a fixed number of control points. It is therefore important to choose a sufficient number of control points for a given load case. Alternatively, the resulting stress state could be analyzed in a post-process and additional control points could be inserted if needed.

4.1 Formulation of the modified Coulomb criterion using SDP

Here, we briefly present the SDP formulation of the modified Coulomb criterion. An SDP formulation of the Coulomb criterion was presented in [Bisbos and Pardalos, 2007, Krabbenhøft et al., 2008, Martin and Makrodimopoulos,

and the modified Coulomb criterion applied here was presented in [Larsen et al., 2009]. For a given stress state σ_c in the concrete, the yield criteria can be written as two *linear matrix inequalities* and two linear inequalities

$$\begin{aligned} \sigma_c \; + k\,\alpha_1\,\mathbf{I} &\succeq 0 \\ \sigma_c \; - \;\alpha_2\,\mathbf{I} &\preceq 0 \\ \alpha_2 &\leq f_A \\ \alpha_2 &\leq \frac{f_c}{k} - \alpha_1 \end{aligned} \tag{4.8}$$

where α_1 and α_2 are scalar variables.

4.2 Approximation to modified Coulomb criterion using SOCP

Despite the attractive properties of the SDP formulation of the modified Coulomb criterion given in the previous section, performance considerations in practical applications calls for a yield criterion based on second-order cones. The major challenge here is to model the tri-axial effects which occur in areas with reinforcement in all three directions.

We assume that the transverse shear stresses are carried in zones with shear reinforcement and in a plane which coincide with the shear reinforcement, i.e. τ_{xy} will only be carried in zones where $A_{sy} > 0$. Figure 3 shows a rectangular beam reinforced with longitudinal reinforcement bars and stirrups. The beam has been discretized into 9 zones as marked with dashed lines. The figure also illustrates the three possible zone types used when modeling cross sections. The zone types differ by the transverse reinforcement present in the zone. The first type has no transverse reinforcement and therefore no transverse normal- or shear stresses resulting in a uni-axial stress state. The second zone type has transverse reinforcement in one of the transverse directions making it similar to a reinforced concrete disk with a biaxial stress state. In the third zone type, reinforcement is present in both of the transverse directions making a tri-axial stress state possible. The zone types are marked by the numbers 1-3 on Figure 3. Separate yield criteria are applied in each of the three zone types. These criteria will be described in detail in the next sections.

4.2.1 Triaxial Stress State

Here, we will propose an approximation to the modified Coulomb criterion using second order cone constraints only. The approximation will, to some extend, be able to utilize the tri-axial stress state in the concrete. The approximation is based on the observation that zones subjected to tri-axial stress states often will have the same amount of reinforcement in the transverse directions. Zones with reinforcement in both directions will often be corner zones, see Figure 3, in which a stirrup wraps around the longitudinal reinforcement, this assumption seems reasonable.

The principal concrete stresses are determined by the eigenvalues of the concrete stress tensor σ_c

$$\begin{bmatrix} \sigma_{cx}-\lambda & \tau_{cxy} & \tau_{cxz} \\ \tau_{cxy} & \sigma_{cy}-\lambda & 0 \\ \tau_{cxz} & 0 & \sigma_{cz}-\lambda \end{bmatrix} = 0 \Rightarrow \tag{4.9}$$

$$(\sigma_{cx}-\lambda)(\sigma_{cy}-\lambda)(\sigma_{cz}-\lambda) - \tau_{cxy}^2(\sigma_{cz}-\lambda) - \tau_{cxz}^2(\sigma_{cy}-\lambda) = 0 \tag{4.10}$$

In [Andreasen, 1985] the separation criterion, Eq. (4.7), for a reinforced solid is, utilizing Eq. (4.1) and Eq. (4.10), approximated on quadratic form under the assumption that $f_A = 0$. We will make a similar

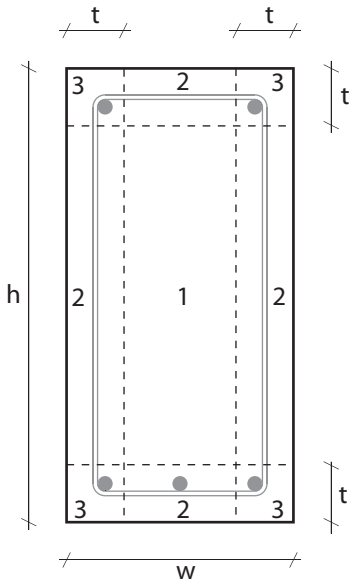

Figure 3: Rectangular beam example with longitudinal rebars and stirrups.

approximation but allow for a separation strength, f_A, in the concrete:

$$-\left(\Phi_x^* - \frac{\sigma_x}{f_c}\right)\Phi_y^*\Phi_z^* + \Phi_z^*\left(\frac{\tau_{cxy}}{f_c}\right)^2 + \Phi_y^*\left(\frac{\tau_{cxz}}{f_c}\right)^2 \leq 0 \tag{4.11}$$

where

$$\Phi_i^* = \frac{A_{si} f_{Yt}}{f_c} + \frac{f_A}{f_c} = \Phi_i + \frac{f_A}{f_c} \qquad for\ \ i = \{x,y,z\} \tag{4.12}$$

This type of constraint can be handled by some solvers (these are known as Quadratic Constrained Programming (QCP) problems) but it is often recommended to use cone constraints because they solve more efficiently, [MOSEK, 2009]. Eq. (4.11) can be translated into a rotated quadratic cone (Eq. (2.6)) as shown below

$$\begin{aligned} 2x_1x_2 &\geq x_3^2 + x_4^2 \\ x_1 &= -\frac{1}{2}\left(\Phi_x^* f_c - \sigma_x\right)\Phi_y^*\Phi_z^* \\ x_2 &= f_c \\ x_3 &= \sqrt{\Phi_y^*}\ \tau_{cxy} \\ x_4 &= \sqrt{\Phi_z^*}\ \tau_{cxz} \end{aligned} \tag{4.13}$$

For the sliding criterion, Eq. (4.6), we will assume that the transverse normal stresses are of equal magnitude i.e., $\sigma_{cy} = \sigma_{cz}$, i.e. equal amounts of transverse reinforcement in both directions. If the transverse normal stresses are not equal, we apply the largest (compression is negative) of the transverse normal stresses in both directions. It should be noted that if the difference between the reinforcement in each direction becomes large, the criterion will be too restrictive. Therefore, a different criterion must be applied in the biaxial stress state as described in the next section.

First, we will assume that σ_{cz} is the largest of the transverse normal stresses. If we substitute σ_{cy} with σ_{cz} in Eq. (4.10) we get

$$(\sigma_{cx}-\lambda)(\sigma_{cz}-\lambda)^2-\tau_{cxy}^2(\sigma_{cz}-\lambda)-\tau_{cxz}^2(\sigma_{cz}-\lambda)=0 \tag{4.14}$$

It is evident that one eigenvalue must be given by

$$\lambda_1=\sigma_{cz} \tag{4.15}$$

The remaining two eigenvalues are computed from

$$\left.\begin{matrix}\lambda_2\\ \lambda_3\end{matrix}\right\}=\frac{\sigma_{cx}+\sigma_{cz}}{2}\pm\sqrt{\left(\frac{1}{2}(\sigma_{cx}-\sigma_{cz})\right)^2+\tau_{cxy}^2+\tau_{cxz}^2} \tag{4.16}$$

Since we do not know the order of the three eigenvalues we must check every combination hereof. From Eq. (4.16) we see that $\lambda_2\geq\lambda_3$ which means that it is sufficient to check three combinations of the eigenvalues. In order to formulate the yield criterion on a second-order cone form, we introduce the auxiliary variable σ_{dz}

$$\sigma_{dz}=\frac{1}{2}(\sigma_{cx}-\sigma_{cz}) \tag{4.17}$$

Case I: $k\cdot\lambda_1-\lambda_3\leq f_c$
Here we assume that λ_1 is the largest of the three eigenvalues. λ_3 must therefore be the smallest and when inserted into Eq. (4.6) we get

$$\begin{aligned}k\cdot\sigma_{cz}-\left(\frac{\sigma_{cx}+\sigma_{cz}}{2}-\sqrt{\sigma_{dz}^2+\tau_{cxy}^2+\tau_{cxz}^2}\right)\leq f_c\Rightarrow\\ \sqrt{\sigma_{dz}^2+\tau_{cxy}^2+\tau_{cxz}^2}\leq f_c-k\cdot\sigma_{cz}+\frac{\sigma_{cx}+\sigma_{cz}}{2}\end{aligned} \tag{4.18}$$

The above inequality is a quadratic cone constraint in compliance with Eq. (2.5).

Case II: $k\cdot\lambda_2-\lambda_1\leq f_c$
Here, λ_1 is assumed to be the smallest eigenvalue making λ_2 the largest. Inserting this into Eq. (4.6) we get

$$\begin{aligned}k\cdot\left(\frac{\sigma_{cx}+\sigma_{cz}}{2}+\sqrt{\sigma_{dz}^2+\tau_{cxy}^2+\tau_{cxz}^2}\right)-\sigma_{cz}\leq f_c\Rightarrow\\ \sqrt{\sigma_{dz}^2+\tau_{cxy}^2+\tau_{cxz}^2}\leq\frac{f_c}{k}+\frac{\sigma_{cz}}{k}-\frac{\sigma_{cx}+\sigma_{cz}}{2}\end{aligned} \tag{4.19}$$

which yields another quadratic cone constraint.

Case III: $k\cdot\lambda_2-\lambda_3\leq f_c$
The last combination is when λ_1 lies between λ_2 and λ_3 which gives the following constraints when inserted into Eq. (4.6)

$$\begin{aligned}k\cdot\left(\frac{\sigma_{cx}+\sigma_{cz}}{2}+\sqrt{\sigma_{dz}^2+\tau_{cxy}^2+\tau_{cxz}^2}\right)-\left(\frac{\sigma_{cx}+\sigma_{cz}}{2}-\sqrt{\sigma_{dz}^2+\tau_{cxy}^2+\tau_{cxz}^2}\right)\leq f_c\Rightarrow\\ \left(\frac{\sigma_{cx}+\sigma_{cz}}{2}\right)(k-1)+\sqrt{\sigma_{dz}^2+\tau_{cxy}^2+\tau_{cxz}^2}(k+1)\leq f_c\Rightarrow\\ \sqrt{\sigma_{dz}^2+\tau_{cxy}^2+\tau_{cxz}^2}\leq\frac{1}{k+1}\left(f_c-\left(\frac{\sigma_{cx}+\sigma_{cz}}{2}\right)(k-1)\right)\end{aligned} \tag{4.20}$$

The above conditions are used when σ_{cz} is the largest of the transverse normal stresses. The case when σ_{cy} is the largest normal stress is handled by interchanging the z-indicies with y, adding an additional three cones and another auxiluary variable σ_{dy} to the set of inequality constraints. We can reduce the number of cones by introducing two more auxiluary variables, α_1 and α_2. The sliding criterion can be written as a combination of two cones, two linear equality constraints and six linear inequality constraints as shown in Eq. (4.21)-(4.30)

$$\sqrt{\sigma_{dz}^2 + \tau_{cxy}^2 + \tau_{cxz}^2} \leq \alpha_1 \tag{4.21}$$

$$\sqrt{\sigma_{dy}^2 + \tau_{cxy}^2 + \tau_{cxz}^2} \leq \alpha_2 \tag{4.22}$$

$$\sigma_{dz} = \frac{1}{2}(\sigma_{cx} - \sigma_{cz}) \tag{4.23}$$

$$\sigma_{dy} = \frac{1}{2}(\sigma_{cx} - \sigma_{cy}) \tag{4.24}$$

$$\alpha_1 \leq f_c - k \cdot \sigma_{cz} + \frac{\sigma_{cx} + \sigma_{cz}}{2} \tag{4.25}$$

$$\alpha_1 \leq \frac{f_c}{k} + \frac{\sigma_{cz}}{k} - \frac{\sigma_{cx} + \sigma_{cz}}{2} \tag{4.26}$$

$$\alpha_1 \leq \frac{1}{k+1}\left(f_c - \left(\frac{\sigma_{cx} + \sigma_{cz}}{2}\right)(k-1)\right) \tag{4.27}$$

$$\alpha_2 \leq f_c - k \cdot \sigma_{cy} + \frac{\sigma_{cx} + \sigma_{cy}}{2} \tag{4.28}$$

$$\alpha_2 \leq \frac{f_c}{k} + \frac{\sigma_{cy}}{k} - \frac{\sigma_{cx} + \sigma_{cy}}{2} \tag{4.29}$$

$$\alpha_2 \leq \frac{1}{k+1}\left(f_c - \left(\frac{\sigma_{cx} + \sigma_{cy}}{2}\right)(k-1)\right) \tag{4.30}$$

4.2.2 Biaxial Stress State

The yield criterion described in the previous section is only useful when the amount of reinforcement in each of the transverse directions does not differ significantly. Therefore, it cannot be used if reinforcement is only present in one of the transverse directions, i.e. zone type 2 on Figure 3. In this section we describe the yield criterion employed in zones with biaxial stress state.
First we assume that $\Phi_z = 0$, $\sigma_z = 0$ and $\tau_{cxz} = 0$ which gives the following concrete stress tensor

$$\sigma_c = \begin{bmatrix} \sigma_{cx} & \tau_{cxy} & 0 \\ \tau_{cxy} & \sigma_{cy} & 0 \\ 0 & 0 & 0 \end{bmatrix} \tag{4.31}$$

In this case one of the eigenvalues is 0 and the remaining two can be determined from

$$\left.\begin{matrix}\lambda_1 \\ \lambda_2\end{matrix}\right\} = \frac{\sigma_{cx} + \sigma_{cy}}{2} \pm \sqrt{\sigma_{dy}^2 + \tau_{cxy}^2} \tag{4.32}$$

where $\sigma_{dy} = \frac{1}{2}(\sigma_{cx} - \sigma_{cy})$. Since λ_1 must be larger than λ_2 the separation criterion, Eq. (4.7), gives

$$\begin{aligned} \lambda_1 \leq f_A \Rightarrow \\ \frac{\sigma_{cx} + \sigma_{cy}}{2} + \sqrt{\sigma_{dy}^2 + \tau_{cxy}^2} \leq f_A \Rightarrow \\ \sqrt{\sigma_{dy}^2 + \tau_{cxy}^2} \leq f_A - \frac{\sigma_{cx} + \sigma_{cy}}{2} \end{aligned} \tag{4.33}$$

For the sliding criterion, Eq. (4.6), we must consider the two cases were the largest concrete principal stress $\sigma_{c1} = 0$ and $\sigma_{c1} = \lambda_1$. If $\sigma_{c1} = 0$ we get

$$\begin{aligned} -\lambda_2 \leq fc \Rightarrow \\ -\left(\frac{\sigma_{cx}+\sigma_{cy}}{2} - \sqrt{\sigma_{dy}^2+\tau_{cxy}^2}\right) \leq f_c \Rightarrow \\ \sqrt{\sigma_{dy}^2+\tau_{cxy}^2} \leq f_c + \frac{\sigma_{cx}+\sigma_{cy}}{2} \end{aligned} \tag{4.34}$$

If $\sigma_{c1} = \lambda_1 \geq 0$, the sliding criterion becomes

$$\begin{aligned} k\lambda_1 - \lambda_2 \leq fc \Rightarrow \\ k\left(\frac{\sigma_{cx}+\sigma_{cy}}{2} + \sqrt{\sigma_{dy}^2+\tau_{cxy}^2}\right) - \left(\frac{\sigma_{cx}+\sigma_{cy}}{2} - \sqrt{\sigma_{dy}^2+\tau_{cxy}^2}\right) \leq f_c \Rightarrow \\ \sqrt{\sigma_{dy}^2+\tau_{cxy}^2} \leq \frac{f_c}{1+k} - \frac{k-1}{k+1}\frac{\sigma_{cx}+\sigma_{cy}}{2} \end{aligned} \tag{4.35}$$

We can do the usual rewriting to reduce the problem from two cones to one cone, one equality and two inequalities

$$\sqrt{\sigma_{dy}^2+\tau_{cxy}^2} \leq \alpha \tag{4.36}$$

$$\sigma_{dy} = \frac{1}{2}(\sigma_{cx} - \sigma_{cy}) \tag{4.37}$$

$$\alpha \leq f_A - \frac{\sigma_{cx}+\sigma_{cy}}{2} \tag{4.38}$$

$$\alpha \leq f_c + \frac{\sigma_{cx}+\sigma_{cy}}{2} \tag{4.39}$$

$$\alpha \leq \frac{f_c}{1+k} - \frac{k-1}{k+1}\frac{\sigma_{cx}+\sigma_{cy}}{2} \tag{4.40}$$

In the case where $\Phi_y = 0$ the y-indices are interchanged with z-indices as shown below

$$\sqrt{\sigma_{dz}^2+\tau_{cxz}^2} \leq \alpha \tag{4.41}$$

$$\sigma_{dz} = \frac{1}{2}(\sigma_{cx} - \sigma_{cz}) \tag{4.42}$$

$$\alpha \leq fA - \frac{\sigma_{cx}+\sigma_{cz}}{2} \tag{4.43}$$

$$\alpha \leq f_c + \frac{\sigma_{cx}+\sigma_{cz}}{2} \tag{4.44}$$

$$\alpha \leq \frac{f_c}{1+k} - \frac{k-1}{k+1}\frac{\sigma_{cx}+\sigma_{cz}}{2} \tag{4.45}$$

4.2.3 Uniaxial Stress State

In the case where there is no transverse reinforcement in either direction we assume a uni-axial stress state and a simple upper- and lower limits on the normal stresses are sufficient

$$-f_c \leq \sigma_{cx} \leq f_A \tag{4.46}$$

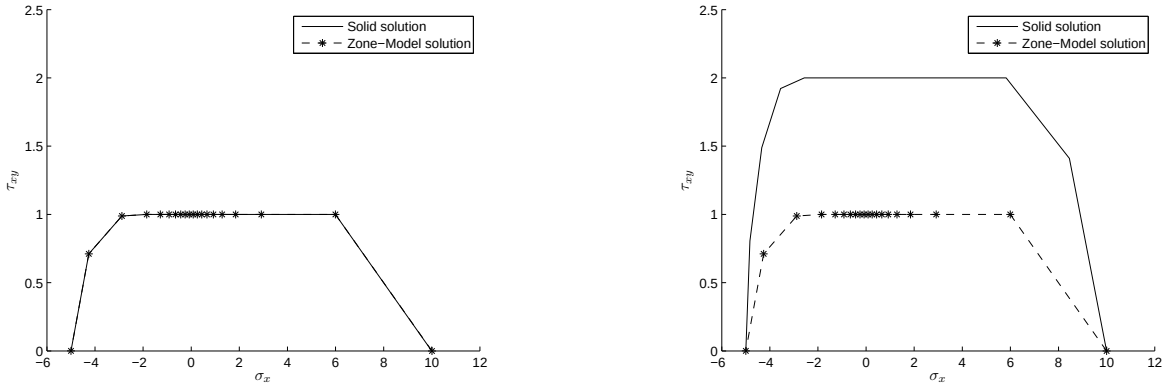

(a) $\Phi = \{10.0, 1.0, 1.0\}$ (b) $\Phi = \{10.0, 5.0, 1.0\}$

Figure 4: Comparison between the exact- and the approximated modified Coulomb criterion.

5 Numerical Tests

In this section we show some numerical examples using the beam element presented here. The first example shows a comparison between the exact yield criterion using SDP constraints and the approximated criterion using SOCP constraints. In the second example, a single element is subjected to some basic load cases and the results are compared to analytical solutions for verification. The third examples utilizes the flexibility of the zone model to analyze a beam with a more complex cross section and compare the results to physical tests.

5.1 Exact vs. Approximate modified Coulomb Criterion

Here we will compare the approximated yield criterion described in section 4.2 with the exact criterion from section 4.1. We will also compare the performance of each method.

Accuracy

For the uni- and bi-axial stress states, the approximate method yields no difference from the exact method. In the tri-axial stress state, the models are compared by plotting a slice in the $\sigma_x - \tau_{xy}$-plane of the yield surface. On Figure 4a the methods are compared for a point in a concrete material with normalized $f_c = 1$, $f_A = 0$ and $k = 4$ and with a reinforcement degree of $\Phi = \{10, 1, 1\}$ in the x, y- and z-direction respectively. Here it is seen, that the results found by both methods are identical which was also expected since the amount of transverse reinforcement is equal in both the y- and the z-direction. On Figure 4b, the amount of reinforcement in the y-direction is increased to 5. Because of the assumptions made in the approximate method, significantly lower capacities will be found by this method. The approximation should therefore be used only when the amount of transverse reinforcement does not differ significantly in each direction.

Performance

We test the performance of the exact method and the approximate method by analyzing a simple beam subjected to pure bending. The beam is discretized using an increasing number of elements and the time taken

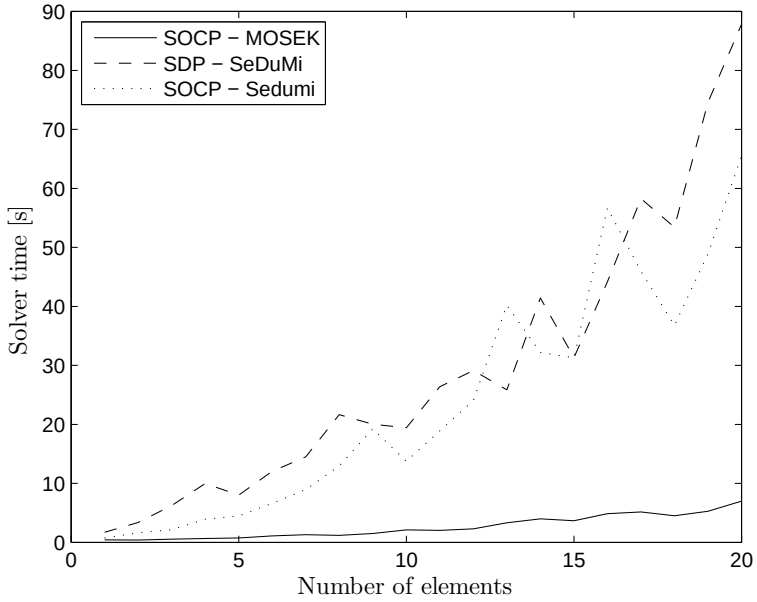

Figure 5: Performance comparison between the exact modified Coulomb criterion and the approximation described in section 4.2

to solve the problem is measured. The free solver SeDuMi, [Sturm, 1999, Pólik, 2005], is used for solving the SDP problems posed by the exact method and the commercial solver MOSEK 5, [MOSEK, 2009], is used to solve the SOCP problems in the approximate method. Additionally, the SOCP problems are tested using SeDuMi in order to compare the performance of the commercial and the free solver. The tests are performed on a IBM ThinkPad T60p laptop with 2GB RAM and running MatLab 2008a under Windows 7. The problems are assembled using the YALMIP interface [Löfberg, 2004] and passed to the solvers. Figure 5 shows the time in seconds used by the solvers to compute the problem depending on the number of elements used to model the beam. As seen from the figure, MOSEK 5 performs significantly better than SeDuMi, which makes the approximate model attractive. One thing to note though is the relatively small difference between the time used by SeDuMi to solve the SOCP and the SDP problems. This could indicate that with enough code optimization, the SDP could perform as good as the SOCP found in MOSEK 5. For now, the approximate method should be used whenever possible due to its improved performance over the exact method.

5.2 Basic Load Cases

For the basic element tests, a simple rectangular beam modeled using the 9 zones shown on Figure 3 is used. The width and height of the beam is 250 *mm* and 600 *mm* respectively and the thickness, t, of the outer zones is 76 *mm*. The reinforcement diameters are 20 *mm* and 6 *mm* for the longitudinal and the stirrups respectively and the cover thickness is 35 *mm*. The material parameters for concrete and reinforcement are as shown below

$$f_{Yt} = 550\ MPa \qquad f_{Yc} = 0$$
$$f_c = 25\ MPa \qquad f_A = 0 \qquad k = 4$$

Static Model	Numerical	Analytical
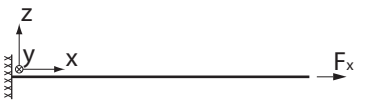	691	691
	−4626	−4500
	272	273
	47	51
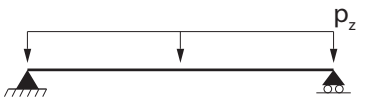	22	22

Table 1: Results obtained from the exact, and the approximate method compared to an analytical solution. Forces are in kN, moments in kNm and line loads in kN/m.

All examples are analyzed using both the exact and the approximate modified Coulomb model. The test results are presented and discussed in the following sections, and a brief summery of the results is given in Table 1. Because the zones in which tri-axial stress states can occur have equal reinforcement in the transverse directions, the results obtained from the exact and approximated methods will be identical, and will here be refered to as the numerical solution.

Pure Tension and Compression

Initially, a single element is subjected to a pure tension and compression state. The yield strength of the longitudinal reinforcement governs the load bearing capacity of the element when subjected to a tensile force, $F_x \geq 0$. The analytical capacity is determined by

$$F_x = \frac{\pi}{4} d^2 f_{Yt} = \frac{\pi}{4} \cdot (20\ mm)^2 \cdot 550\ MPa = 691\ kN$$

and the numerical load capacity is found to be 691 kN which is identical to the analytical solution.
Assuming a uni-axial stress state in the concrete, the analytical load capacity in compression can be found from

$$F_x = -(w \cdot h \cdot f_c) = -(300\ mm \cdot 500\ mm \cdot 25\ MPa) = -4500\ kN$$

Because some tri-axial effects are possible in the corner zones, the numerical capacity found in compression is slightly higher than the analytical: $F_x = -4626\ kN$. Figure 6a shows the normal stress distribution in the cross section when subjected to $F_x = -4626\ kN$, and here it is seen how the corner zones are able to carry stress values larger than the uni-axial compression strength.

Uni-axial Bending

Since discontinuities can only exist at the borders between zones, the bending capacity of a cross section depends on how it is modeled. Assuming a uni-axial stress state in the concrete, the negative bending capacity about the local y-axis can be determined to $M_y = 273\ kN$ which gives a compression zone depth of 69 mm. Because the height of the top zones is 76 mm, a discontinuity in the normal stresses cannot occur exactly at 69 mm. The placement of longitudinal reinforcement within a zone should not be offset to

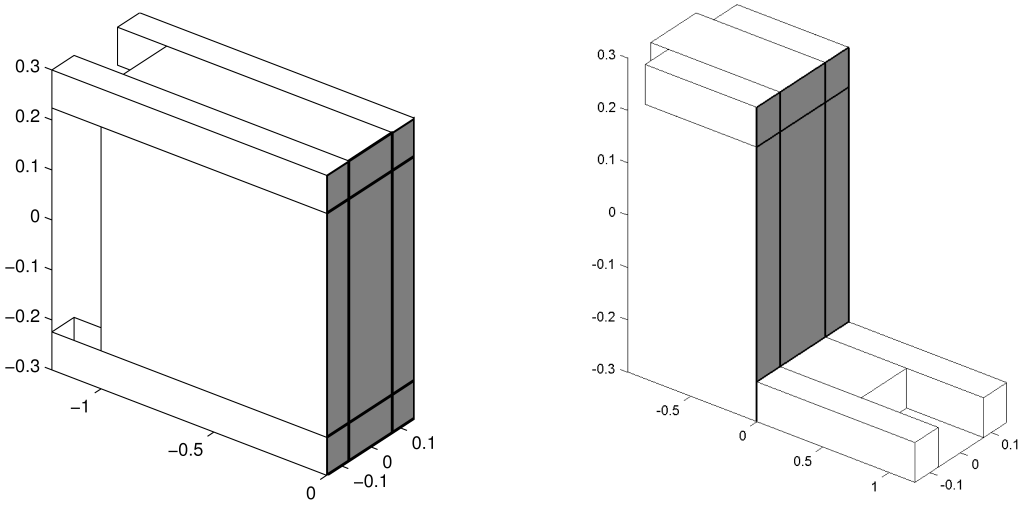

(a) Compression (b) Bending

Figure 6: Illustration of the normal stress distribution in the beam cross section.

much from the geometric center because this could influence the internal leaver arm and effect the bending capacity. In this case, the rebar is offset slightly towards the center which increases the leaver arm while the larger compression zone reduces it. The overall effects are marginal and the numerical moment capacity is found to be slightly less than the analytical: $M_y = 272\ kNm$. Even though the difference here is small, the example illustrates the importance of using a sufficient zone mesh when modeling a cross section and to carefully consider the zone layout with respect to the reinforcement. The bending capacity is also tested by applying a constant line load to a 10 m long simple supported beam. The load capacity is determined to be 21.7 kN/m which yields a bending moment of $M_y = -272\ kNm$. Figure 6b shows the normal stress distribution in the cross section at the center point of the beam when subjected to $M_y = -272\ kNm$.

Pure Torsion

When the rectangular element is loaded by a constant torsional moment, the numerical load bearing capacity is determined to $M_x = 47\ kNm$. To be able to compare this with an analytical solution, we consider the cross section as a thin-walled closed section as described in [Nielsen, 1999] with a thickness of $t = 76\ mm$. Because the resulting bending moment must be equal to zero, only the four rebars in the corners are considered active in the case of pure torsion. If these rebars are distributed evenly over the thin-walled section, a shear strength of $f_v = 3.22\ MPa$ is obtained. The torsional capacity can then be determined from the following expression

$$M_x = 2 \cdot f_v \cdot t \cdot (w-t)(h-t) = 51\ kNm \tag{5.1}$$

The analytical result is slightly larger than the numerical one because it neglects the effects of the combined shear stresses in the corner zones. Since the numerical model uses the full tri-axial stress state, these are taken into account here.

Concluding remarks

The above examples has shown that the element is capable of modeling simple beams subjected to basic load cases. It was also seen, that the tri-axial effects could be handled using both the exact implementation

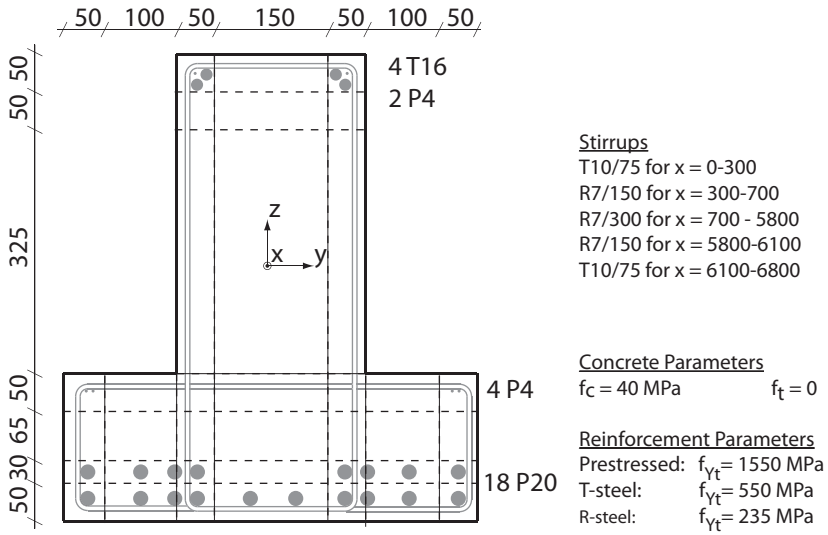

Figure 7: Cross section of inverse T-beam with zone division model.

of the modified Coulomb criterion and the approximated criterion.

5.3 Analysis of inverse T-Beam

The rectangular beam analyzed in the previous section is similar to the one presented in [Niebling et al., 2007]. The major advantage of the element presented here is its ability to model more complex cross sections. This final example demonstrates how the flexible zone model can be used to determine the load bearing capacity of the inverse T-beam shown on Figure 7. The beam is 6.8 m long and the shear reinforcement varies along the length as described in the figure. Because a single element must have the same shear reinforcement throughout, 5 elements are required to model the beam. The cross section is modeled using 37 zones as illustrated on Figure 7 and the material parameters are noted on the figure.
Initially, a constant bending moment is applied to the beam and the uni-axial bending capacity of the cross section about the y-axis is found to be $M_y = 2073\ kNm$. The beam is then simply supported at both ends and a constant line load is applied along the geometric centerline. The numerical load bearing capacity is then found to be $p_z = 119\ kNm$. It should be noted that the maximum bending moment is only 689 kNm and that the load bearing capacity is therefore governed by the shear strength of the beam. As part of a renovation project in Copenhagen, Ramboll conducted a series of tests on beams similar to the one shown on Figure 7. Five tests were carried out and the average capacity was here found to be $p_z = 136\ kNm$ which is approximately 13% higher than the numerical lower bound solution obtained here. Tests conducted on the concrete material indicated that the yield strength was a bit higher the the design strength used here: $f_c \approx 46\ MPa$. The reinforcement steel was not tested, but the actual yield strength values are usually higher than the design values specified by the manufacturer. Because the capacity is governed by the stirrups, this could be a possible reason for the higher test results. Despite of these uncertainties in material properties, the numerical result are considered to be quite good.

6 Conclusion

We have presented a method for determining the load bearing capacity of 3D beams subjected to both bending- and torsional moments as well as normal and shear forces. The method circumvents the need for

a complex yield criteria based on section forces by representing the internal stress state by a discrete set of zones. The material constraints are then applied directly at the stress-state level. The modified Coulomb failure criterion is used to constrain the stress state in the concrete. Two different methods are employed to solve the non-linear problem posed by this criterion. The first method is Semidefinite Programming, which makes it possible to implement the modified Coulomb criterion exactly. It does suffer from some performance issues on the current solvers, and a method using only second-order cones was therefore developed to reduce computation times. This method makes good approximations to the modified Coulomb and is sufficient for most analysis cases.
The numerical model was tested using a range of basic load cases. The results were then compared with analytical results and it was found that the correlation was very good. An inverse T-beam with complex reinforcement layout was also modeled and analyzed and the numerical results were compared to those obtained from physical tests. The load bearing capacity found by the numerical model was only 13% less than those found from the tests which is considered very good when taking the uncertainties of the material properties into account.

References

[Anderheggen and Knopfel, 1972] Anderheggen, E. and Knopfel, H. (1972). Finite element limit analysis using linear programming. *International Journal of Solids and Structures*, 8(12):1413–1431.

[Andreasen, 1985] Andreasen, Bent Steen Nielsen, M. P. (1985). Armering af beton i det tredimensionale tilfælde. *Bygningsstatiske Meddelelser*, 56(2-3).

[Bisbos and Pardalos, 2007] Bisbos, C. and Pardalos, P. (2007). Second-order cone and semidefinite representations of material failure criteria. *Journal of Optimization Theory and Applications*, 134(2):275–301.

[Damkilde and Hoyer, 1993] Damkilde, L. and Hoyer, O. (1993). An efficient implementation of limit state calculations based on lower-bound solutions. *Computers and Structures*, 49(6):953–962.

[Damkilde et al., 1994] Damkilde, L., Olsen, J. F., and Poulsen, P. N. (1994). A program for limit state analysis of plane, reinforced concrete plates by the stringer method. *Bygningsstatiske Meddelelser*, 65(1):1–26.

[Dantzig, 1963] Dantzig, G. B. (1963). *Linear programming and extensions*. Princeton University Press, Princeton, N.J.,.

[Fredsgaard and Kirk, 1979] Fredsgaard, S. and Kirk, J. (1979). Ruptus - et program til brudstadieberegninger. *ADB-Udvalget*.

[Grant and Boyd, 2008a] Grant, M. and Boyd, S. (2008a). Cvx: Matlab software for disciplined convex programming.

[Grant and Boyd, 2008b] Grant, M. and Boyd, S. (2008b). Graph implementations for nonsmooth convex programs. *Recent Advances in Learning and Control*, pages 95–110.

[Karmarkar, 1984] Karmarkar, N. (1984). A new polynomial-time algorithm for linear programming. *Combinatorica*, 4(4):373–395.

[Krabbenhøft et al., 2008] Krabbenhøft, K., Lyamin, A., and Sloan, S. (2008). Three-dimensional mohr-coulomb limit analysis using semidefinite programming. *Communications in Numerical Methods in Engineering*, 24(11):1107–1119.

[Krenk et al., 1994] Krenk, S., Damkilde, L., and Hoyer, O. (1994). Limit analysis and optimal design of plated with equilibrium elements. *Journal of Engineering Mechanics*, 120(6):1237–1254.

[Larsen et al., 2009] Larsen, K. P., Poulsen, P. N., and Nielsen, L. O. (2009). Limit analysis of solid reinforced concrete structures. In *Computational Technologies in Concrete Structures (CTCS'09)*, pages 1216–1226.

[Löfberg, 2004] Löfberg, J. (2004). Yalmip : A toolbox for modeling and optimization in matlab. In *Proceedings of the CACSD Conference*, Taipei, Taiwan.

[Makrodimopoulos and Martin, 2006] Makrodimopoulos, A. and Martin, C. M. (2006). Lower bound limit analysis of cohesive-frictional materials using second-order cone programming. *International Journal for Numerical Methods in Engineering*, 66(4):604–634.

[Martin and Makrodimopoulos, 2006] Martin, C. M. and Makrodimopoulos, A. (2006). Finite-element limit analysis of mohr-coulomb materials in 3d using semidefinite programming. *Journal of Engineering Mechanics*, 134(4):339–347.

[MOSEK, 2009] MOSEK (2009). The mosek optimization toolbox for matlab manual. version 5.0.

[Nesterov and Nemirovsky, 1988] Nesterov, Y. and Nemirovsky, A. (1988). A general approach to polynomial-time algorithms design for convex programming. *Centr. Econ. & Math. Inst., USSR Acad. Sci., Moscow, USSR,*.

[Niebling et al., 2007] Niebling, J., Vinther, A., and Larsen, K. P. (2007). Numerisk modellering af plastiske betonkonstruktioner (in danish). Master's thesis, Department of civil engineering, Byg-DTU.

[Nielsen, 2008] Nielsen, L. O. (2008). Concrete plasticity notes. Technical report, Department of Civil Engineering, Byg-DTU.

[Nielsen, 1999] Nielsen, M. P. (1999). *Limit Analysis and Concrete Plasticity*. CRC Press.

[Pólik, 2005] Pólik, I. (2005). Addendum to the sedumi user guide. version 1.1.

[Poulsen and Damkilde, 2000] Poulsen, P. N. and Damkilde, L. (2000). Limit state analysis of reinforced concrete plates subjected to in-plane forces. *International Journal of Solids and Structures*, 37(42):6011–6029.

[Sturm, 1999] Sturm, J. F. (1999). Using sedumi 1.02, a matlab toolbox for optimization over symmetric cones. *Optimization Methods and Software*, 11(1):625–653.

[Vandenberghe and Boyd, 1996] Vandenberghe, L. and Boyd, S. (1996). Semidefinite programming. *SIAM Review*, 38:49–95.

Paper III

"Limit Analysis of Reinforced Concrete Shells"

K.P. Larsen, P.N. Poulsen & L. O. Nielsen

Submitted to: *International Journal of Solids and Structures*

Limit Analysis of Reinforced Concrete Shells

K.P. Larsen[†]

Ramboll Denmark, DK-2300 Copenhagen, Denmark,
Department of Civil Engineering, Technical University of Denmark, DK-2800 Kgs. Lyngby, Denmark
e-mail: kpl@ramboll.dk

P.N. Poulsen, & L.O. Nielsen

Department of Civil Engineering, Technical University of Denmark, DK-2800 Kgs. Lyngby, Denmark
e-mail: pnp@byg.dtu.dk and lon@byg.dtu.dk

Abstract

In this paper we present a new shell finite element for reinforced concrete structure modeling based on lower bound limit state analysis. The element employs a layered disk approach to define the internal stress state in the shell, and the need for a section force based yield criterion is circumvented by applying yield conditions on the stress state level. The stress state is decomposed into concrete and reinforcement stresses for which separate yield criteria are applied. Therefore, the element includes the transverse shear stresses in the yield criterion and shear reinforcement can be modelled. The modified Coulomb criterion is used to constrain the tri-axial stress state in the concrete while simple limits are imposed on the axial reinforcement stresses. Examples are given in which the element is used to model plate and disk structures and the results obtained are very good. An example is shown in which methods that disregards the transverse shear stresses overestimates the load bearing capacity of the given structure.
Keywords *rigid perfect plasticity; limit analysis; numerical methods; semidefinite programming*

1 Introduction

Limit state analysis based on the extremum principles is a useful tool for assessing the load bearing capacity of reinforced concrete (RC) structures. Over the last decades, several methods for manual limit state analysis have been developed. Even for structures of moderate complexity, these problems are a significant challenge to solve manually which makes numerical tools attractive. Whether these methods are based on the upper bound theorem or the lower bound theorem, they pose a convex optimization problem.

One of the first numerical optimization methods employed for limit analysis was Linear Programming (LP) using the Simplex algorithm (Dantzig, 1963). This method only allowed for linear inequality constraints on the stresses and non-linear constraints had to be linearised if they were to be solved as LP problems. This approach was taken in (Anderheggen and Knopfel, 1972) where the conic yield criterion for plates in bending (Nielsen, 1969), see (Nielsen, 1999), was linearised to transform it into an approximated LP problem. The Interior-Point algorithm presented by (Karmarkar, 1984) has become popular because of its efficiency and ability to solve large problems. Furthermore, it was shown by (Nesterov and Nemirovsky, 1988), see (Nesterov and Nemirovskii, 1994), that the algorithm could be generalized to solve not only LP problems but also problems with non-linear constraints. This gave rise to Second-Order Cone Programming (SOCP) which allows for quadratic cone constraints on the decision variables. The SOCP method was applied by (Makrodimopoulos and Martin, 2006) in which the Coulomb criterion for plane stress states were formulated. The latests addition to the family of convex optimization methods using the interior-point algorithm is Semidefinite Programming (SDP). This method is the most general of the three mentioned here and allows constraints in the form of positive semidefinite matrices. SDP has been applied by (Bisbos and Pardalos, 2007; Krabbenhøft et al., 2008) to analyze structures of frictional materials with cohesion using the Coulomb criterion in three dimensions.

The finite element method has become one of the most widely adopted approaches for numerical structural analysis, and several elements for limit state analysis have been developed. Elements for modeling of RC structures subjected to plate bending, (Krabbenhoft and Damkilde, 2002), for disk structures subjected to in-plane forces, (Poulsen and Damkilde, 2000), and for shell structures, (Engkilde, 2008). exists, but without including the transverse shear in the yield condition. In (Niebling et al., 2007), a shell model was presented which defined the internal stress state through a set of layered disks. Each layer was considered as an RC disk in a plane stress state and the conic yield criterion applied. While this model was capable of modeling RC shell structures, it neglected the effects of the transverse shear stresses present in the cross section. If these are to be taken into consideration, the stress state within the element becomes tri-axial and a yield criteria based on plane stress theory becomes inadequate.

This paper presents a new shell element which includes the effects of the transverse shear stresses in the structure. The element uses a layered disk approach similar to (Niebling et al., 2007) in which the total stress state is decomposed into concrete and reinforcement stresses. The modified Coulomb criterion is applied to the concrete stresses while simple upper and lower bounds are applied to the reinforcement. Three numerical examples are given which illustrates the use of the element. In the first example, the element is used as a disk element to model an unreinforced beam subjected to four point bending. The second example shows a plate subjected to a combination of uni-axial bending and transverse shear. In the third and final example, a triangular plate supported on three columns and subjected to a point load.

2 Lower Bound Limit Analysis

Lower bound limit analysis has been used for analysis of rigid plastic structures for many years. Methods such as Strut-and-Tie Models (Moersch, 1922), the Stringer-Method (Lundgren, 1949) and Homogeneous Stress Fields (Nielsen, 1969), has made it possible to perform manual lower bound limit analysis of simple structures. Because all of these methods requires some optimization, they can pose a significant challenge even for simple structures. Over the last decades, numerical optimization routines have become more efficient which, combined with the increase in computer hardware performance, has made numerical methods attractive for solving lower bound limit analysis problems of considerable size and complexity.
The methods mentioned above are based on the lower bound theorem which states that *a safe and statically admissible stress distribution will not be able to cause collapse in a structure*. Since this encompasses all solutions that fulfils the equilibrium equations, static boundary conditions and obeys the yield criteria at any point within the structure, multiple solutions can exists for a given structural problem. Because we are interested in finding the solution which results in the largest possible load bearing capacity, and because the yield criteria are convex, the lower bound theorem naturally poses a convex optimization problem. The equilibrium finite element formulation of this problem is shown below and is used in the following:

$$\begin{aligned} &\text{minimize} && -\lambda \\ &\text{subject to} && -R\,\lambda + H\,\Psi = R^0 \\ & && \Sigma \in C_t \end{aligned} \tag{2.1}$$

Here, λ is the load factor which is sought maximized, H is the equilibrium matrix representing the equilibrium equations and static boundary conditions while R and R^0 are the proportional and constant load vectors respectively. Ψ is a vector containing the stress parameters, also called the decision variables, required to define the stress state in the structure. Eq. (2.1) is linear in λ and Ψ. Σ is the stress state at a number of control points within the structure and it is constrained by a set of convex constraints C_t. The stress state at a control point in the element is denoted $\sigma \in \Sigma$ and determined from interpolation of the stress parameters:

$$\sigma = N\Psi \tag{2.2}$$

where N is a matrix containing the interpolation functions.
The optimization algorithm required to solve a given problem depends on the type of restrictions used to constrain the stress state, which in turn depends on the chosen yield criteria. In the Semidefinite Programming method considered here, the convex constraints are limited to *Linear Matrix Inequalities* or *LMI's* which are written as (Vandenberghe and Boyd, 1996):

$$C_t = \{X \succeq 0\} \tag{2.3}$$

where $X \succeq 0$ means that the symmetric matrix X is positive semidefinite, i.e. $s^T X s \geq 0$ for any vector s. This allows for inequality constraints to be placed on the eigenvalues of the matrix X, i.e. the principal stresses when X represents the 2D or 3D stress tensor. In (Bisbos and Pardalos, 2007; Krabbenhøft et al., 2008) it was shown how SDP could be used to formulate the Coulomb criterion in the tri-axial stress state.

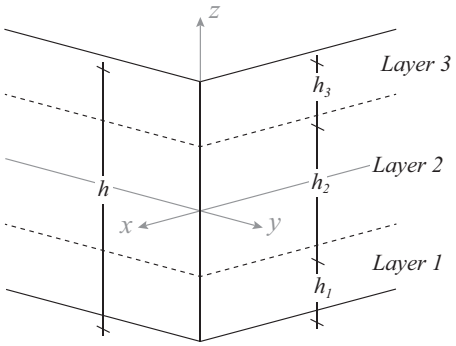

Figure 1: Plane shell structure modeled using three layered disks.

2.1 Plane Shell Structure

A shell structure is characterized by membrane and bending behaviour and is often modeled by plane shell elements characterized by disk (in-plane) and bending behaviour. One approach for handling a plane shell structure is to consider it as a set of layered disks. When combined, these will be able to carry the cross section forces, e.i. bending and torsional moments as well as in-plane disk forces. To obtain a lower bound solution, the yield surface for reinforced concrete disks (Nielsen, 1969), see (Nielsen, 1999), can then applied in each layer. This approach was taken by (Niebling et al., 2007) were a 3D shell element using three layers was presented. While this element was shown efficient for modeling both disk-, plate bending- and shell structures, it neglected the effects of the transverse, or out-of-plane, shear stresses. If these are to be taken into account, the resulting stress state becomes tri-axial which can not be handled by the SOCP methods used in (Niebling et al., 2007). However, SDP can be used to model and analyze reinforced concrete solids with tri-axial stresses using the modified Coulomb criterion, (Larsen et al., 2009). Here we will expand on the work done by (Niebling et al., 2007) by including the transverse shear stresses into the yield criterion.

The layered disks provide a discrete representation of the internal stress state in the shell from which the section forces can be derived. Fig. 1 illustrates the layered disk principle using three disks. The thickness of the disk is $h = \sum_{k=1}^{n} h_k$. The element stresses refers to a local orthogonal coordinate system (x,y,z) where z is perpendicular to the element plane and $z = 0$ at the center plane.

The stress state at a point within the element is considered as a combination of concrete and reinforcement stresses, and yield criteria are applied to these separately as described in further detail in the next section. Here, we will assume that the total transverse normal stresses, σ_z, are zero over the thickness of the shell and the stress state at a point within a disk layer is defined by the stress tensor σ:

$$\sigma = \begin{bmatrix} \sigma_x & \tau_{xy} & \tau_{xz} \\ \tau_{xy} & \sigma_y & \tau_{yz} \\ \tau_{xz} & \tau_{yz} & 0 \end{bmatrix} \tag{2.4}$$

We also assume that the in-plane stress components, σ_x, σ_y and τ_{xy}, are constant over the height of a layer as illustrated on Fig. 2a. The transverse shear stresses, τ_{xz} and τ_{yz}, are constant over the height of the center layer and decreases linearly to zero over the height of the outer layers as

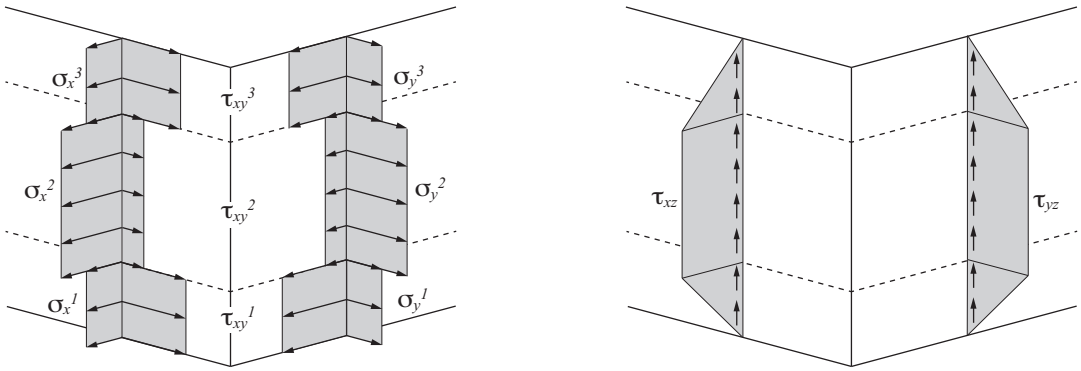

(a) Distribution of in-plane stresses over the cross section.

(b) Distribution of transverse shear stresses over the cross section.

Figure 2: Stress distribution over the element cross section.

illustrated on Fig. 2b. The shell section forces can be determined from summation of the stresses in the disk layers as:

$$m_x^{(j)} = \sum_{k=i}^{a} \sigma_x^{(k)}\ h_k\ z_k^{(j)} \tag{2.5}$$

$$m_y^{(j)} = \sum_{k=i}^{a} \sigma_y^{(k)}\ h_k\ z_k^{(j)} \tag{2.6}$$

$$m_{xy}^{(j)} = \sum_{k=i}^{a} \tau_{xy}^{(k)}\ h_k\ z_k^{(j)} \tag{2.7}$$

$$q_x = \sum_{k=i}^{a} \tau_{xz}^{(k)}\ h_k \tag{2.8}$$

$$q_y = \sum_{k=i}^{a} \tau_{yz}^{(k)}\ h_k \tag{2.9}$$

where j is the order of the moment, a is the number of layers and z_k is the distance in the z-direction from the central plane to the center of layer k. It should be noted that the 0th order moment is equal to the normal force i.e. $m_i^{(j)} = n_i$. Furthermore, the 1st order moment is also refered to as just the moment, i.e. $m_i^{(1)} = m_i$.
To ensure a statically admissible stress field, a set of equilibrium equations must be fulfilled. The equations given below ensures in-plane equilibrium:

$$f_x\lambda + \sigma_{x,x} + \tau_{xy,y} + \tau_{xz,z} = -f_x^0 \tag{2.10}$$

$$f_y\lambda + \sigma_{y,y} + \tau_{xy,x} + \tau_{yz,z} = -f_y^0 \tag{2.11}$$

Here f_i and f_i^0 are the proportional and constant volume loads in the i'th direction. The volume loads are assumed constant over the cross section such that it can be defined from the in-plane

surface loads as $p_i = hf_i$ and $p_i^0 = hf_i^0$. The notation $\sigma_{i,j}$ refers to the partial derivatives of σ_i with respect to j. Because σ_z is assumed equal to zero, transverse equilibrium is obtained through equilibrium between the surface load and the transverse shear forces

$$-p_z\lambda + q_{x,x} + q_{y,y} = p_z^0 \tag{2.12}$$

where p_z and p_z^0 are the proportional and constant surface loads perpendicular to the element plane respectively.

2.2 Yield Criteria

To ensure that the obtained solution is in a safe state, yield constraints must be applied to the stresses in the disk layers. We decompose the total stress state given in Eq. (2.4) into concrete- and reinforcement stresses

$$\sigma = \sigma_c + A_s\sigma_s \tag{2.13}$$

where σ_c is the concrete stress tensor

$$\sigma_c = \begin{bmatrix} \sigma_{cx} & \tau_{cxy} & \tau_{cxz} \\ \tau_{cxy} & \sigma_{cy} & \tau_{cyz} \\ \tau_{cxz} & \tau_{cyz} & \sigma_{cz} \end{bmatrix} \tag{2.14}$$

and σ_s is a diagonal matrix containing the normal stresses in the reinforcement

$$\sigma_s = \begin{bmatrix} \sigma_{sx} & 0 & 0 \\ 0 & \sigma_{sy} & 0 \\ 0 & 0 & \sigma_{sz} \end{bmatrix} \tag{2.15}$$

The matrix A_s contains the reinforcement area per unit area perpendicular to the local element axes

$$A_s = \begin{bmatrix} A_{sx} & 0 & 0 \\ 0 & A_{sy} & 0 \\ 0 & 0 & A_{sz} \end{bmatrix} \tag{2.16}$$

It should be noted, that even though $\sigma_z = 0$, transverse normal stresses can still be present in the concrete and reinforcement respectively. The shear stresses in the rebars are disregarded and these are therefore carried only in the concrete. The separation of the total stresses into concrete- and reinforcement stresses allows for yield constraints to be applied to these separately. Since the rebars are primarily subjected to a uni-axial stress state, linear upper- and lower limits can be applied to these

$$-f_{Yc} \leq \sigma_{si} \leq f_{Yt} \tag{2.17}$$

where f_{Yt} and f_{Yc} are the uni-axial tensile- and compression strength respectively. The concrete stresses are constrained by the modified Coulomb yield criterion

$$\begin{aligned} k\,\sigma_{c1} - \sigma_{c3} &\leq f_c \\ \sigma_{c1} &\leq f_A \end{aligned} \tag{2.18}$$

where f_c is the uni-axial compression strength of the concrete and f_A is the separation strength. The material parameter k is determined from the frictional angle, ϕ. Here, $k = 4$ is used which is equivalent of a frictional angle of $\phi \approx 37^\circ$. Because of its discontinuous nature, the modified Coulomb criterion has traditionally been difficult to handle in numerical applications. For this element, we will employ the method described by (Larsen et al., 2009), in which the modified Coulomb criterion is formulated using linear matrix inequalities. The formulas are summarized below

$$\begin{aligned} \sigma_c \; + k\,\alpha_1\,\mathbf{I} &\succeq 0 \\ -\sigma_c \; + \; \alpha_2\,\mathbf{I} &\succeq 0 \\ \alpha_2 &\leq f_A \\ \alpha_2 &\leq \frac{f_c}{k} - \alpha_1 \end{aligned} \tag{2.19}$$

where α_1 and α_2 are scalar variables and $\mathbf{I}$ is the identity matrix.

3 Finite Element Formulation

In the previous section, a brief description of a plane stress structure and its associated equilibrium equations was given. It was also shown how the cross section force could be defined from a discrete representation of the internal stress state using a layered disk model. In this section, an element suitable for implementation in an equilibrium based finite element framework is presented. The element is chosen as a planar triangular element to which a local orthogonal coordinate system (x, y, z) is associated. The geometric shape of the element is defined by three nodes, (n^1, n^2, n^3), in an order defining the positive z-direction through the right-hand rule, see Fig. 3. The element unit normal is a unit vector in the positive z-direction. The element edges are numbered such that the first edge, e_1, is opposite n_1 and so forth, see Fig. 3. The local coordinate axes of edge i is defined by the outward unit normal perpendicular to the edge in the element plane, n_n, a unit vector along the edge in the node order, n_t, and the element normal n as illustrated on the figure.

With $P_d(\zeta)$ representing an arbitrary polynomium in coordinate ζ of degree d, the surface loads are chosen as

$$p_x, p_y = P_1(x,y) \qquad p_z = P_0(x,y) \tag{3.1}$$

From Eq. (2.10) - Eq. (2.11) it then follows that

$$q_x, q_y = P_1(x,y) \qquad m_x^{(j)}, m_y^{(j)}, m_{xy}^{(j)} = P_2(x,y) \tag{3.2}$$

The yield criteria described in section 2.2 is employed at a number of control points within element. At each control point, the yield criterion is applied once in each layer. In the center layer, the stress state is constant in the z-direction so the yield criteria are applied in the center point. In the outer layers, the shear stresses are zero at the element surface and non-zero at the interface towards the center layer. Since the transverse shear stresses varies linearly over the layer thickness, it is sufficient to apply the yield criteria at the interface. Because a quadratic moment field, and thereby also a quadratic normal stress field, is employed, a strictly lower bound solution

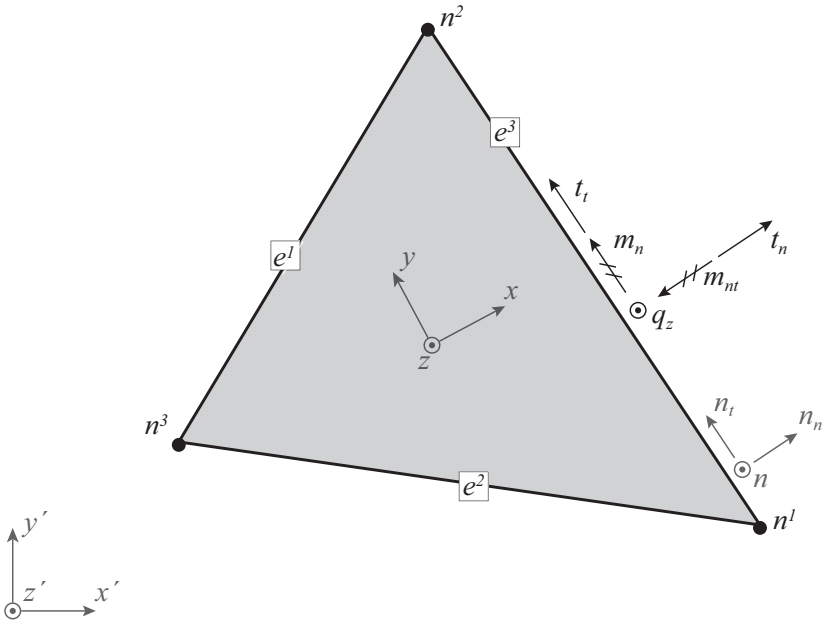

Figure 3: Geometric properties of a triangular element.

cannot always be obtained by using a fixed number of control points. It is therefore important to use a sufficient number of control points to adequately constrain the solution. Alternatively, a post-processor could be used to check the resulting stress state and insert additional control points if needed. This method was implemented in (Niebling et al., 2007).
Static boundary conditions are applied as prescribed traction forces and moments along the element edges. The tractions along an edge is found by transforming the cross section forces into the local edge coordinate system. The tractions along an edge are compute from

$$t = T^e \, f \tag{3.3}$$

where

$$f = \left[n_x, n_y, n_{xy}, m_x, m_y, m_{xy}, m_x^{(2)}, m_y^{(2)}, m_{xy}^{(2)}, q_x, q_y \right]^T \tag{3.4}$$

is a vector containing the section forces at the given point along the edge and

$$t = \left[t_n, t_t, m_n, m_{nt}, m_n^{(2)}, m_{nt}^{(2)}, q_n \right]^T \tag{3.5}$$

is a vector with the tractions in local edge coordinates. The local edge transformation matrix, T^e, is assembled from the edge normal n_n components in the local coordinate system $n_n = (n_{nx}, n_{ny})$

$$T^e = \begin{bmatrix} T^m & & & \\ & T^m & & \\ & & T^m & \\ & & & T^q \end{bmatrix} \tag{3.6}$$

where

$$T^m = \begin{bmatrix} n_{nx}^2 & n_{ny}^2 & 2n_{nx}n_{ny} \\ -n_{nx}n_{ny} & n_{nx}n_{ny} & n_{nx}^2 - n_{ny}^2 \end{bmatrix} \tag{3.7}$$

and

$$T^q = \begin{bmatrix} n_{nx} & n_{ny} \end{bmatrix} \tag{3.8}$$

Equilibrium between adjacent elements is ensured by requiring traction continuity along the shared edges. Since adjacent elements are not necessarily in the same plane, the tractions have to be transformed into the same coordinate system, here the global coordinate system. This is achieved by multiplying T^e with a global transformation matrix T:

$$T = \begin{bmatrix} n_n^T & n_t^T & & & & n^T \\ & & n_n^T & n_t^T & & \\ & & & & n_n^T & n_t^T \end{bmatrix} \tag{3.9}$$

The continuity condition for each edge in the structure can be constructed by summarizing the incident traction forces as

$$-t\lambda + \sum_{i=1}^{k} T_i P_i f = t^0 \tag{3.10}$$

where k is the number of incident elements to the edge, P_i and T_i are the transformation matrices associated with incident element i and t and t^0 are the proportional traction forces respectively.
While a statically admissible solution could be obtained on section force level by ensuring n_i, q_i and m_i equilibrium across element boundaries, the internal stress state across boundaries might not be statically admissible. Since adjacent elements are not required to have identical cross section layouts, it is not possible to require full stress continuity across the boundaries. It is though possible to improve the solution by requiring $m_n^{(2)}$ and $m_{nt}^{(2)}$ continuity between elements. This ensures that the distribution of total stresses does not differ significantly in adjacent elements along shared edges. On free boundaries, the second-order moments can be used to determine the amount of internal stress redistribution allowed in the cross section. If the second-order moment is required equal to zero, no redistribution of stresses can occur between the layers, though internal redistribution between concrete and reinforcement is possible within the layer. If the second-order moment is allowed a non-zero value at a free boundary, the total stresses can be redistributed between layers as long as they are in equilibrium with the external loadings. Reinforcement placed in the outer layers can therefore induce stresses in the center layer simulating the effects of closed stirrups along the edge.
It should be noted that the actual element is only capable of modeling faceted shell structures since the twisting moments cannot be transferred between elements that are not in the same plane.

4 Numerical Examples

The element has been tested using basic load cases such as tension, compression, pure shear and bending, in which all numerical results were equal to the analytical solutions. The examples given

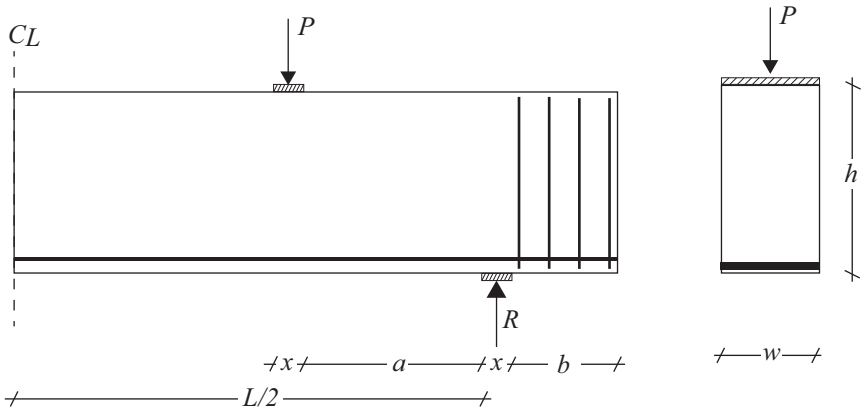

Figure 4: Beam without shear reinforced subjected to 4-point bending.

in this section illustrates how the element can be used to model different structural types. In the first example, the element is used as disk elements to model a beam without shear reinforcement subjected to four point bending. In the second example a plate subjected to a combination of uni-axial bending and transverse shear is analyzed and the numerical results are compared to an analytical $M-V$ failure curve. In the third and final example, a triangular plate supported on three columns and subjected to a point load is analyzed and the effects of including transverse shear stresses in the yield criterion is illustrated.
In all examples, the separation strength of the concrete, f_A, is set equal to zero and the second order moments, $m_n^{(2)}$ and $m_{nt}^{(2)}$, are allowed $\neq 0$ on free boundaries. The free solver SDPT3 (Toh et al., 1998; Tütüncü et al., 2003) was used to solve all examples and YALMIP (Löfberg, 2004) was used as interface to the solver. Both SDPT3 and YALMIP are implemented as MatLab Toolboxes.

4.1 Unreinforced Shear Beam

In the first example, the element will be used as a disk element to model and analyze the load bearing capacity of a beam without shear reinforcement subjected to four point bending. This problem has been treated in (Jensen, 1981) in which the constant stress triangles was used to obtain a lower bound solution manually.

Here we consider a beam with a span of L, width w and height h as shown in Fig. 4. The beam is simply supported on a rigid support plate with length x and the point load P is assumed to be transferred through a rigid plate of equal length x as illustrated in the figure. The distance between the rigid plates is denoted a. Longitudinal stringer reinforcement with cross section area A is placed along the bottom of the beam and shear reinforcement is placed in a distance of b behind the support to ensure sufficient anchorage of the stringer reinforcement.
In (Jensen, 1981), formulas for the load capacity based on a lower bound solution is given. These

formulas will be used to verify the numerical results and are summarized below

$$\frac{\tau}{f_c} = \begin{cases} \frac{1}{2}\left(\sqrt{1+\left(\frac{a}{h}\right)^2} - \frac{a}{h}\right) & for\ \ \Phi \geq \frac{1}{2} \\ \frac{1}{2}\left(\sqrt{4\,\Phi(1-\Phi)+\left(\frac{a}{h}\right)^2} - \frac{a}{h}\right) & for\ \ \Phi \leq \frac{1}{2} \end{cases} \tag{4.1}$$

where $\tau = \frac{P}{wh}$ and Φ is the reinforcement degree in the longitudinal direction

$$\Phi = \frac{T_Y}{h\ w\ f_c} = \frac{A\ f_{Yt}}{h\ w\ f_c} \tag{4.2}$$

For the numerical experiments, a beam with span $L = 12000\ mm$, width $w = 300\ mm$ and height $h = 600\ mm$ is used. The uni-axial compression strength of the concrete is $f_c = 25MPa$. The beam is meshed using 160 elements as shown in Fig. 5. The force P is applied as a proportional pressure load, t_y, over the length $x = 100mm$. b is kept constant at $2x$. The reinforcement degree in the longitudinal direction is $\Phi = 0.1$ and it is smeared over the height of $100mm$ such that

$$\Phi_x = \frac{h}{y}\Phi = 0.6 \tag{4.3}$$

The meshing of the beam with the applied reinforcement is illustrated in Fig. 5. Behind the support, a shear reinforcement of $\Phi_y = 0.1$ is applied to ensure anchorage of the longitudinal reinforcement. The beam is analyzed for different values of a and the numerical results are compared

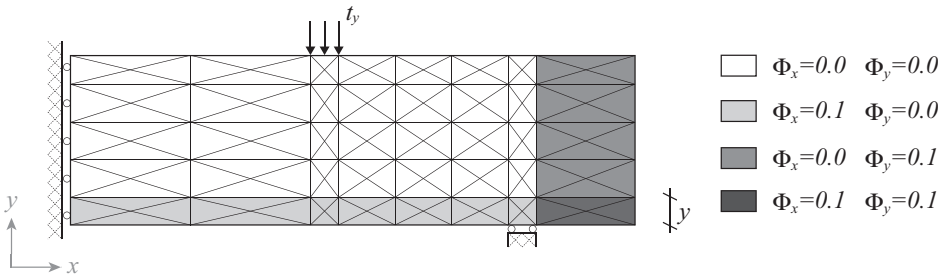

Figure 5: Sketch of meshed beam without shear reinforced subjected to 4-point bending.

to the analytical solution given in Eq. (4.1).The analytical solution assumes that a compression zone is formed from the load down to the support in which there is a uni-axial stress state. Such a zone can not be formed using the mesh shown in Fig. 5 and a slight redistribution of the stresses is required. This redistribution requires some shear stresses to be present, which, due to the lack of reinforcement, requires a tensile strength of the concrete. Numerical tests are therefore made for different values of f_{ct} where:

$$\frac{f_{ct}}{f_c} = \alpha\frac{\sqrt{0.1 f_c}\ [MPa]}{f_c} \qquad (f_c \text{ in MPa}) \tag{4.4}$$

Fig. 6 shows the numerical results compared with the analytical solution. As seen in the figure, lower load bearing capacities are found for all values of f_{ct} when a is small. For $a = h$, a slightly

higher capacity is found when f_{ct} is greater than zero, while low capacities are found for $f_{ct} = 0$. As a increases, the bending moment becomes more dominant and the influence of f_{ct} therefore decreases. As seen from the figure, the numerical results converges towards the analytical solution for increasing values of a.

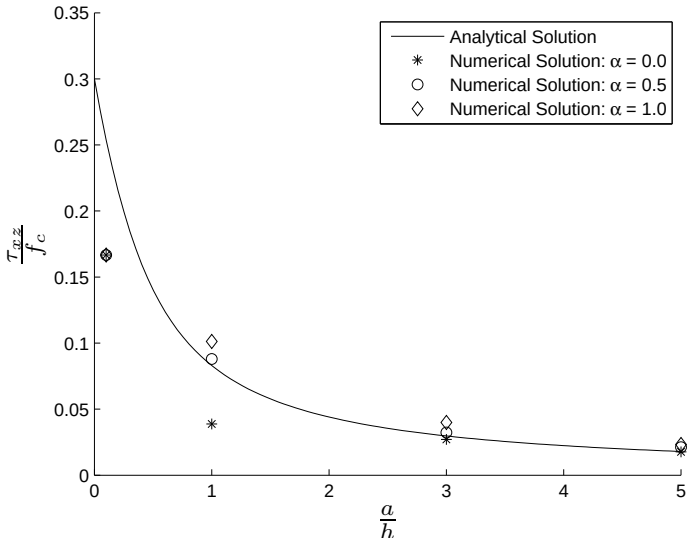

Figure 6: Comparison between the numerical model and the analytical solution. Numerical results are shown for different values of f_A.

4.2 Combined Bending Moment and Transverse Shear

In this example, the element is tested when subjected to a combination of bending moments and transverse shear forces. We consider a very short, simply supported plate with length L, width w and height h as shown in Fig. 7. The plate is reinforced in the longitudinal direction in top and bottom and shear reinforcement is applied as closed stirrups, which are assumed to be closely spaced: that is the stirrup reinforcement is smeared over the cross section and replaced by an equivalent reinforcement degree ϕ:

$$\phi = A_{sz}\frac{f_{Yt}}{f_c} \tag{4.5}$$

where A_{sz} is area of shear reinforcement per unit area in the Lw-plane.
The plate is loaded by a constant bending moment m_n^0 along the supported boundary and a uniform surface load p as shown in the figure. At the supported boundary, the cross section will be subjected to a combination of the bending moment m_n^0 and the transverse shear force $q_n = pL/2$. The shear force is assumed to be transferred to the supports through rigid plates as illustrated in the figure. In (Nielsen, 1999), the combined effect of shear and bending moment has been considered using the stringer method, where tension and compression is treated as concentrated stringer forces in top and bottom, and shear is carried as constant shear stresses between the stringers. We will here assume that the compression stringer has sufficient capacity to carry the loading such

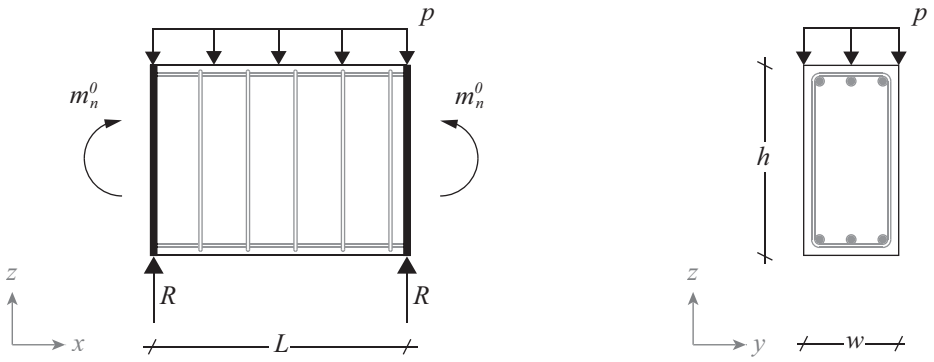

Figure 7: Short plate subjected to uniform loading and a constant bending moment.

that the load capacity is governed by the tensile stringer and the shear reinforcement. In (Grob and Thürlimann, 1976), an analytical expression for the $m_n - q_n$ yield surface is derived:

$$\left(\frac{q_n}{T_y}\right)^2 - 2\,\frac{\phi}{\Phi}\left(1 - \frac{m_n}{h'\,T_Y}\right) \leq 0 \tag{4.6}$$

where h' is the height of the shear zone. The reinforcement degree Φ is defined as

$$\Phi = \frac{A_s\, f_{Yt}}{w\, h'\, f_c} = \frac{T_Y}{w\, h'\, f_c} \tag{4.7}$$

where A_s is the area of the stringer reinforcement and T_Y is the yield capacity of the tensile stringer. The above expression will be used as reference for the numerical results.
The plate shown in Fig. 7 is modeled using 4 elements as shown in Fig. 8. To minimize the influence of the bending moment caused by the uniform load, the beam length is set very low:

$$\frac{L}{h} = \frac{1}{60} \tag{4.8}$$

The analytical solution assumes infinitely thin stringers. To simulate this as close as possible, the outer layers are kept thin:

$$h_1 = h_3 = \frac{h}{60} \tag{4.9}$$

The reinforcement degree in the outer layers Φ_x^1 and Φ_x^3 is determined from the reinforcement degree Φ as

$$\Phi_x^1 = \Phi_x^3 = \frac{h - h_1}{h_1}\Phi \tag{4.10}$$

The numerical $m_n - q_n$ yield surface is created by varying the constant moment, m_n^0 in the interval $0 \leq m_n^0 \leq m_n^p$, where

$$m_n^p = T_y\, h' \tag{4.11}$$

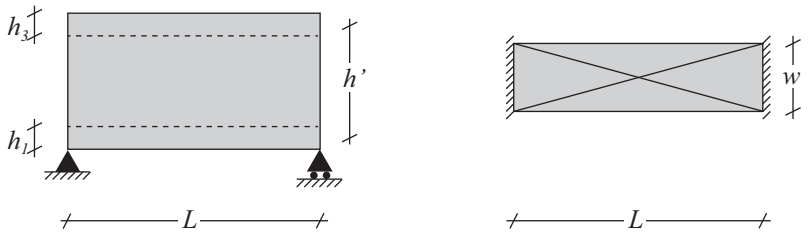

Figure 8: Short plate modelled using 4 shell elements.

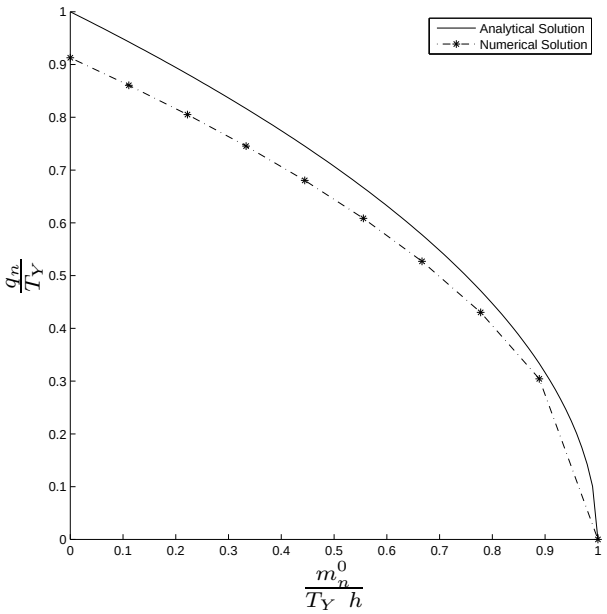

Figure 9: Comparison between the numerical and analytical yield surface.

is the bending capacity of the cross section. Fig. 9 shows a comparison between the numerical results and the analytical solution given in Eq. (4.6). From the figure it is seen that identical solutions are obtained when the plate is subjected to pure bending while the numerical capacity is slightly lower when shear becomes dominant. The analytical solution neglects the effect of shear stresses in the stringers, these are taken into account in the numerical model, which is why a lower capacity is found by the numerical model when compared with the analytical stringer model.

4.3 Triangular Plate on Point Supports

In this example, a triangular slab supported by three columns and subjected to a downward point load, P, as illustrated in Fig. 10, is analyzed. For the numerical test, a is set equal to $1m$ and the thickness of the plate is set to $300mm$ and divided into layers such that $h_1 = h_2 = h_3 = 100mm$. The concrete compression strength is $f_c = 15MPa$ and reinforcement is added to the top and bottom

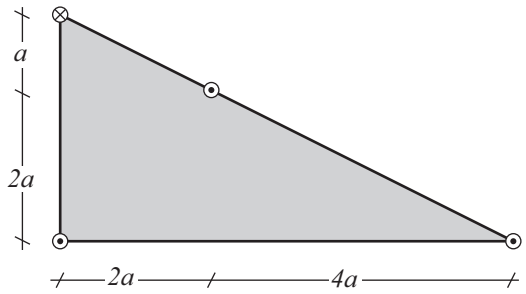

Figure 10: Triangular plate supported on 3 columns and load by a pointload.

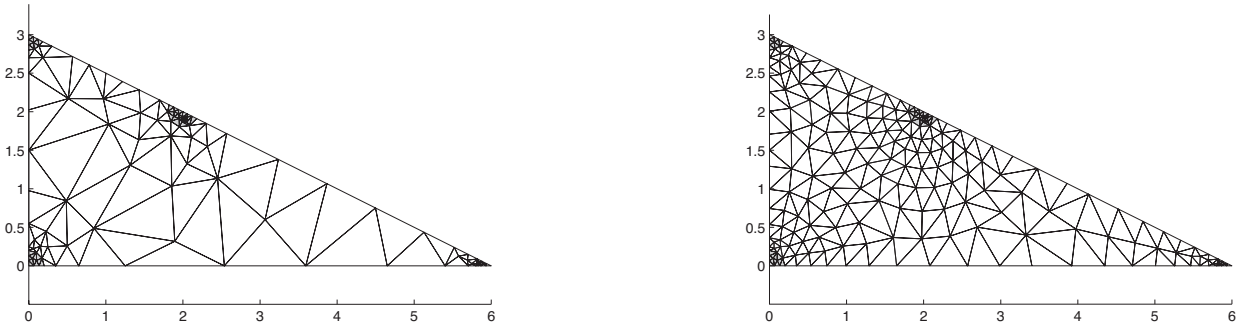

(a) Coarse mesh: 166 elements

(b) Fine mesh: 351 elements

Figure 11: Finite element model of the triangular plate.

layers such that

$$\Phi_x^{(1)} = \Phi_x^{(3)} = 0.1 \tag{4.12}$$

$$\Phi_y^{(1)} = \Phi_y^{(3)} = 0.1 \tag{4.13}$$

The plastic bending capacity of the cross section is $m_p = 30kNm/m$ and shear reinforcement is added in the entire plate such that $\Phi_z = 0.1$. The column supports are modelled by supporting the plate over a circular sector with radius $0.2m$. The point load is similarly applied as a constant surface load over a circular sector with the same radius. The plate is meshed and analyzed using a coarse mesh of 166 elements, Fig. 11a, and a fine mesh of 351 elements, Fig. 11b. An upper bound solution for P_m (identical to a numerical lower bound solution) based on moment yield line theory and rigid in transverse shear is given by

$$P_m = \frac{12m_p}{2+\sqrt{5}} \tag{4.14}$$

which gives $P_m = 85kN$ for the given m_p.
From numerical analysis, a load bearing capacity of $P_{m+s} = 38.4kN$ is found using the coarse mesh wile a slightly higher value of $P_{m+s} = 39.2kN$ is found using the fine mesh. The reduced capacity is a consequence of combined moment and shear failure in the plate, something which

is not accounted for by P_m. In this example, the moment based solution yields a capacity which is more than twice that of the numerical model and the example illustrates the importance of considering transverse shear stresses when analyzing certain plate structures in which combined shear and bending occurs.

5 Conclusion

We have presented a new shell element capable of performing lower bound limit state analysis of reinforced concrete shell structures. The element can model membrane and plate bending behaviour and it includes the transverse shear stresses into the yield criterion. The element employs a layered disk model to describe the internal stress state in the shell element and the yield criteria are applied at a stress state level. The internal stress state is decomposed into concrete and reinforcement stresses to which separate yield criteria are imposed. The modified Coulomb criterion is applied to the concrete stresses and formulated as a combination of linear matrix inequality constraints and linear inequality constraints. The reinforcement is assumed subjected to uni-axial stresses only and is constrained by simple upper- and lower limits. The optimization problem is then solved using a general purpose Semidefinite Programming algorithm.
It is shown how the element can model both plate and disk structures and comparison with analytical solutions showed good agreement. Furthermore, it was shown how the load bearing capacity of certain plate structures are significantly overestimated if the transverse shear stresses are not included in the yield criterion.

References

Anderheggen, E. and Knopfel, H. (1972). Finite element limit analysis using linear programming. *International Journal of Solids and Structures*, 8(12):1413–1431.

Bisbos, C. and Pardalos, P. (2007). Second-order cone and semidefinite representations of material failure criteria. *Journal of Optimization Theory and Applications*, 134(2):275–301.

Dantzig, G. B. (1963). *Linear programming and extensions*. Princeton University Press, Princeton, N.J.,.

Engkilde, P. J. (2008). Armerede betonskallers plastiske bæreevne (plastic load carrying capacity of reinforced concrete shells) (in danish). Master's thesis, Department of civil engineering, Byg-DTU.

Grob, J. and Thürlimann, B. (1976). Ultimate strength and design of reinforced concrete beams under bending and shear. *International Association for Bridge and Structural Engineering*, 36(2):105–120.

Jensen, J. F. (1981). *Plasticitetsteoretiske løsninger for skiver og bjælker af jernbeton (Plastic solutions for disks and beams of reinforced concrete)*. PhD thesis, Structural Research Laboratory, Technical University of Denmark, Copenhagen. No. R-141.

Karmarkar, N. (1984). A new polynomial-time algorithm for linear programming. *Combinatorica*, 4(4):373–395.

Krabbenhøft, K., Lyamin, A., and Sloan, S. (2008). Three-dimensional mohr-coulomb limit analysis using semidefinite programming. *Communications in Numerical Methods in Engineering*, 24(11):1107–1119.

Krabbenhoft, K. and Damkilde, L. (2002). Lower bound limit analysis of slabs with nonlinear yield criteria. *Computers and Structures*, 80(27-30):2043–2057.

Larsen, K. P., Poulsen, P. N., and Nielsen, L. O. (2009). Limit analysis of solid reinforced concrete structures. In *Computational Technologies in Concrete Structures (CTCS'09)*, pages 1216–1226.

Löfberg, J. (2004). Yalmip : A toolbox for modeling and optimization in matlab. In *Proceedings of the CACSD Conference*, Taipei, Taiwan.

Lundgren, H. (1949). *Cylindrical Shells*. Danish Technical Press, Institution of Danish Civil Engineers.

Makrodimopoulos, A. and Martin, C. M. (2006). Lower bound limit analysis of cohesive-frictional materials using second-order cone programming. *International Journal for Numerical Methods in Engineering*, 66(4):604–634.

Moersch, E. (1922). *Der Eisenbetonbau - Seine Theorie und Anwendung*. Verlag Konrad Wittwer, Stuttgart, 5. auflage edition.

Nesterov, Y. and Nemirovskii, A. (1994). *Interior-Point Polynomial Methods in Convex Programming*. Society for Industrial and Applied Mathematics.

Nesterov, Y. and Nemirovsky, A. (1988). A general approach to polynomial-time algorithms design for convex programming. *Centr. Econ. & Math. Inst., USSR Acad. Sci., Moscow, USSR,*.

Niebling, J., Vinther, A., and Larsen, K. P. (2007). Numerisk modellering af plastiske betonkonstruktioner (in danish). Master's thesis, Department of civil engineering, Byg-DTU.

Nielsen, M. P. (1969). Om jernbetonskivers styrke (on the strength of reinforced concrete discs). page 254. Polyteknisk Forlag.

Nielsen, M. P. (1999). *Limit Analysis and Concrete Plasticity*. CRC Press.

Poulsen, P. N. and Damkilde, L. (2000). Limit state analysis of reinforced concrete plates subjected to in-plane forces. *International Journal of Solids and Structures*, 37(42):6011–6029.

Toh, K. C., Todd, M., and Tütüncü, R. (1998). Sdpt3 - a matlab software package for semidefinite programming. *Optimization Methods and Software*, 11:545–581.

Tütüncü, R. H., Toh, K. C., and Todd, M. J. (2003). Solving semidefinite-quadratic-linear programs using sdpt3. *Mathematical Programming*, 95(2):189–217.

Vandenberghe, L. and Boyd, S. (1996). Semidefinite programming. *SIAM Review*, 38:49–95.